Amount of Carbon Dioxide Fraction Determination by TDLAS: Evidences for a *Potential Primary Method Directly Applied* in Gas Analysis

Von der Fakultät für Lebenswissenschaften

der Technischen Universität Carolo-Wilhelmina

zu Braunschweig

zur Erlangung des Grades eines

Doktors der Naturwissenschaften

(Dr. rer. nat.)

genehmigte

D i s s e r t a t i o n

von Jorge Koelliker Delgado

aus Celaya, Mexiko

1. Referent: Prof. Dr. Karl-Heinz Gericke

2. Referent: Priv. Doz. Dr. Peter Ulbig

eingereicht am: 27. Feb. 2006

mündliche Prüfung (Disputation) am: 12. Apr. 2006

2006

Vorveröffentlichungen der Dissertation

Teilergebnisse aus dieser Arbeit wurden mit Genehmigung des Fachbereichs für Chemie und Pharmazie, vertreten durch den Mentor in folgenden Beiträgen vorab veröffentlicht:

Publikationen

- Werhahn O., Koelliker Delgado J., Schiel D.; *Kalibrationsfreie Bestimmung von Stoffmengenanteilen – Potenziale für Quantenkaskadenlaser in der Gas Analytik*; Technisches Messen, 72, 6: 396 - 405 (2005)

- Werhahn O., Koelliker Delgado J., Schiel D.; *Laserspektrometrie für die Gasanalytik*, PTB-Mitteilungen 115, 4: 305 - 309 (2005)

Tagungsbeiträge

- Koelliker Delgado J., Werhahn O., Schiel D.; *Absolute measurements of amount of substance fractions by laser spectroscopy*. (Poster) 69. Jahrestagung der Deutschen Physikalischen Gesellschaft, Berlin, März (2005)

- Werhahn O., Koelliker D. J., Schiel D.; *Gasanalytik mit Quantenkaskadenlasern*. (Vortrag) 69. Jahrestagung der Deutschen Physikalischen Gesellschaft, Berlin, März (2005)

- Werhahn O., Koelliker D. J., Schiel D.; Gas *Analysis with Quantum Cascade Lasers*. (Poster) 5th International Conference on Tunable Diode Laser Spectroscopy, Florence, Italy, Juli (2005)

- Padilla Viquez G. J., Koelliker Delgado J., Werhahn O., Jousten K., Schiel D.; *Traceable molecular linestrengths for gas analysis applications*. (Poster) eingereicht zur Conference on Precision Electromagnetic Measurements, Turin, Italy, Juli (2006)

Abstract

Tunable diode laser absorption spectroscopy (TDLAS) is a very powerful measurement technique, able to determine *amount of substance fractions* of gases from *major* to *trace* levels. Compared with other traditional methods used in gas analysis, TDLAS is very selective and fit for *in-situ* or *field* measurements. This work regards its ability to perform *calibration-free* measurements of amount of substance fractions serving as the first *potential primary method of measurement directly applied* (PMDA) in gas analysis. Establishing such a PMDA would be an important contribution to the fundamental concepts in the Metrology in Chemistry in terms of the international comparability of measurement results. This PMDA effectively reduces the uncertainty of field measurement results being independent of relatively large traceability chains supported by e. g. primary gas mixtures. Thus, improvements in the reliability and accuracy of measurement results can be achieved. Additionally, a direct traceability to the SI units avoid the manipulation mistakes that could occur in larger traceability chains. The method based on the application of the Beer-Lambert law. The measurement equation of the method considers all significant uncertainty sources and all correction factors that substantially contribute to the uncertainty budget. For the first time a *GUM-compliant*, *transparent* and *complete* uncertainty budget for calibration-free amount of carbon dioxide fraction measurements by TDLAS is given.

The performance of the *calibration-free* method was proved measuring amount of carbon dioxide fractions x_{CO_2} of gravimetrically prepared CO_2 in N_2 gas mixtures in the interval of $1 \cdot 10^{-2}$ to $10 \cdot 10^{-2}$ mol/mol. The TDLAS based x_{CO_2} results were compared with respective gravimetric values. Given the expanded uncertainty of the TDLAS-based x_{CO_2} values of < 2 % (k=2), this comparison showed concordance within the uncertainty of the gravimetric reference values. Based on these achieved uncertainties, it is argued that this PMDA-TDLAS method is *fit-to-intended-use* in e. g. the monitoring of CO_2 emissions in different combustion processes, including stack and automotive exhaust emission tests.

To improve the TDLAS-based method a new traceable linestrength value for the R12 line of the $\nu_1+2\nu_2+\nu_3$ band of CO_2 was measured. The uncertainty of the R12 line was improved from 2 - 5 % given in HITRAN to 1.1 % (k=2).

The good performance of the PMDA-TDLAS method was also proved in two applications at extreme opacity conditions: the measurement of x_{CO_2} in a commercially certified multi-component gas mixture used for the calibration of vehicle exhaust emissions sensors with $x_{CO_2} \approx 14 \cdot 10^{-2}$ mol/mol and in CO_2 measurements in room air with $x_{CO_2} \approx 400 \cdot 10^{-6}$ mol/mol. For the multi-component gas mixture the *apparent bias* was -0.55 %, which was concordant within the uncertainty of the certified value $\pm$ 1 % (k=2). This bias was not significant related to the uncertainty of 2 % (k=2) of the TDLAS based x_{CO_2} value. Thus, TDLAS has also the potential to be used calibration-free as certification method for gaseous reference materials. For the CO_2 measurements in room air a synthetic gravimetric gas mixture of CO_2 in N_2 was also prepared and measured by TDLAS. The *apparent bias* of the TDLAS based x_{CO_2} was +0.93 %. It was also concordant within the 1 % (k=2) uncertainty of the gravimetric x_{CO_2} and the bias was also not significant considering the uncertainty of the TDLAS based x_{CO_2} value of 3.3 % (k=2).

Table of Contents

1 Introduction

1.1 Motivation

Tunable diode laser absorption spectroscopy (TDLAS) is a very powerful measurement technique, able to determine *amount of substance fractions* of gases from *major* to *trace* levels. Purity can also be determined if the linestrength and the isotopic abundance of the measured substance are known. For purity analysis of gas species, TDLAS has the advantages of using only one measurement technique, and of potentially rendering uncertainties similar to those obtained when analyzing the impurities. Resolving the lines of 2 isotopologues in one spectrum allows also the estimation of isotopic ratios [1-4] or resolving 2 lines of an isotope for a gas specie produces the measurement of temperature [5]. With the use of three resolved lines for a gas specie in one spectrum the measurement of temperature and amount of substance can be established [6]. With the appropriate stability control, TDLAS can be used as a secondary method [7] for the certification of gas mixtures reference materials [120], because it will have the repeatability and reproducibility that other traditional techniques - like gas chromatography - may achieved.

The advantages of TDLAS are based on the laser source characteristics that conventional radiation sources do not offer, particularly: high *radiant power*, *monochromaticity* and *directionality*. The small linewidth of the laser radiation allows high selectivity for gas species. This *monochromaticity* of the laser source can maintain undisturbed the spectrum of the measured gas by instrumental linewidth contribution, while the laser is tuned over a molecular absorption line. *Directionality* can be used for the generation of larger optical pathlengths [8], especially for multi-reflection gas cells and *open-path free-of-sampling* gas analysis.

To grade the TDLAS, some traditional measurement techniques in gas analysis are compared in Table 1.1. There is a set of measurement techniques that render precise results, but they need calibration procedures. Others offer the potential to be used as *free-of-calibration*, but they are not suit for *field* (or *in situ*) measurements. For example, GC and MS are very precise measurement techniques, but no techniques that can be applied to *real-time*, *sample free* and *non-destructive* measurements. Contrary TDLAS can fulfill these needs. In FTIR the spectral lines have a limited resolution and pathlengths can not be accurately known due to the lack of directionality of the light source, by the same this technique is not suit for free-of-calibration measurements. TDLAS has other two advantages: changes of the optical pathlength allow to measure from pure to trace levels of concentrations and a change of the laser source allows also a variation in the line intensity. Two disadvantages of the TDLAS are: it is not a universal technique, and one laser is useful to detect only one or a couple of substances at once. However, the selectivity of TDLAS to specific substances is an advantage for the *in situ* measurement of substances of known identity.

From the point of view of the techniques in laser spectroscopy, a selected group of optical techniques is compared in Table 1.2. Among them, only the direct detection and the differential absorption, and cavity ring down are those who are both suit for *in situ* and *free-of-calibration* measurements. Cavity ring down (CRDS) has been proposed by some authors as a potential primary method of measurement for gas analysis [9], but it is a measurement technique that is one of the best researched

optic techniques of the last years [10], thus CRDS is not considered in this work, but only the other two techniques.

Table 1.1: Selected measurement techniques for gas analysis.

Measurement technique	Free-of-calibration possibilities?	In situ?	Sample destructive?	Real time measurement?	Main characteristics or applications fields
Gas chromatography (GC)	No	Yes (compact GCs)	Yes	No	Universality limited, very precise,
Mass spectrometry (MS)	Yes as IDMS	No	Yes	-	Universal, very precise
Non dispersive infrared spectroscopy (NDIR)	No	No	No	No	Selective and precise
Fourier transform infrared spectroscopy (FTIR)	No	Yes	No	Possible	Universal
Tunable diode laser absorption spectroscopy (TDLAS)	Yes	Yes	No	Possible	Selective for pure to trace gases

Table 1.2: Selected techniques for laser spectroscopy.

Spectroscopic technique	In situ?	Free-of-calibration possibilities?
Direct absorption (DA)	Yes [11]	Yes [11]
Differential absorption (DiA)	Yes [11]	Yes [11]
Frequency Modulation spectroscopy (FM-S)	Yes [11]	No [11]
Photoacoustic spectroscopy (PAS)	No [11]	No [12]
Cavity ring down spectroscopy (CRDS)	Yes [13]	Yes [10]
Light detection and ranging (LIDAR) and Differential optical absorption spectroscopy (DOAS)	No [13, 14]	No [13]

The spectrum of applications of TDLAS in gas analysis ranges from the basic needs sectors**:** health [15], food [16] and agriculture [17] to the commodities sectors: such as energy [18, 19], industry [20, 21] and environment [22, 23]. The main emphasis in applications has been given to the environmental sector [24]. TDLAS has, at least in research, invade many fields of applications for gas analysis in environmental measurements for vehicle exhaust emissions, stack emissions and air quality monitoring [18, 22, 24]; in health for non invasive medicine by breath tests [15]; in agriculture for the control of gases in fruit ripening [17], in energy for control of combustion processes [18]; and in industry for example in the control of gases in process optimization [21].

Definitively, the advantages of TDLAS have been exploited in research reports for field [25], non-intrusive, sampling free, in situ [18, 26, 27] or open path [20, 25] measurements or for measurements under difficult conditions of temperatures and pressures [6, 18]. Despite some efforts have been made for performing free-of-calibration gas analysis by TDLAS - as the so called absolute methods [14, 27, 28] or primary methods [30, 31, 32] - only a few has been written about the uncertainty of such measurements. Today, the uncertainty of measurement is a technical requirement for test and calibration laboratories [33] as a measure of the quality of the results, which allows effectively to compare results. Nowadays, not only the uncertainty but also the traceability of measurement results are both key technical requirements in chemistry for the accreditation of chemical laboratories under

ISO17025-(1999) [33]. Quality systems like ISO 9000-(2000) require now also the fulfillment of traceability of measurement results [34].

Uncertainties achievable in gravimetry - the traditional and most extended potential primary method of measurement used to generate reference gas mixtures - are of the order of 10^{-4} for amount of substance fractions [35]. At present, "state-of-the-art" analytical methods are capable of measurement uncertainties of about 10^{-3} [35]. However, uncertainties of 10^{-3} can be achieved in the preparation of chemical standards traceable to the SI-unit of mass, but this does not provide the capability to analyze unknown samples [35]. The agreement of results between laboratories for calibration gas mixtures at the highest metrological level in the gas analysis field is of about 10^{-2} [36, 37], depending on the substance, matrix and the concentration. The Avogadro constant is known with an uncertainty being of the order of 10^{-7}. This could be seen as the ultimate uncertainty achievable in chemistry. It gives an idea of the ultimate waited uncertainties. Smaller uncertainties than this can be possible, but only with the biggest efforts. Without adherence to the SI of units to establish such an improvement in uncertainty is - in some cases - more difficult to probe.

The possibility to use TDLAS for *field measurements*, *direct measurements*, *on line*, *in situ*, *open path*, in some cases *without sampling* and without calibration of the substance being measured brings fundamental metrological advances. That is, the application possibility of TDLAS in an absolute way (without calibration of the substance being measured). Despite the performance of TDLAS could maybe not achieve the performance of a primary method of measurement [38] for every substance under study in gas analysis. But in practice, the fit-to-intended-use of the TDLAS method (fit for purpose) is more important than promoting free-of-calibration, absolute or primary methods claims. In other words, this means that the method is useful to monitor a substance in a given application with the accuracy needed. The adequacy to use is facilitated only by the estimation of measurement uncertainty that is not possible to realize without traceability. Uncertainty estimation also allows to identify the main influence quantities contributing to the overall uncertainty of the measurement, thus introduce improvements in the measurement procedure or to identify the limits of a measurement technique.

There are several ways to establish the traceability of chemical measurement results [39, 40] and some guidelines are available [41]. In gas analysis, for static gas mixtures it is typical to have a large traceability chain originated in National Metrology Institutes (NMIs) with a number of linkages of at least 4 to 5 measurement values, e.g. for the regulated USA EPA-traceability protocol for the certification of gaseous standards [42]. This regulated way is a good alternative for the establishment of traceability in practice, where the tendency is to reduce the number of linkages in the traceability chains for supporting the field measurement results. For example, the automotive industry requested that one of the NMIs (NIST) provide gas mixtures with uncertainties lower than those claimed for a kind of gaseous certified reference materials [43]. Because of the uncertainty of manipulation of gas mixture analysis in large traceability chains, uncertainties for field measurements in gas analysis of 5 % seems to be optimistic in not isolated cases. For example, in Switzerland concentrations of airborne pollutants are required to be given with an uncertainty lower than $\pm$15 % [44]. Other way of establishing traceability is the direct traceability concept of measurement results to the SI system of units [39, 40]. This concept is based on an accurate measurement equation traced back directly to the SI of units

[38]. Direct traceability prevents mistakes in large traceability chains and effectively reduces the number of linkages to the SI units. This calibration-free direct traceability concept is especially important for measurement results, where the standard methods fail [8].

Comparisons of reference spectra from available quantitative collections show that the agreement of reported intensities is frequently ± 10 % or worse [1.1]. The uncertainty in line strengths of the HITRAN 2004 database could be < 1 % or even ≥ 20 %, depending on the line, the substance, and if the results come from appropriate calibrated facilities or from other sources, including the use of quantum-mechanic models and numerical calculations [45]. For example, for carbon dioxide only three lines are reported with an uncertainty < 1 %, and from the main isotope $^{12}C^{16}O_2$ only one line is reported at this level of uncertainty, more normal are the uncertainties given in an interval between 2 and 10 % uncertainty. In science and research, it is not common practice to use fundamental metrological principles, it means, the use of recognized measurement standards or comparison with them, maintenance of the traceability of measurements results and uncertainty estimations according to the international method for estimation of uncertainty (GUM) [46]. The uncertainties given in the databases not explicitly conform with the GUM, also the traceability of measurement results is not always established or can be demonstrated. This is because the important fundamentals and the full application of the metrological principles in Chemistry are relatively new.

It could be thought that the application of the TDLAS technique without calibration and the limits of the Beer-Lambert law for gas analysis are already in place since some decades, but recent discovers, improvements and international arrangements evidence the still in development real power of the TDLAS technique in industry for enough accurate gas analysis (fit-to-intended-use):

- the limits of signal averaging in spectroscopy [47, 1993],
- use of reliable laser sources and detection technologies [8, 2001],
- improved studies of the lineshapes, although the fundamentals were in place since the 1960s [48, 2003],
- born of new lineshape theories [49, 1997],
- formal international recognition of measurement standards in gas analysis [50, 1999],
- starting of internationally rigorous application of Metrology in gas analysis [51, 1991],
- formal application of the traceability concept to chemical measurements [52, 1990],
- formal recognition of the traceability and uncertainty as scientific-technical requirements for calibration and test laboratories [33, 1999],
- internationally accepted methodology for estimating the uncertainty of measurement [46, 1993],
- even more, in case of this thesis, improvement of the uncertainty estimation for refraction index of silicon [53, 2002].

Also the motivation of this thesis is to have an active future influence on the type approval proof of commercial and normative designs of TDLAS measurement systems that can operate free-of-calibration. Because until now, absolute instruments

for gas analysis have not been developed [54]; especially with TDLAS that simultaneously fulfill new stringent requirements, e. g. that of ISO 17025.

1.2 Objectives

The main objective of this thesis was to design a measurement system to show that TDLAS can be used as a method directly traceable and without calibration of the substance being measured in a quantitative reliable way.

As consequence, a methodology for the evaluation of the free of calibration performance for gas analysis was presented. Such methodology considered all significant uncertainty sources and all correction factors that substantially could contribute to the uncertainty of measurement results.

As an example, the carbon dioxide molecule was selected to prove a free-of calibration performance that completely conforms with internationally accepted metrological principles for gas analysis.

The applications selected to be proved were:

a) the indoor air quality monitoring of carbon dioxide, and

b) the analysis of carbon dioxide in a commercially certified multi-component gas mixture.

The fit-to-intended-use can be definitively evaluated by providing complete and transparent uncertainty budgets for these applications and for the free-of-calibration performance evaluation verified by static gravimetric gas mixtures.

2 Scientific Bases of Measurements

In this chapter the theoretical foundations governing the use of spectroscopy with tunable diode lasers for gas analysis are presented. Measurement principles, equations and conditions assumed for the application of the measurement technique in gas analysis are introduced. Section 2.1 presents the fundamentals of the carbon dioxide (CO_2) NIR-electromagnetic spectrum, section 2.2 deals with the principles governing quantitative single line spectroscopy and 2.3 with the metrological bases of the measurements.

2.1 The Near-Infrared Spectra of CO_2

As a good approximation the total energy of a molecule can be represented by the sum of the electronic, the vibrational and the rotational energy

$$E_{total} = E_{elec} + E_{vib} + E_{rot} \qquad (2.1).$$

The molecular energy eigenstates are separated by characteristic molecular transition energies. The separation of the vibrational eigenstates corresponds to the IR spectrum.

2.1.1 The Molecular Structure

Linear molecules such as CO_2 can generally be treated as diatomics with regard to their *moments of inertia*. The *moment of inertia* about the A-axis (along the molecule), is approximately zero, $I_A = 0$, and the other two moments are equal, $I_B = I_C$. Because the moment of inertia for CO_2's end-over-end rotation is much larger than for diatomics, the rotational constant will be correspondingly smaller (Table 2.1). The *moment of inertia* can be related to a molecule's rotational constant via the relation

$$B_0 = \frac{h}{8 \cdot \pi^2 \cdot I_B \cdot c} \qquad (2.2).$$

The quantum number for a linear polyatomic molecule's *angular momentum* (*rotational quantum number*) is *J*. Since CO_2 is linear and symmetric, it does not have a permanent *dipole moment*. Thus, CO_2 is only spectroscopically active in the IR when a dipole is induced due to bending or asymmetric stretching.

Table 2.1: Some properties of CO_2 [55].

Property	Value
Bond length	$r_0(C\text{-}O)$ = 1.162 Å
Rotational constant	B_0 = 0.390 cm^{-1}
Symmetry number	σ = 2

2.1.2 Vibrations and Symmetry

CO_2 has four *vibrational modes*, of which two bending modes are degenerate, as depicted in the lower part of Figure 2.1 and listed in Table 2.2. The two stretching modes, symmetric and antisymmetric, are parallel vibrations, since the vibrations occur parallel to the main symmetry axis, and the bending modes are perpendicular, since they induce changes of the position of the atoms in the molecule that are

perpendicular to the main symmetry axis. Only the vibrations that induce a *dipole moment* are spectroscopically active in the infrared. The top part of Figure 2.1 shows the two axes of symmetry of CO_2, including an infinite number of C_2 axes that align through the C atom and perpendicular to the bonds. These axes are two-fold symmetric, thus, a rotation of 180° produces an indistinguishable change. In addition, CO_2 has the C_∞ axis along the molecule, about which an infinite number of rotations produces no distinguishable change in orientation. Because CO_2 has an ∞-fold axis C_∞ that is perpendicular to an infinite number of planes of symmetry, it belongs to the point group $D_{\infty h}$ and has a symmetry number $\sigma = 2$ [56].

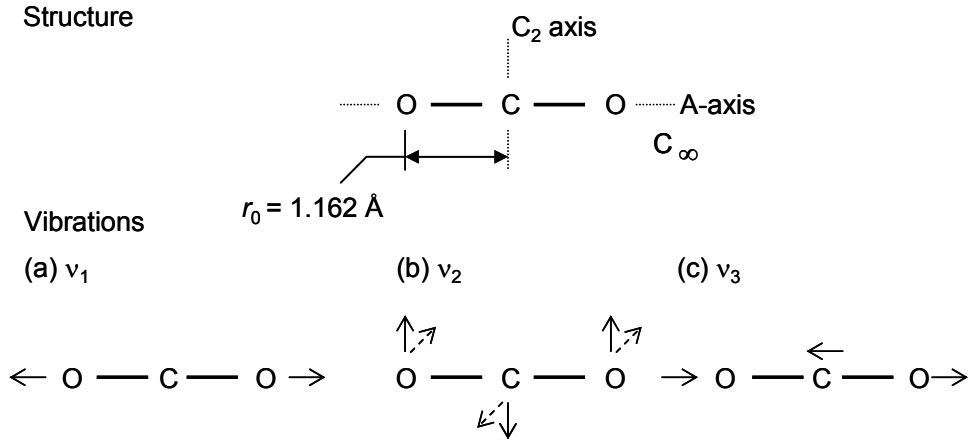

Figure 2.1: CO_2 symmetry axes (top panel), and vibrational modes (bottom panel): (a) symmetric stretch, ν_1; (b) bending, ν_2; (c) antisymmetric stretch, ν_3.

Table 2.2: Fundamental vibrations, frequencies, types, and description for CO_2 [55].

Vibration	Wavenumber / cm^{-1}	Type	Description	IR-active?
ν_1	1388	Parallel	Symmetric stretch	No
ν_2	667	Perpendicular	Bending (Degenerate)	Yes
ν_3	2349	Parallel	Asymmetric stretch	Yes

If the anharmonicity of the vibrations is taken into account, the classical vibrational motion contains not only the fundamental but also the overtone frequencies $2\nu_i$, $3\nu_i$, ⋯, and furthermore the combination tones $\nu_i + \nu_k$, $\nu_i - \nu_k$, $2\nu_i + \nu_k$, ⋯. Therefore, overtone and combination bands may also occur if they are connected with a change of dipole moment. However, they will be weaker than the fundamentals, since anharmonicities in general are slight. This kind of overtone and combination bands are the bands tested in this work.

2.1.3 Nomenclature of IR Spectra

CO_2 has a center of symmetry, and thus, it is susceptible to the effects of the *nuclear spin*. Because CO_2 is a member of the $D_{\infty h}$ point group, alternate rotational levels have different statistical weights, with odd rotational levels having a zero weight, while even levels have a weight of one. Thus, the odd levels for CO_2 are missing. The selection rules for CO_2's rovibrational spectra are that the rotational quantum number can change $\Delta\nu = \pm 1$, such that $\Delta J = \pm 1$. Standard notation for a transition

uses *P* to denote quantum rotational changes of ΔJ = -1, and *R* for ΔJ = +1 with respect to the low lying level.

A particularity of the CO_2 vibrations is that they show *Fermi resonances* (e. g. the ν_1 and the first overtone of the ν_2), and that the degenerated mode is influenced by *Coriolis coupling*. The result of these effects is that the classical notation scheme used by Herzberg and others that describes the vibrational modes breaks down in certain instances. Extended notation schemes have been employed by Hitran96 and others [57, 58] to describe different vibrational bands. Hitran96 notation uses 5 parameters to distinguish different bands with the following system: $\nu_1\,\nu_2\ell\nu_3\mathrm{r}$, for which ν_1, ν_2 and ν_3 denote the classical vibrations; ℓ is the angular momentum of the bending mode; and r is a ranking index that uses the energy level to clarify bands that have similar quanta.

Table 2.3: Labelling for the Fermi triad at 2 μm using Herzberg and HITRAN notation schemes.

Band Center/μm	Band Center/cm^{-1}	Herzberg	HITRAN $\nu_1\,\nu_2\ell\nu_3\mathrm{r} \leftarrow \nu_1\,\nu_2\ell\nu_3\mathrm{r}$
1.957	5109	$2\nu_1+\nu_3$	20011←00001
2.006	4984	$\nu_1+2\nu_2+\nu_3$	20012←00001
2.057	4861	$4\nu_2+\nu_3$	20013←00001

A plot of CO_2 NIR spectra is shown in Figure 2.2. As the band labels on the plot reveal, the NIR is populated by weak overtone and combination bands. The 2 μm region contains 3 main bands known as the Fermi triad. The labelling for these three bands using Herzberg and Hitran96 notation are listed in Table 2.3. The band used for CO_2 sensors in this thesis is the $\nu_1+2\nu_2+\nu_3$ band centered at 2.006 μm.

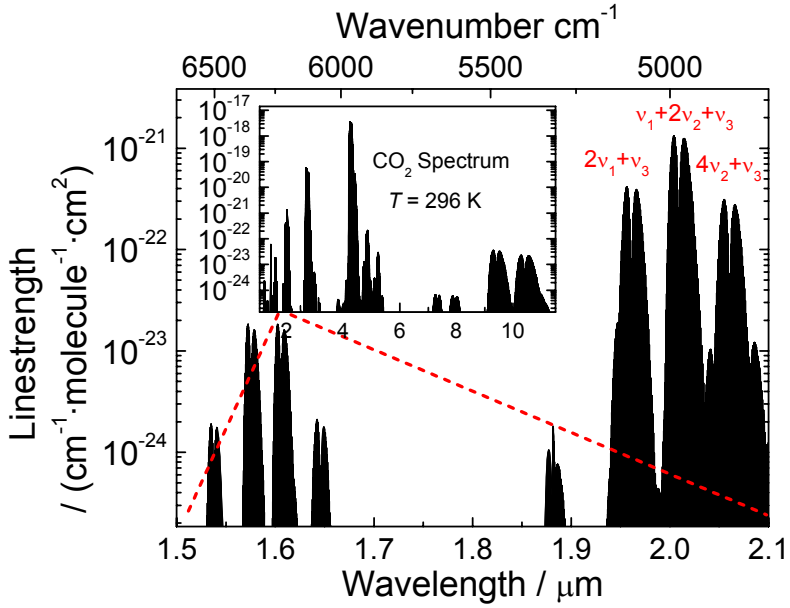

Figure 2.2: CO_2 NIR spectra: absorption bands labelled using Herzberg notation [45].

2.1.4 Partition Function

The total internal molecular partition function, $Q(T)$, is used to determine how *molecules in thermodynamic equilibrium* are distributed among the various energy states at particular temperatures, which is important for the temperature dependence of linestrength (see 2.2.2). It can be described *classically* as a product of the nuclear, rotational, and vibrational partition functions, Q_{nuc}, Q_{rot}, and Q_{vib}, respectively (2.3), if the interactions between vibrations and rotations are neglected [56]

$$Q(T) = Q_{nuc} \cdot Q_{rot} \cdot Q_{vib} \tag{2.3}.$$

The nuclear partition function is described by

$$Q_{nuc} = (2I_C+1)\cdot(2I_O+1)^2 = 1 \tag{2.4}$$

where I_C = 0 and I_O = 0 are the nuclear spins of the carbon and oxygen atoms, respectively. Thus, accounting for nuclear spin does not affect the overall partition function, but rather affects only the statistics of the different rotational levels, as discussed above.

Because CO_2 is a linear molecule, its rotational partition function can be approximated by a diatomic rigid rotor (RR), namely

$$Q_{rot} = \frac{k_B \cdot T}{\sigma \cdot h \cdot c \cdot B_0} \tag{2.5}$$

where σ = 2 is the symmetry number for CO_2, h is Planck's constant, k_B is Boltzmann's constant, c is the speed of light, and B_0 is the rotational constant for CO_2 (Table 2.1).

The simple harmonic oscillator (SHO) model for the vibrational partition function of CO_2 yields

$$Q_{vib} = \left[1-\exp\left(\frac{-h\cdot c\cdot \nu_1}{k_B\cdot T}\right)\right]^{-1}\left[1-\exp\left(\frac{-h\cdot c\cdot \nu_2}{k_B\cdot T}\right)\right]^{-2}\left[1-\exp\left(\frac{-h\cdot c\cdot \nu_3}{k_B\cdot T}\right)\right]^{-1} \tag{2.6}$$

for which the fundamental vibration frequencies are listed in Table 2.2 with a double degeneracy for the ν_2 mode. Thus, the classic total internal partition function for CO_2, neglecting vibration-rotation coupling, anharmonicities, and non-rigidities, is

$$Q(T)_{CO_2} = \frac{\frac{k_B \cdot T}{\sigma \cdot h \cdot c \cdot B_0}}{\left[1-\exp\left(\frac{-h\cdot c\cdot \nu_1}{k_B\cdot T}\right)\right]^{1}\left[1-\exp\left(\frac{-h\cdot c\cdot \nu_2}{k_B\cdot T}\right)\right]^{2}\left[1-\exp\left(\frac{-h\cdot c\cdot \nu_3}{k_B\cdot T}\right)\right]^{1}} \tag{2.7}$$

The total internal partition function used in this work was taken from the estimation used for the HITRAN database, which is in detail described in [57, 59]. This approach is an improvement of the usual *classical approximation* for the independent temperature variation of the rotational and vibrational components of the partition

function given above [57]. Following a brief description of it is presented. For the main isotope $^{12}C^{16}O_2$, a sum over all main energetic states of the molecule is used, with all *symmetry* and *degeneracy factors* accounted for. It is written

$$Q(T) = \frac{1}{\sigma}\sum_{\forall E}(2 \cdot J + 1) \cdot g_n \cdot e^{-\frac{E}{k_B \cdot T}} \tag{2.8}$$

This method called *direct summation* is potentially the most accurate [59]. An *energy cutoff* is chosen. The first 1456 vibrational energy states are obtained and (2.8) is evaluated with the appropriate *full nuclear spin degeneracy factor* (g_n). The summation is done over all these energy levels (E) at each temperature of interest (T). The factor $2 \cdot J+1$ arises from J spatial *degeneracy*. The energy levels were calculated by the authors using

$$E(v, J) = G_v + B_v \cdot J \cdot (J+1) - D_v \cdot J^2 \cdot (J+1)^2 + H_v \cdot J^3 \cdot (J+1)^3 + \cdots \tag{2.9}.$$

The molecular constants in this equation were obtained from direct *numerical diagonalization* (DND) results from Wattson and Rottman [60]. DND is an adaptation of the *variational method* for solving the quantum mechanical equations of the rovibrational molecular Hamiltonian. Wherever possible, the molecular constants G, B, D and H for a given vibrational state were determined by weighted linear least-squares fitting of observed line positions involving that state [61]. This last condition was the case of the energetic state used in this thesis [61], warranting in some way a final traceable link to the SI of units through measurements - in this case the meter or second - and not limited to the use of quantum mechanical models.

The total internal partition function, $Q(T)$ so obtained for each temperature T is then fitted using a *simplex non linear minimization algorithm* [62]. Then HITRAN database (1996 and 2000 versions) can calculate each value of linestrength at temperature T or the user can calculate the values of a provided third order *polynomial-fit* (2.10), for which the coefficients a, b, c, and d are listed in Table 2.4.

$$Q(T) = a + b \cdot T + c \cdot T^2 + d \cdot T^3 \tag{2.10}$$

Table 2.4: Coefficients of the polynomial expression for $Q(T)$ in (2.10) from Hitran96 [57] for CO_2.

Coefficient	$70 < T < 500$
a	-1.3617
b	9.4899e-1
c	-6.9259e-4
d	2.5974e-6

The uncertainty estimation of $Q(T)$ via the polynomial expression for the principal CO_2 isotope is < 0.1 % for the 70-415 K range and the maximum deviation between all results was < 0.5 % for 70-700 K when different methods of calculation of $Q(T)$ were used [59]. Applying the *classic* equation (2.7) and the *polynomial* expressions of $Q(T)$ for $^{12}C^{16}O_2$ (2.10), the total internal partition functions agree within 0.3 % in the temperature interval used for this thesis 293–298 K. Using the partition function in higher ranges of temperature is risky as the uncertainty grew up significantly, e. g.

4 % for the 415-2005 K interval [59], that could be a limitation of accuracy when applying the method at high temperatures.

For all other isotopic species of CO_2 the classical approach for estimation of $Q(T)$ was used, i. e., the total internal partition functions were calculated by the product assumption where both Q_{vib} and Q_{rot} were from direct summations. In these cases the uncertainty estimation of $Q(T)$ reported is < 1 % at ambient temperature. For temperatures around 2000 K this uncertainty is informed to be higher than 20 % [59].

2.2 Quantitative Absorption Spectroscopy

2.2.1 Beer-Lambert Law

According to *J*. H. Lambert, when a *parallel beam* of *monochromatic radiation* of radiant power $I(\lambda)$ enters a *homogeneous absorbing material*, the radiation transmitted through a layer of thickness *z* will have the radiant power

$$I(\lambda, z) = I(\lambda) \cdot \exp\{-k(\lambda,T) \cdot z\} \tag{2.11}$$

where $k(\lambda,T)$ is a positive constant called the *absorption coefficient* of the material. It is normally expressed in cm^{-1} units. A. v. Beer found that in many cases the absorption coefficient is proportional to the concentration of the absorbing material. When applying high resolution spectroscopy to gas analysis a convenient form of the Beer contribution is given by

$$k(\lambda,T) = S_i(T) \cdot \phi(\lambda, T, P, x_B) \cdot n(p,T) \tag{2.12}$$

which allows to relate the absorption coefficient with the line strength of a substance $S_i(T)$ in a transition i, having a density of absorbing molecules $n(p,T)$ and a line-shape function $\phi(\lambda, T, P, x_B)$ of a resolved absorption peak.

The theory governing absorption spectroscopy is embodied in the conjunction of the Beer-Lambert law, which relates the interaction between light and absorber of electromagnetic radiation

$$I(\lambda,z) = I(\lambda) \cdot \exp\{- S_i(T) \cdot \phi(\lambda, T, P, x_B) \cdot n(p,T) \cdot z\} \tag{2.13}.$$

Introducing the absorbance $\alpha(\lambda)$

$$\alpha(\lambda) = -\ln\left[\frac{I(\lambda,z)}{I(\lambda)}\right] \tag{2.14}$$

The ratio of transmitted and incident light is known as transmittance T.

Combining (2.13) and (2.14) for $z = L$ one gets

$$\alpha(\lambda) = S_i(T) \cdot n(p,T) \cdot \phi(\lambda, T, P, x_B) \cdot L \tag{2.15}$$

with *L* being the optical pathlength.

As the molecular density n in gas phase is highly temperature and pressure dependent, it does not seem to be the best quantity for expressing results of the substance being measured. With the use of the *ideal gas law*

$$p = n(p,T) \cdot k_B \cdot T \tag{2.16}$$

where p is the partial pressure of the substance, k_B is the Boltzmann constant and T the temperature of the gas, and applying the *law of partial pressures*

$$p = x_j \cdot P_{total} \tag{2.17}$$

the combination of (2.15), (2.16) and (2.17) gives

$$\alpha(\lambda) = S_i(T) \cdot \phi(\lambda, T, P, x_B) \cdot x_j \cdot P_{total} \cdot L / (k_B \cdot T) \tag{2.18}$$

which allows to express results of the measured entity in amount of substance fraction. The amount of substance fraction quantity x_j has the advantage to be independent of the surrounding conditions, specifically from temperature and pressure (P_{total}). Additionally, the quantity x_j has the same unit as the majority of traceable reference material values in gas analysis used for calibration purposes.

2.2.2 Linestrength

For the quantification of the absorption capacity of a single molecular absorption line the use of the term linestrength is preferred instead of the more general term line intensity. Several non SI-units for the linestrength are unfortunately still being used (e. g. $cm^{-2} \cdot atm^{-1}$) in communicating scientific results, despite the wide international acceptance of the SI of units. Thus, $cm^{-1} \cdot molecule^{-1} \cdot cm^2$ is the preferred unit, because it is compatible with the SI, avoiding the use of non SI units and conversion factors, and allowing by this an easier understanding and comparison of results.

Radiative transfer theory for a two states of a vibrational-rotational system delivers the definition of the spectral linestrength

$$S_i(T_{ref}) = \frac{8 \cdot \pi^3}{3 \cdot h \cdot c} \cdot \nu_{0,i} \cdot \frac{I_a \cdot g'' \cdot \exp\left(-c_2 \cdot E''_i / T_{ref}\right)}{Q(T_{ref})} \cdot \left[1 - \exp\left(-\frac{c_2 \cdot \nu_{0,i}}{T_{ref}}\right)\right] \cdot \Re_i \cdot 10^{-36} \tag{2.19}$$

The deduction of (2.19) is presented in [57]. In (2.19) S_i is the linestrength for the transition i at the reference temperature T_{ref} , h is the Planck constant, c is the speed of light in vacuum, $\nu_{0,i}$ is the spectral transition frequency, I_a is the natural terrestrial isotopic abundance, c_2 is the second radiation constant = $h \cdot c / k_B$, E''_i is the lower state energy for the transition i. $\Re_i$ is the weighted transition-moment squared and *g"* the *state statistical weight* in the absorbing state. The weight includes electronic, vibrational, rotational, and nuclear statistics. $\Re_i$ is independent of both temperature and isotopic abundance and can therefore be considered the real molecular property [57].

The term $\exp(-c_2 \cdot E''_i / T_{ref})$ in (2.19) accounts for the ratio of Boltzmann populations, and the fourth term on the right for the effect of stimulated emission. Equation (2.19)

makes evident that the linestrength of an absorption transition depends on the population in the lower quantum state, which is a function of the Boltzmann fraction, and the probability of the transition, which depends on the specific spectroscopic constants associated with that molecule's particular transition.

Two preconditions are important when using (2.19). First, when local thermodynamic equilibrium is assumed, the population partition between states is governed by the Boltzmann statistic. Second, the linestrength is weighted according to the natural terrestrial isotopic abundances given in [57]. When this natural isotope mixture is changed, this weight must be renormalized.

Since the linestrength depends on the Boltzmann fraction of molecules in the absorbing (or lower quantum) state, the linestrength is a function of temperature. Thus, it has to be referred to a reference temperature T_{ref}. In order to facilitate the comparison of results, this temperature was chosen here to be 296 K, the same like the one of the HITRAN database, following called $T_0 = T_{ref}$.

The linestrength $S_i(T)$ for a particular transition i at temperature T can be converted from the ratio of linestrengths with (2.19) at temperature T and T_0, rendering the following equation,

$$S_i(T) = S_i(T_0) \cdot \frac{Q(T_0)}{Q(T)} \cdot \exp\left[-\frac{h \cdot c \cdot E''_i}{k_B} \cdot \left(\frac{1}{T} - \frac{1}{T_0} \right) \right] \cdot \left[1 - \exp\left(\frac{h \cdot c \cdot \nu_{0,i}}{k_B \cdot T} \right) \right] \cdot \left[1 - \exp\left(\frac{h \cdot c \cdot \nu_{0,i}}{k_B \cdot T_0} \right) \right]^{-1} \quad (2.20)$$

In (2.20), the total internal partition function is calculated from (2.10).

2.2.3 Spectral Line shapes

Due to Heisenberg's uncertainty principle, the energy uncertainties of the upper and lower energy levels of a transition i at central transition wavelength $\lambda_{0,i}$ produce a line of finite width called "natural line width" of Gaussian line shape. Typical *line shape functions* of an isolated absorption line are shown e. g. in Figure 2.3. The frequency interval at which the intensity is half the maximum is the *full width at half-maximum* (FWHM), called more briefly linewidth or half-width. The term *half width at half maximum* (HWHM) is also used in many references, thus, clearance of using full- or half- width is often needed. In this work FWHM is used.

A line shape function $\phi(\lambda)$ reflects the relative variation in the absorption coefficient with wavelength around a transition i centered at $\lambda_{0,i}$. When $\phi(\lambda)$ is normalized, the wavelength integrated value is equal to unity

$$\int_{\lambda} \phi d\lambda = 1 \quad (2.21).$$

The line shape function $\phi(\lambda, T, P, x_B)$ introduced in (2.12) is in general a function of the wavelength, temperature, total pressure and perturber x_B (matrix or medium surrounding the gas specie).

Several broadening mechanisms influence the line shape of an absorption line in gas phase. They are due to phenomena in the medium that perturb the energy levels of the transition or the way in which individual atoms or molecules interact with light. For measurement conditions at or below the normal atmospheric pressure, there are three major mechanisms that might contribute to the shapes of infrared absorption lines: 1) Doppler broadening, 2) Collisional broadening and 3) Collisional narrowing.

2.2.3.1 Doppler Broadening

The Doppler effect is due to the thermal motion of the absorbing molecules. It is an inhomogeneous effect because the probability of transition of absorption is not equal for all the molecules of a certain gas species. It depends on the velocity component class of the random motion of molecules described by a Maxwellian velocity distribution function. When the molecule has a velocity component in the propagation direction of a beam of light, a shift in the absorption frequency is observed. This effect is called the Doppler shift.

The Doppler half-width (FWHM) is then given by,

$$\Delta\tilde{\nu}_{\mathrm{D}} = 2\cdot\tilde{\nu}_0\cdot\left(\frac{2\cdot k_{\mathrm{B}}\cdot T\cdot\ln 2}{m\cdot c^2}\right)^{1/2} \tag{2.22}$$

The distribution of the Doppler shift (or half-width) renders a Gaussian line shape, which is described by the function,

$$\phi_{\mathrm{D}}(\tilde{\nu}) = \frac{2}{\Delta\tilde{\nu}_{\mathrm{D}}}\cdot\left(\frac{\ln 2}{\pi}\right)^{1/2}\cdot\exp\left\{-4\cdot\ln 2\cdot\left(\frac{\tilde{\nu}-\tilde{\nu}_0}{\Delta\tilde{\nu}_{\mathrm{D}}}\right)^2\right\} \tag{2.23}$$

For most ambient gases at ambient temperatures and pressures below 2 kPa [63], the line shape is dominated by the Doppler effect.

2.2.3.2 Collisional Broadening

Interaction between particles (molecules, atoms, etc.) leads to collisional broadening. This is due to energy shifts of the excited state and a resulting decrease of the lifetimes. The line shape for collisional broadening has the form of a Lorentzian function

$$\phi_{\mathrm{C}}(\tilde{\nu}) = \frac{1}{2\cdot\pi}\cdot\frac{\Delta\tilde{\nu}_{\mathrm{C}}}{(\tilde{\nu}-\tilde{\nu}_0)^2+(\Delta\tilde{\nu}_{\mathrm{C}}/2)^2} \tag{2.24}$$

with the wavenumber difference $\Delta\tilde{\nu}_{\mathrm{C}}$ being the Lorentz line shape's half-width (FWHM). This collisional half-width - for the interrogated species A - is often modelled as the product of the system pressure and the sum of the amount of substance fraction for each perturber species B multiplied with its species-dependent *collisional broadening coefficient* $\gamma_{\mathrm{A\text{-}B}}$

$$\Delta\tilde{\nu}_C = P \cdot \sum_B x_B \cdot 2 \cdot \gamma_{A-B} \qquad (2.25).$$

The notation for the different broadening coefficients is $\gamma_{A\text{-}B}$, where A is the molecule whose line shape is being studied and B is the collision partner (or perturber) that interacts with species A to broaden its absorption line. Thus, $\gamma_{CO_2-CO_2}$ is the broadening coefficient for CO_2-CO_2 collisions (self-broadening, γ_{self}), and $\gamma_{CO_2-N_2}$ is the coefficient for CO_2 line shape broadening due to collisions with N_2 (nitrogen-broadening). Averaged O_2 and N_2 coefficients are contained in air-broadening coefficients, γ_{Air}. Values of $\gamma_{A\text{-}B}$ are determined experimentally and are published for specific transitions and specific collision partners.

Figure 2.3 compares a Gaussian and a Lorentzian normalized line shape with areas equal to unity. In addition, the line shapes have the same half-width. In order to cover most of the peak area (approx. 99.73 %) by an integration, at least an interval of $\pm\ 3{\cdot}\Delta\nu_D$ is necessary for the Gauss profile. To get the same coverage for the Lorentz profile even $\pm\ 9{\cdot}\Delta\nu_D$ is needed.

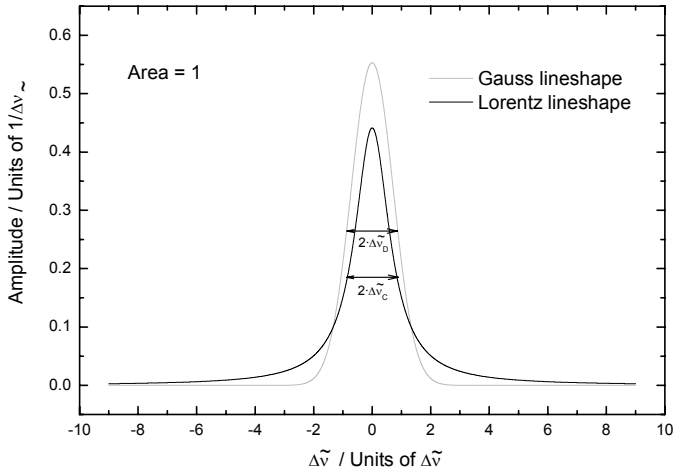

Figure 2.3: Comparison of Gauss & Lorentzian line shapes with the same half-width.

2.2.3.3 Voigt Profile

When both broadening mechanisms are present, the intensity profile is given by a convolution of the Lorentzian and Gaussian line shapes, called Voigt profile.

There is not a closed-form expression for the Voigt profile. Rather, the Voigt line shape function is given by the integral convolution expression of the Doppler effect and the pressure broadening

$$\phi_V(\tilde{\nu}) = \int_{-\infty}^{+\infty} \phi_D(\tilde{u}) \cdot \phi_C(\tilde{\nu} - \tilde{u}) \cdot d\tilde{u} \qquad (2.26)$$

Various approximations of that integral [64, 65] and new improvements have been recently proposed [66, 67, 68]. The Voigt fit used here was that from Origin®. It has the form

$$\phi_V(\tilde{\nu}) = \frac{2\cdot\ln(2)}{\pi^{3/2}}\cdot\frac{\Delta\tilde{\nu}_C}{\Delta\tilde{\nu}_D{}^2}\cdot\int_{-\infty}^{+\infty}\frac{e^{-t^2}}{\left(\sqrt{\ln(2)}\cdot\frac{\Delta\tilde{\nu}_C}{\Delta\tilde{\nu}_D}\right)^2+\left(\sqrt{4\cdot\ln(2)}\cdot\frac{\tilde{\nu}-\tilde{\nu}_0}{\Delta\tilde{\nu}_D}-t\right)}\cdot dt \qquad (2.27)$$

where *t* is an integral variable defined as

$$t = \frac{2\cdot\sqrt{\ln(2)}\cdot\tilde{u}}{\Delta\tilde{\nu}_D} \qquad (2.28)$$

and $\sqrt{\ln(2)}\cdot\Delta\tilde{\nu}_C/\Delta\tilde{\nu}_D$ which is called the damping constant a. This a is the Voigt parameter that indicates the relative significance of Doppler and collisional broadening, with a increasing as the effect of collisional broadening increase.

2.2.3.4 Collisional Narrowing

Collisional narrowing (or Dicke narrowing) has the effect of reducing the size of the Gaussian linewidth. In other words, it makes the line appear to have a Doppler half-width that is smaller than that calculated by (2.22). Collisional narrowing is primarily a kinetic collisional effect sometimes described in terms of hard and soft collision models. Consideration of collisional narrowing produces at least two other refined lineprofile models, namely the Rautian-Sobelman (hard-collision model) and the Galatry (soft-collision model) [48, 69] and refined theories of line shapes [49].

2.3 Metrological Bases

The expression of measurement results in the international system (SI) of units is - unfortunately - not yet a common practice in science. That makes it difficult to compare the results of measurements, because they are referred and expressed in different measurement scales [70]. A simple conversion to SI Units is not sufficient. Instead, the concept of Metrology requires that all significant quantities are measured in a reliable relation to the SI units.

The Consultative Committee for Amount of Substance (CCQM) was set up in 1993. It advices the International Committee for Weights and Measures (CIPM) on matters related to the accuracy and comparability of chemical measurements [71]. CIPM is the scientific and legal guardian of the SI units, including that for *amount of substance*: the mole. CCQM's present activities concern *primary methods* for measuring amount of substance, international comparisons and establishment of *international equivalence* between national laboratories [72]. The CCQM is involved in measurements of analytes of key sectors, which demand improved reliability in measurements in chemistry due to powerful commercial and public pressures. Between these sectors are: environmental monitoring, international trade in food and drugs, clinical practice, human health and safety, forensic medicine, advanced materials research, and energy [73].

2.3.1 Traceability

One of the most important concepts in metrology is that of the *traceability of measurement results*. It summarizes the sense of existence of metrology. That is to achieve the comparability of measurement results by means of traceability chains, which link them with the SI units or an internationally recognized reference. An example of a traceability chain for field measurements in gas analysis is shown in Figure 2.4. There, a number of 4 links (double arrows) are provided starting by the material realization of the SI unit of the kilogram and ending in the field measurement value supported by the units in which the result is expressed. These units are e. g. mol and kg, in the amount of substance fraction mol/mol or the mass fraction kg/kg. For the fundamental link up with the mol unit are used: the Avogadro constant (N_A), consequently the value of the molar mass in the periodic table, the identity and the purity of the substance. The first link in the traceability chain relies on the use of a *primary method* of measurement. The next 2 links of comparison measurements are done with the purpose of increase the availability of calibration gas mixtures. In these steps are involved the national metrology institute, reference laboratories and finally in the fourth link the users. The given uncertainties (U) are only presented as approximations.

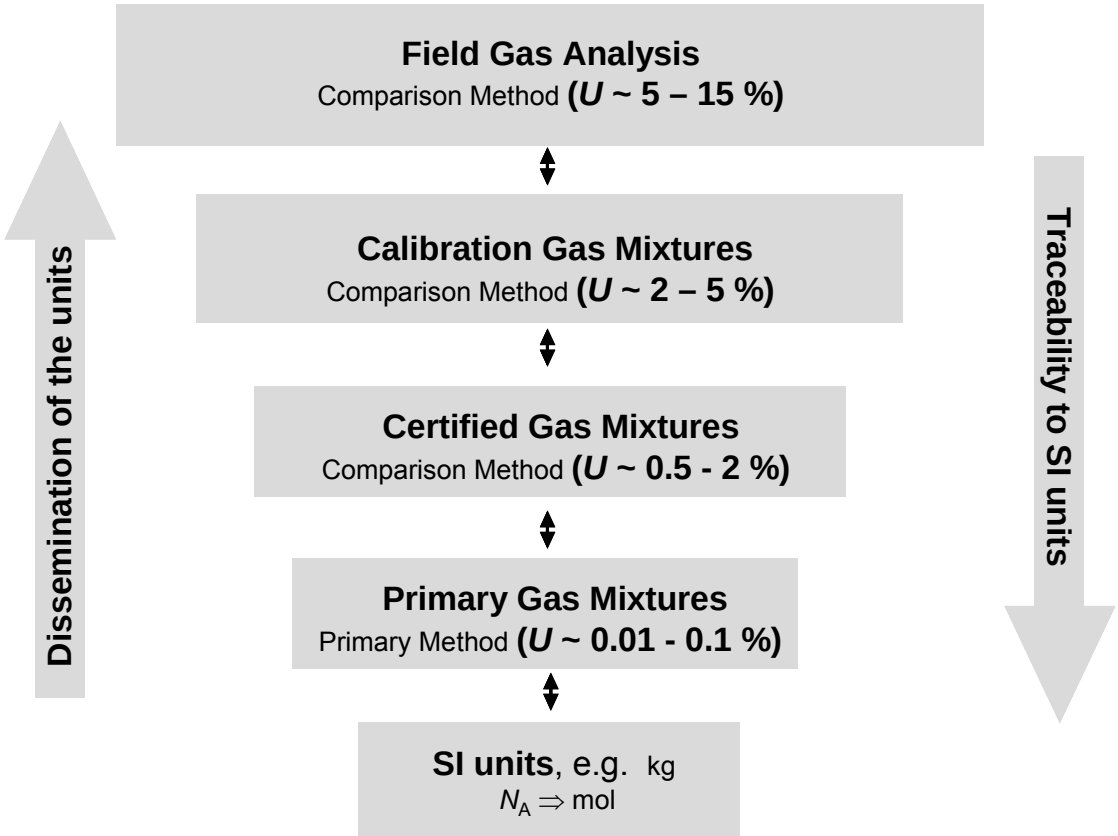

Figure 2.4: Traceability chain for gas analysis. The traditional scheme for static gas mixtures (certified reference materials) is shown. The kind of method involved is generally described. The percent relative uncertainty (U) is shown. The traceability chain is used to support the reliable unbroken comparison to the SI units of field measurement results.

Traceability is defined as the property of the result of a measurement or the value of a standard whereby it can be related to *stated references*, usually *national or*

international standards, through an *unbroken chain of comparisons* all having *stated uncertainties* [74]. At least three key elements are identified in this definition to be necessary for establishing traceable measurement results: a) use of stated references, b) an unbroken chain of comparisons starting from the realization of SI units towards the measurement in question and c) an uncertainty statement for each comparison.

It has been identified 4 routes that can be followed for the establishment of traceability of chemical measurement results [40]. In the case of gas analysis examples of the applied references and methods are presented in Figure 2.5. The first route in this figure is that of the use of a certified gas mixture (use of a reference material), which was already described (Figure 2.4). The second route involves the use of reference points, this is the case of some reliable reference data - traceable FTIR spectra for hazardous air pollutants (HAP) [75]- , and reference instrumentation - standard reference photometer (SRP) to quantify ozone in ambient air [40] -. The third route is the use of reference measurements which is mainly dedicated to measurements performed by highly experienced laboratories - as examples of this called references laboratories at the highest metrological level are the Institute for Reference Materials and Measurements IRMM [76] and the Bureau International des Poids et Mesures (BIPM) laboratory of gas metrology [77] -. The fourth route is that of interest of this work. It is the use of primary methods directly applied to field (or *in-situ*) gas analysis. All the four routes involve the use of *primary methods*. Some *potential primary methods* are also depicted in the same picture. By mean of this methods the link to the SI unit can be realized. Normally primary methods in chemistry are very complex and costly and therefore, mainly used in National Metrology Institutes (NMIs). The direct use of a primary method as shown in this work is an exception, however, involving very important advantages.

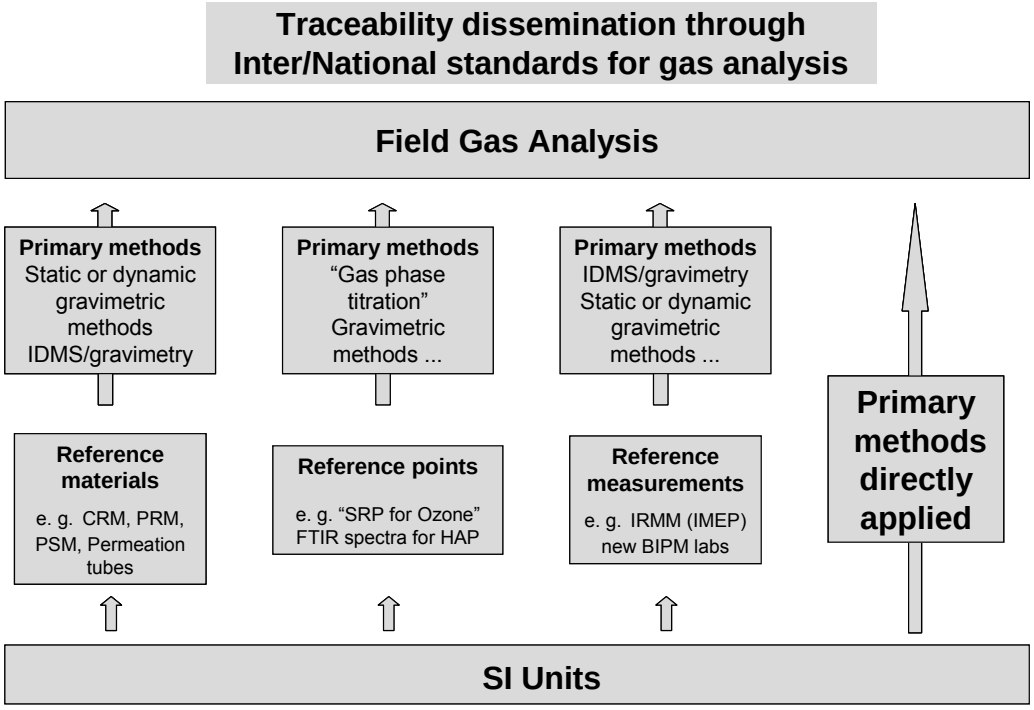

Figure 2.5: International measurement standards for gas analysis.

This primary method directly applied acquires a huge importance for methods with the potential of being applied to field measurements, such as in the case of TDLAS. The definition of a primary method of measurement in Chemistry has been extensively discussed [38, 78-80]. It means basically that the measurement equation does not depend from a measurement standard (reference material) of the same substance (or of any other substance) being measured, that the measurement method must be completely understood, and that all influence quantities [74] are traced back to the SI units. The use of empirical constants or fits of models to data whose accuracy cannot be proved in the measurement equation should be avoided [81].

2.3.2 International Standards of Measurements

In gas analysis and in most of the metrology in chemistry applications, a certified reference material (here a certified gas mixture) constitutes the standard of measurement. Some exceptions are the use of reference points e. g. the ozone photometer [40] and some reference data e. g. [75]. Reference gas mixtures spans from purity gases until low level amount of substance values of binary and multi-component gas mixtures. They can be prepared statically or dynamically. One of the most extended preparation methods is the static method, particularly by gravimetry, because when it is correctly applied it renders low uncertainties and traceability to the SI units. The kind of references used in gas analysis was already presented in Figure 2.5.

2.3.3 Uncertainty of Measurements

The uncertainty of a measurement result is defined in the international vocabulary of metrology VIM [74] as a parameter, associated with the result of a measurement, that characterises the dispersion of the values that could reasonably be attributed to the measurand. With the appliance of the traceability concept, it can be said that the uncertainty of measurement is the interval of values where the “conventional value” could reliably be found. The most extended and internationally accepted method for the estimation and expression of measurement uncertainty (GUM) is that of [46]. In order to differentiate the GUM compliant uncertainty claims from other rough estimations of uncertainty, adjectives like *complete* or *transparent* are sometimes added to the term uncertainty budget. One important necessity for the complete estimation of measurement uncertainty at any metrological level is the use (if possible) of SI-traceable measurement results for all influence quantities. A traceability chain is a priori requirement for evaluating the uncertainty budget of a measurement result [39].

The GUM method can be applied to all kinds of measurements and to all types of input data. This universality makes it the ideal method for evaluating and expressing the uncertainty of a measurement result [46]. The GUM-compatible uncertainty is:

- *internally consistent*: it is directly derivable from the components that contribute to it and is independent of how these components are grouped and of the decomposition of the components into subcomponents,

- *transferable*: it allows to use directly the uncertainty evaluated for one result as a component in evaluating the uncertainty of another measurement in which the first result is used,

- *probabilistic approachable*: it has an interval with a coverage probability or level of confidence.

The goal of the GUM is to promote full information on how *uncertainty statements* are derived and to provide a basis for the *comparison of measurement results* [46].

The method of the GUM has been extensively described. Therefore, for general understanding of the method only a brief description of it is given here. Those interested can be remitted to the reference document [46].

The GUM is based on the concept of a measurement equation. In most cases a *measurand f* - it means, the particular quantity being measured [74] - is not measured directly but is determined from other input quantities x_1, x_2, … x_n through a functional relationship g

$$f = g(x_1, x_2, \ldots, x_n) \tag{2.29}$$

The relationship g may be explicitly written down or determined experimentally or exist only as an algorithm that must be evaluated numerically [46]. The function g should contain every quantity, including all corrections and corrections factors, that can contribute a significant component of uncertainty to the result of the measurement.

Generally, several input quantities may contribute to the uncertainty of a measurement, according to their respective uncertainties. Regarding the method the numerical value of the uncertainty of an input quantity is estimated, input uncertainties are divided into two groups

type A: those, which are evaluated by statistical methods,

type B: those, which are evaluated by other means.

The method consist basically in the estimation of standard uncertainties $u(x_i)$ by statistical calculation - for type A estimation of uncertainty given as an standard deviation of the mean -, or by reduction of uncertainties - in type B estimation of uncertainty - using the known or assumed probability density functions (PDFs) of the input quantities. The PDFs are models that represent the - for the measurement - state of knowledge of the quantity.

Standard uncertainties are combined using the *law of propagation of uncertainty*. A convenient form of this law from equation 13 and 15 of [46] is

$$u_c^2(f) = \sum_{i=1}^{N} \left(\frac{\partial f}{\partial x_i} \right)^2 \cdot u^2(x_i) + 2 \sum_{i=1}^{N-1} \sum_{j=1}^{N} \left(\frac{\partial f}{\partial x_i} \right) \cdot \left(\frac{\partial f}{\partial x_j} \right) \cdot u(x_i) \cdot u(x_j) \cdot r(x_i, x_j) \tag{2.30}$$

here, $u_c(f)$ is the combined uncertainty and $\partial f / \partial x_{i \text{ or } j}$ are the sensitivity coefficients. The second term of (2.30) represents the correlation - if exists - between the influence quantities x_i, x_j, and $r(x_i, x_j)$ is the correlation coefficient given by

$$r(x_i, x_j) = \frac{u(x_i, x_j)}{u(x_i) \cdot u(x_j)} \tag{2.31}$$

where $u(x_i, x_j)$ is the covariance between x_i and x_j.

Covariance can be described as the relationship between two input quantities [82]. It can be calculated with

$$u(x_i, x_j) = \frac{1}{n-1} \cdot \sum_{k=1}^{N} (x_{ki} - \bar{x}_i) \cdot (x_{kj} - \bar{x}_j) \tag{2.32}$$

The combined uncertainty is multiplied by a coverage factor k to obtain an overall uncertainty called the expanded uncertainty $U(f)$ with an associated probability of finding the *conventional value* in that interval. The expanded uncertainty is given by

$$U = k \cdot u_c(f) \tag{2.33}.$$

To determine the coverage factor of the combined uncertainty, at first the effective degrees of freedom ν_{eff} have to be calculated from the Welch-Satterthwaite formula

$$\nu_{eff} = \frac{u_c^4(f)}{\sum_{m=1}^{N} \frac{u^4(x_m)}{\nu_m}} \tag{2.34}$$

where ν_m are the degrees of freedom of each influence quantity x_m.

The coverage factor k is obtained by

$$k = t_p(\nu_{eff}) \tag{2.35}$$

from the *t*-distribution table for the calculated ν_{eff} and the required level of confidence p.

The expanded uncertainty, the coverage factor and the level of confidence are normally part of the report for uncertainty budgets that fulfill the GUM.

2.3.4 Bias and Uncertainty: Criteria for Validation and Performance

The method used in this work called "*absolute*" or "*free-of-calibration*" and can be reserved as a method that has the potential to be a primary method directly applied, because it does not need a calibration by means of references of the analyte. In this thesis *absolute* or *free-of-calibration* terms are used interchangeably to denote the same meaning.

The method uses molecular specific parameters (linestrength of the absorption line) for the calculation of the concentration of molecules. This has a lot of advantages – already mentioned in the introduction (s. 1) – for the practical use of the method involving a certain form of verification. However, one has to be aware that the measurement of the molecular specific parameter comprises the calibration procedure. Furthermore, the measurement uncertainty achieved here does hardly fulfill all the requirements of a potential primary method of measurement (PMM), specially the requirement of having the highest metrological qualities [78] - meaning a low uncertainty of measurement [79] - already showed by any other PMM [38] for the same gas specie and matrix, e. g. as gravimetric preparation or as isotope dilution mass spectrometry (IDMS) applied to gas analysis [35-37, 83]. These low uncertainties have been proved in laboratory conditions, e. g. for the certification of reference gas mixtures; but such methods are not appropriate for field measurements, where the uncertainties will have uncertainties of the same magnitude order as those obtained for long traceability chains. A useful magnitude order of uncertainty for TDLAS would give it all the potential to be a PMM directly applied.

An important property of a PMM is that it is able to produce unbiased measurement results [38]. It means, it is able to produce reliable values of measurands. If TDLAS performs free of calibration (absolute performance), it has to produce also unbiased measurement results. This should be proved by comparison with another primary method [38]. The other primary method used here is gravimetry.

The gravimetric preparation of gas mixtures produces independent values based in the mass values of weighed high pure gases. The mass values are converted to amount of substance fraction by means of the knowledge of molar masses and composition of the pure gases or parent gases. This is carried out by use of the next expression

$$x_j = \frac{\sum_{A=1}^{P} \frac{m_A x_{jA}}{\sum_{j=1}^{n} x_{jA} M_j}}{\sum_{A=1}^{P} \frac{m_A}{\sum_{j=1}^{n} x_{jA} M_j}} \tag{2.36}$$

where:

x_j is the amount of substance fraction of the component j in the final mixture,
P is the total number of parent gases,
n is the total number of components in the final mixture,
m_A is the mass of the parent gas A determined by weighing,
x_{jA} is the amount of substance fraction of the component j in parent gas A,
M_j is the molar mass of the component j.

The gas mixtures used here were prepared gravimetrically (s. 3.3). The resulting amounts of CO_2 fractions measured by TDLAS were therefore compared with the respective gravimetric values. The comparison has to be done considering the corresponding individual uncertainties of both values.

The criteria to verify the absolute performance of a method needs a definition of *bias* for understanding the existence of biased or unbiased measurement results. The standard ISO 5725-1 defines *bias* as the difference between the expectation of the *test results* and *an accepted reference value* [84]. This is the *bias* definition used here. "*Real" bias* is here used to denote when the test results are not concordant with the reference value within the uncertainties. *Apparent bias* is when test results are concordant within uncertainties, but the mean value of test results differs from the reference value.

An additional definition needed is that of a *test result*. In terms of ISO 5725-1, it is the result of carrying out a specific test method, and it is valid to one as also to a number of individual observations. As the purpose of this work is limited to the performance of a method, the definition of *test result* is only limited to several or a large series of *test results* in order to have the trueness of the method. This trueness is expressed as the bias of the method.

In this work, bias is presented in percent relative bias by

$$Bias\,/\,\% = \left(\frac{x_{\mathrm{TDLAS}} - x_{\mathrm{Grav.}}}{x_{\mathrm{Grav.}}} \right) \cdot 100 \qquad (2.37),$$

where the laser spectroscopy values of amount of CO_2 fraction (x_{TDLAS}) are compared with those of the reference values, derived from gravimetric based values ($x_{\mathrm{Grav.}}$).

3 Measurement Systems

This chapter describes the measurement systems and their associated instrumentation used to determine amount of CO_2 fraction values employing TDLAS (3.1), respective linestrength measurements (3.2) and gravimetric amount of CO_2 fraction values (3.3).

3.1 TDLA Spectrometer for Amount of Substance Fraction Measurements

The setup of the optical absorption spectrometer for gas analysis consists of three components: the radiation source (3.1.1), the gas absorption cell (3.1.2) and the detection system (3.1.3). Peripheral instruments described in 3.1.4 are also needed for operation and the controlling of the system.

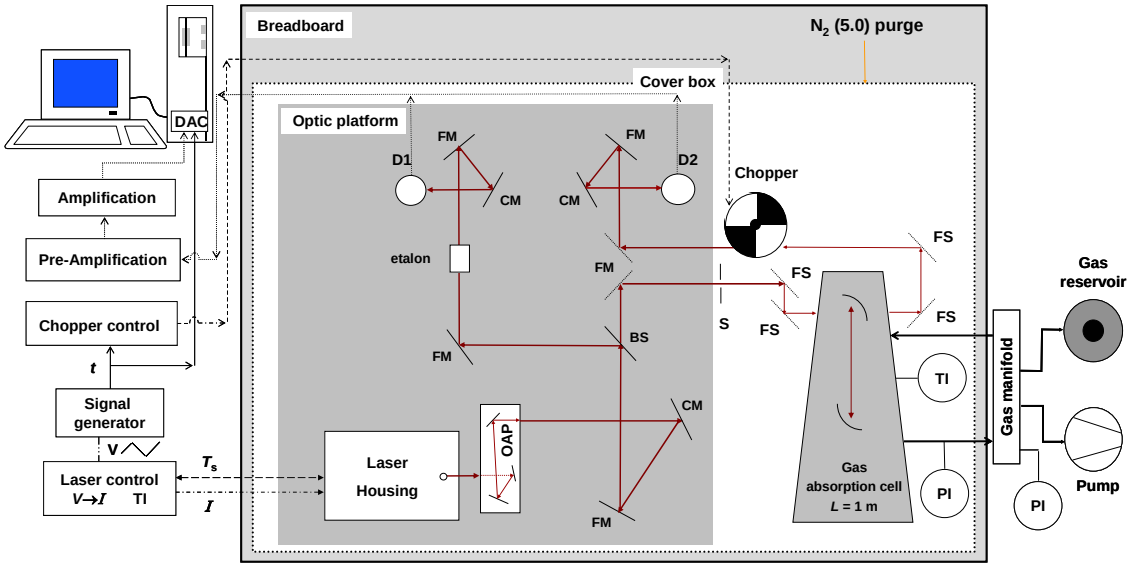

Figure 3.1: Spectrometer setup. OAP: off-axis parabolic mirror, FM: flat gold mirror, CM: concave mirror, FS: flat silver mirror, BS: beam splitter, S: iris, TI: temperature indicator, PI: pressure indicator, D1 and D2: detectors, DAC: digital-analogical converter, *t*: trigger, T_s: laser substrate temperature, *I*: current, V: voltage.

Figure 3.1 depicts the basic setup of the tuneable diode laser absorption spectrometer. The optical components of the spectrometer are mounted to an optical table with a breadboard (Newport, model M-RPR-46-8). For easiness of interchange between different parts, the measurement system is designed in modules. An optic platform on the breadboard is used for: collimation of the laser beam, separation in two measurement beams and detection. The laser beam is collimated by 1 off-axis parabolic mirror (f=100 mm, alfa = 26.375°) and separated in two beams by a splitter. One beam is used as reference signal to measure the initial intensity of the laser, or as frequency marker beam by means of a removable solid Si-etalon. The other beam is directed through the absorption cell to measure the absorption of the gas sample.

3.1.1 Radiation Source

The TDLA- spectrometer is equipped with a continuous wave (cw), thermoelectrically cooled, distributed-feedback (DFB) tuneable GaInSbAs diode laser (TDL) emitting around 2.004 μm (Nanoplus, model 057/4-15). To operate the laser a certain laser current has to be applied and the laser temperature has to be controlled. The current-temperature combination determines the emission wavelength. Specification for the tuning range of 0.26 nm/°C is given. The laser controller, the laser housing (s. Figure 3.1) and the thermoelectric cooling were home made (PTB).

For reliable calibration-free gas analysis the laser has to be tuneable, single-mode and narrow line width. In order to assure high selectivity and sensitivity therefore, the laser source has to be properly characterized prior to use in gas analysis.

The spectral characterization of the laser emission was performed using high-resolution Fourier Transform Infrared (FTIR) Spectroscopy. The laser radiation was coupled to an IFS-120 HR Bruker as external light source. The IFS-120 HR has a maximum resolution of 0.0021 cm^{-1}. Although the laser line width itself is much smaller, mode charts and single-mode operation can be proved by FTIR. Measuring the respective FTIR-spectra for each current-temperature combination and subsequently folding them together the emission characteristic shown in Figure 3.2 was obtained. Mode charts were measured with a fixed laser temperature for laser currents varying between the threshold current of 30 mA and a maximum current of 48 mA (Figure 3.2a). This figure shows that the laser power increases as the laser current increases. The change of wavenumber with current applied to the laser was estimated to be 0.03 cm^{-1}/mA. Complementary measurements were carried out to determine the temperature tuning of the laser for a fixed laser current. The overall tuneability of the laser is shown in Figure 3.2b. There, by varying the laser temperature between 18.00 and 29.85 °C a spectral bandwidth of 4.5 cm^{-1} could be covered. These measurements were performed with a reduced FTIR resolution of 0.006 cm^{-1}, therefore, the changes in intensity of the laser spectra in this figure are attributed to insufficient FTIR resolution. An average value for temperature laser tuning was found to be 0.38 cm^{-1}/K.

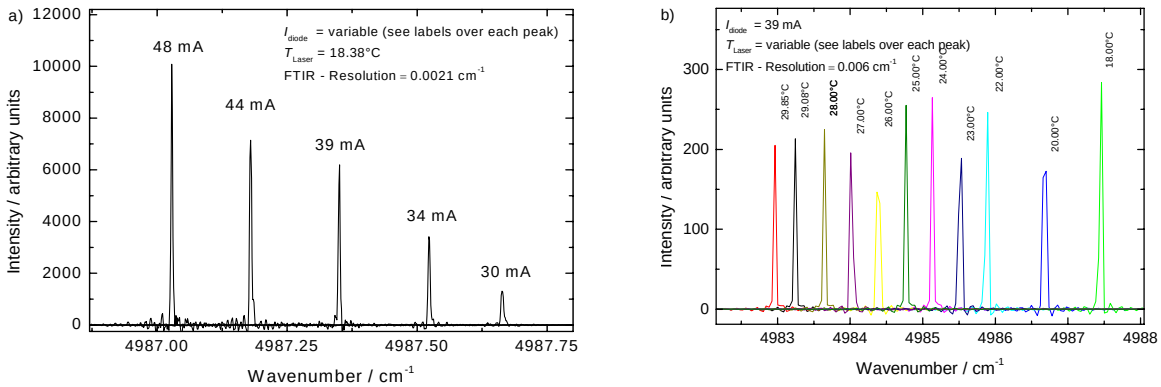

Figure 3.2: Mode charts of laser emission spectrum. a) Varying current. b) Varying temperature.

By applying the maximum FTIR resolution, the laser emission shown in Figure 3.3 was measured. As it can be seen in Figure 3.3a the laser is single-mode confirmed by the absence of any other emission line within the wide investigated frequency interval. The manufacturer-specified side-mode-suppression ratio of >30 dB was verified by this kind of FTIR measurements. By applying a Gauss fit to the measured laser emission spectrum of Figure 3.3b, a laser emission line width (FWHM, W in this figure) $\leq$ 0.00336 cm^{-1} was obtained. This measurement of the laser line width confirmed the manufacturer line width specification of <100 MHz (0.0033 cm^{-1}). The sample points in Figure 3.3b show that, despite the high-resolution available by the FTIR IFS-120, the width of the measured laser line is limited by the resolution of the FTIR. The maximum resolution of this instrument is nearly 5 times smaller than the Doppler width of carbon dioxide lines around 4987 cm^{-1} having a value of ~ 0.009 cm^{-1} at 296 K. Thus, the laser line width is much smaller than that of the CO_2 lines ensuring the laser can be used to perform Doppler-limited spectroscopy.

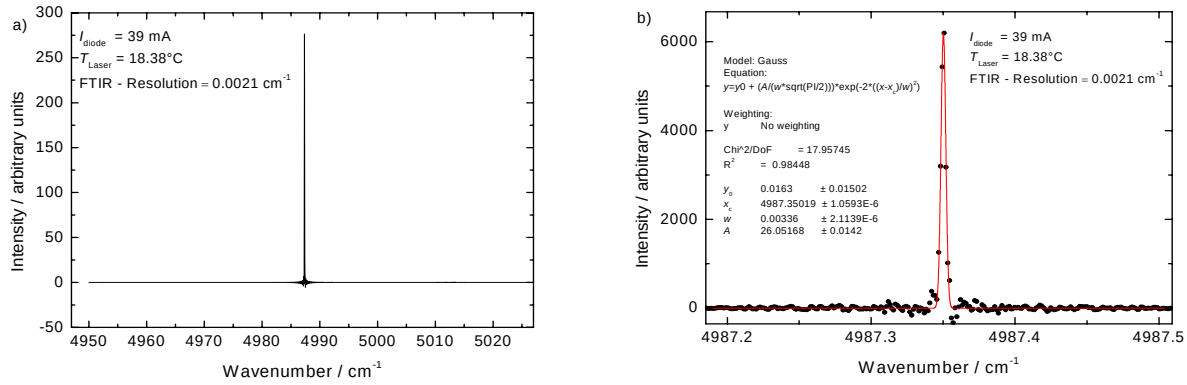

Figure 3.3: FTIR spectrum of the DFB-Laser for fixed *T* and *I*. a) Wide scanned frequency interval. b) Frequency interval around sweep depth.

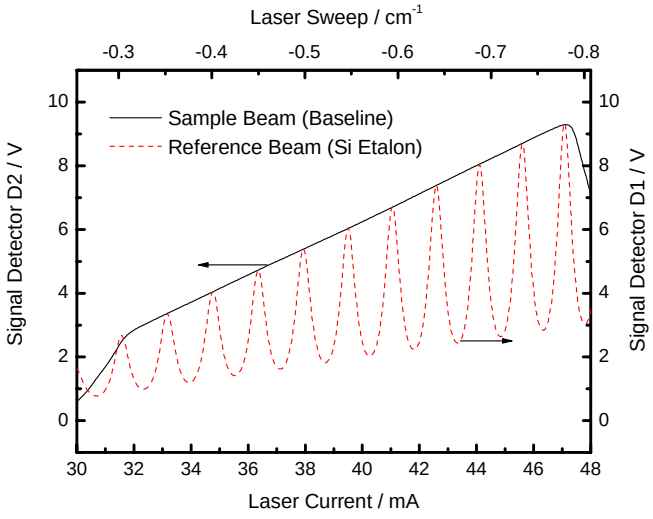

Figure 3.4: Typical laser tuning behavior.

In order to be used for the gas analysis measurements the laser has to be tuned over a molecular absorption line. Laser tuning can be achieved by temperature or current modulation (Figure 3.2). Due to its higher modulation rate, current tuning was preferred. By adjusting the laser temperature manually the start wavelength was fixed. Subsequently the laser current was modulated applying a triangular modulation signal to the modulation input port of the laser controller. The 5 Hz modulation signal was generated by a signal generator (Agilent, model 33120A) whose synchronously generated TTL-output signal served as master-clock for the whole data acquisition (s. 3.1.3). The sweep interval governed by the amplitude of the current modulation was adapted to the width of the CO_2-line. In Figure 3.4 a typical tuning behavior is shown. Given the current modulation amplitude of 18 mA, a sweep interval of 0.55 cm^{-1} could be monitored. The wavenumber sweep is seen in Figure 3.4 as the number of maxima in the signal response of detector D1. That corresponds to the transmission of an Si-etalon placed in the reference beam. Due to the known free-spectral range (FSR ~ 0.05 cm^{-1}) of the etalon the wavenumber sweep of the laser can be determined from the number of fringes in the etalon transmission signal. A current increase is directly proportional to the laser power because more electrical power produces more optical power. The negative wavenumber scale in Figure 3.4 is because an increase in current produces more heat and as a result of the increased temperature or current, the emission wavelength increases - the wavenumber sweep has a negative direction - (s. Figure 3.2b).

3.1.2 Gas Absorption Cell

A multi-reflection gas cell (Figure 3.5) with a total pathlength of 1 m was used (Perkin-Elmer 127-00611). The cell body is constructed of cast aluminium equipped with chrome plated brass fittings. Neoprene rubber is used for gasket material. The gas cell has a gas sample input and a gas sample output connected to the gas manifold as shown in Figure 3.1. The output serves for connecting the pressure sensor. The maximum rate of leakage specification for the cell is < 0.2 Pa/min.

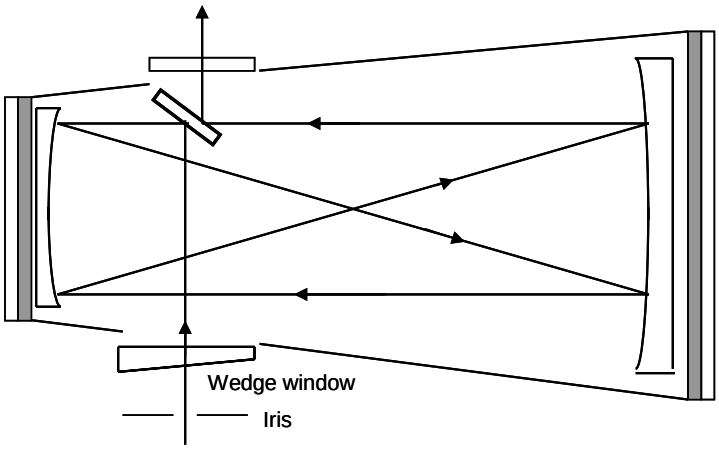

Figure 3.5: Gas absorption cell.

In front of the entrance window of the gas absorption cell, the light beam diameter is controlled by an iris (s. Figure 3.5 or 3.1). It is used to control the light “leakage” due to radiation not following the total pathlength of the gas cell (s. Figure 3.5). To avoid this effect an aperture diameter of the iris of 0.8 cm was used.

3.1.3 Detection and Data Acquisition System

Each measurement beam terminated into an extended indium-gallium-arsenide (XInGaAs) photo detector (Laser components, model J18-18I-R01M-2.2). The electrical signals coming from the detectors (D1 and D2 in Figure 3.1) are first electronically conditioned by individual preamplifiers and amplifiers. The amplifiers have the capability to adjust the gain and the offset of each input signal (S_{in}) according to

$$S_{out} = \text{gain} \cdot (S_{in} + \text{offset}) \qquad (3.1).$$

The amplified signals were sent to a data acquisition card (DAC). The DAC (ADLINK technology Inc, model PCI-9114-DG) had a programmable range (± 10 V, ± 5.0 V, ± 2.5 V, ± 1.25 V) with a maximum acquisition speed of 100 kHz and a vertical resolution of 16 bit. The DAC is controlled by an in-house software developed in Visual Basic 6.0. The software allows displaying and saving the signals of both detectors in a batch or continuous way, including the storage of signals for a multiple scan average.

A variable speed light beam chopper (HMS, model 221) shown in Figure 3.1, was used to measure the background when the laser beam is blocked. The chopper wheel rotation was phase-locked to the TTL-output trigger signal and by this synchronized with the DAC.

3.1.4 Peripheral Instrumentation of the Measurement System

For the conversion from time or sample point (SP) units - resulting from the digitization by the DAC - to the wavenumber domain (cm^{-1}), a calibration of the relative wavenumber-scale was done by a Si-etalon of 29.90 mm length. The etalon was mounted in a base that can be screwed to the optic platform (Figure 3.1). Fixing the etalon in this way assures the reproduction of the position of the etalon when it had to be removed for the absorption measurements.

A contact Pt-100 sensor (TI in Figure 3.1) on the gas cell measured the temperature of the gas sample assuming equivalence of temperatures between the walls outside and gas inside the absorption cell. The sensor was connected to a Testo 650 (accuracy specification of 0.1°C).

For the evacuation of the gas cell a turbomolecular pumping system (Saskia, model CD-160) was used. The vacuum system achieves an ultimate total pressure of $1.5 \cdot 10^{-7}$ hPa at the input of the pump. A gas sampling system (gas manifold in Figure 3.1) connects the vacuum pump and the gas cell. It is designed to realize static or dynamic measurements. Two capacitance detector gauges (CDG) measured the sample pressure, having an operation interval of 0-10 hPa (MKS, model 626AX11TDE) and 0-1000 hPa (MKS, model 626AX13TDE), respectively (PI in Figure 3.1). The first CDG was connected near to the input of the vacuum-pump, and the second was connected directly to the gas cell. A reading controller for the two pressure indicators (MKS, model PDR2000) was used. The capacitance measurement principle for pressure has the advantage that the sensor response is independent of the gas species. The gas sampling system was made of 6 mm SS-

tubing connected in an array with 6 diaphragm valves (Swagelok series DS). Two needle valves located at the input of the sample and at the input of the pump, could be used for dynamic measurements. For a fast interchange of samples and configuration of the gas cell, fast connectors were used.

3.2 TDLA Spectrometer for Linestrength Measurements

For the measurement of linestrengths a special designed TDLA-Spectrometer at PTB-Institute Berlin was used. A detailed description of the spectrometer system setup can be found in [85]. A brief description of the spectrometer setup shall be given in the following.

Figure 3.6 shows a sketch of the setup. Ideally, for linestrength measurements undisturbed or isolated gas molecules of the specific species are needed. This is achieved in practice by the measurement of the most as possible purified gas at low pressure. The ideal pressure range is that at which the spectroscopy is Doppler-limited. That is at high vacuum conditions. In order to achieve sufficient signal strength at low pressures, the optical pathlength was increased by the use of a multi-reflection long-pass gas cell of the Herriott type, as it is depicted in Figure 3.6. Details of the optimized cell design for the linestrength measurements are given in [85]. In a Herriott cell two concave spherical mirrors with identical radius of curvature R are placed on a common axis opposite to each other. One of the mirrors has an entrance hole which also serves as exit for the beam. The number of reflections in the cell depends on the physical distance of the two mirrors. As one mirror is fixed and the other can be moved, this distance can be varied. With an interferometer the distance of the movable mirror from an initial known position was measured [85, 86]. The optical pathlength could be selected and adapted to the measurement requirements (from 7 to 60 m). The total gas pressure inside the Herriott cell was measured with a 10 hPa interval capacitive detector gauge (CDG). For the purpose of temperature monitoring a Pt-100 gauge was mounted inside the Herriott cell. Temperature and pressure measurements in the Herriott cell were traced back to PTB-standards.

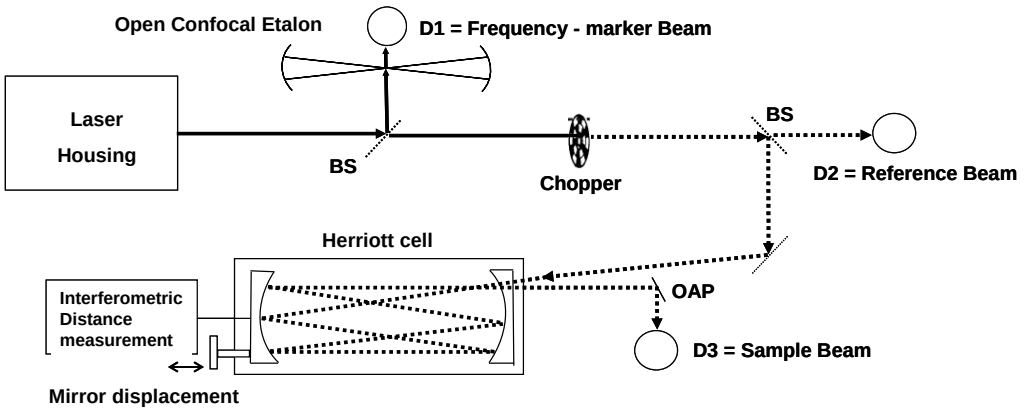

Figure 3.6: Spectrometer setup for linestrength measurements. D1, D2 or D3: detector; BS: beam splitter; OPA: off-axis parabolic mirror.

The same laser system was used for the linestrength measurements as it was operated for the amount of CO_2 fraction determination (s. section 3.1.1). The laser

beam was split in three *measurement beams*: the *reference beam*, the *sample beam* and the *frequency marker beam* as it is shown in Figure 3.6. The *reference beam* works as the initial (or incident) power monitor of the laser, the *sample beam* is directed through the Herriott cell and the *frequency marker beam* was coupled through an open confocal etalon (*FSR* 0.01 cm^{-1}) in order to measure the relative wavelength change during the current tuning of the laser.

Each *measurement beam* was equipped with a LN_2-cooled detector (D1, D2, D3). The laser light was chopped. The output signals from *reference* and *sample beams* were detected with lock-in technique. The signal containing the frequency marker was directly detected. An oscilloscope was used for data acquisition, digitization and displaying of the signals. The data acquisition was controlled by a Labview module communicated with the oscilloscope. The Labview platform saves also temperature, total and residual pressures in the Herriott cell, allowing an evaluation of stability and repeatability of this quantities during the measurements.

3.3 System for Preparation of Static Gas Mixtures by Gravimetry

Reference gas mixtures were prepared by gravimetry. The desired amount of CO_2 fraction to be prepared is approximated by the partial pressure of the respective main components (CO_2 and N_2) in gas phase. The definitive value of the added amount for each parent gas is determined by weight. Gas mixture components are transferred to a properly evacuated spherical reservoir. Following, the empty sphere m_0, the sphere with the added first gas compound m_1, and finally the sphere with the additionally added second compound m_2 were weighed. The determination of mass of the added first parent gas was calculated by the difference of masses $m_1 - m_0$ and that of second parent gas by the difference of $m_2 - m_1$. With knowledge of the composition of the parent gases the amount of CO_2 fraction is calculated by means of (2.36).

The method for preparation of reference gas mixtures by gravimetry is described in [87]. The procedure implemented here is following presented. Each gas mixture between 0.01 to 0.1 mol/mol CO_2/N_2 was prepared directly from high purity parent gases (CO_2 4.6, N_2 5.0). The high purity parent gases were transferred using a gas manifold. The addition of each parent gas to the spherical reservoir was assured by difference of pressure. At the beginning of the preparation process the sphere was evacuated until a pressure of 1 mPa using the turbomolecular pump system of the TDLAS system (s. Figure 3.1). Previous to the addition of each parent gas, the filling system was at least 3 times purged and evacuated with the parent gas in turn to be added to the mixture. After the addition of the balance gas and previous to the weighing of the mixture, the sphere was quickly mixed using freely movable metal sheets located inside the gas container. The weighing was performed by a single step in a balance H135 (Mettler, d = 0.1 mg, Max. cap. = 1000 g). Zero level indication of the balance was corrected at the beginning of the weighing process. Temperature, pressure and relative humidity of the weighing room is registered to probe the non significant variation of the density of air [87].

A scheme of the filling system for gas mixtures is presented in Figure 3.7. The gas manifold is fabricated of a monolithic piece of hollowed stainless steel. It has 6 interconnected ports: one for the manometer, one for a vacuum-meter (isolated during mixture-filling with a valve), two for the gas mixture to be prepared and two for the parent gases. All ports are isolated from the vacuum pump during gas mixture

filling with a valve situated between the manifold and the vacuum pump. Gas mixture filling approximation by partial pressure was done with a manometer of a full scale range of 1.00 MPa with 0.01 hPa of minimum analogical scale division. An auxiliary vacuum meter (pirani cold cathode gauge, Balzers) indicates the vacuum achieved between purges.

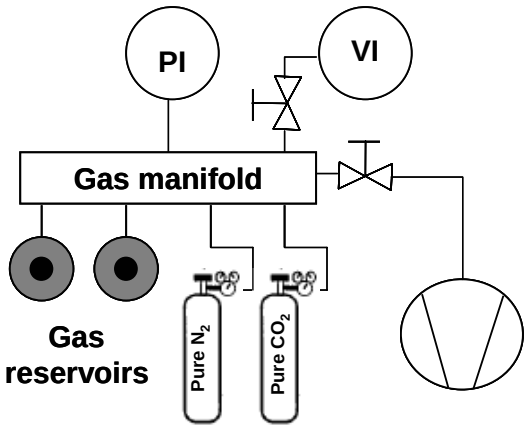

Figure 3.7: Filling system for the preparation of reference gas mixtures.

Figure 3.8: Spherical gas reservoir.

The material of the spherical gas reservoir was stainless steel and the characteristics of the sphere were already described in [88]. The sphere (Figure 3.8) had a 316 stainless steel diaphragm valve (Swagelok DL series) with a Helium leak test of $4 \cdot 10^{-9}$ std cm^3/s at the seat and all seals of the valve.

Static reference gas mixtures are normally prepared in big volume cylinders (5 to 20 L) at filling pressures of ~ 12 MPa (depending on the gas mixture vapour pressure), leading to long life times (several years). In this thesis, small volume reservoirs (1 L) of spherical form (Figure 3.8) were used with a filling pressure of about 0.7 MPa. The performance of such gas mixtures has been already proved to be successful for use in vehicle emission measurements for the pattern approval of vehicle exhaust gas meters [88]. Using these mixtures the PTB has an entry of international recognition of calibration and measurement capabilities (CMC) in the Mutual Recognition Arrangement (MRA) of the CIPM with an uncertainty of $4 \cdot 10^{-3}$ (k=2) [89, 90].

Preparing static gas mixtures in a spherical, small volume at lower filling pressures, has several advantages. The spherical form of the cylinder has the minimum internal surface area being in contact with the gas mixture, which minimize any possible adsorption effect. Binary gas mixtures can be prepared quickly, in nearly 15 minutes, including the single weighing. In this way, it is possible to perform easily the correction for the buoyancy effect of air in the weight, because of the insignificant variation in the environmental conditions [91]. There is also non significant volume change of the sphere during filling because of the relatively low filling pressure, as it is the case of bigger cylinders [87]. Delay times before weighing are avoided because of the over heating of the gas mixture after the addition of the component at high pressure [87].

4 Measurements of Amount of Carbon Dioxide Fraction

The amount of CO_2 fraction was determined using TDLAS without any calibration. The measurement equation for the determination was based on (2.18) with the linestrength calculated with (2.20) and the line shape function with a Voigt profile (2.27). The absorbance was derived from the incident and the transmitted laser power with (2.14). One beam measurements could have been performed, but two beam measurements were used, because they rendered more unbiased results. In order to verify the TDLAS-measured amount of CO_2 fraction results, they were compared with those obtained by gravimetry.

4.1 Line Selection

The infrared spectrum of CO_2 was presented in Figure 2.2. The fundamental band (i. e. with the highest linestrengths) is located in the mid infrared around 4.2 - 4.3 μm. This fundamental band is accessible by lead-salt diode lasers or by quantum cascade lasers. However, these are laser technologies still in development compared with those of near-infrared diode lasers [8, 24]. The reason for the most developed technology of near-infrared diode laser sources and detectors is the use of the cheap mass-production capabilities in telecommunications and consumer electronics extended over the 2μm region [24]. Sensitivities in direct-detection-NIR measurements can be increased by use of multi-reflection gas cells. Thus, CO_2 measurements with laser emitting in the NIR are useful not only for laboratory but also for practical applications.

In order to perform calibration-free amount of CO_2 fraction measurements first of all an unambiguous identification of the absorption line being selected for the measurement has to be assured if literature linestrength values should be used. The line identification was achieved by tuning the laser to different lines, measuring the respective absorption profile for pure CO_2 gas and subsequent comparison with spectroscopic data from literature, i. e. with data obtained from HITRAN. Figure 4.1 shows all CO_2 lines that could be tuned to with laser temperatures between 15 and 30°C compared with the respective spectrum retrieved from HITRAN. With the knowledge of the relative linestrengths the more intense lines can easily be identified by comparison, confirming also the laser temperature tuning scale. With these measurements it was possible to compare the measured intensities (bottom panel of Figure 4.1) with those from HITRAN (top panel of Figure 4.1). The top panel of Figure 4.1 shows the labeling of the lines in the R-branch (R6, R8, R10, R12, R14) of the $\nu_1+2\nu_2+\nu_3$ band for $^{12}C^{16}O_2$. The other identified lines with much lower intensities correspond to lines of adjacent bands of CO_2. In Figure 4.1 the linestrength values for the $^{12}C^{16}O_2$ isotope (from R6 to R14) increase with the wavenumber. The line with the maximum strength accessible with the laser in this R-branch is the R16 line (not shown). For the selection of the line that shall be used in calibration-free TDLAS two parameters play the key role: linestrength for sensitivity and isolation from other absorption lines for selectivity. The selected line should have the highest linestrength and the best isolation from neighboring or interfering spectral features.

In the top panel of Figure 4.1 it is evident that the line most isolated from any other CO_2 line is the R12 line. The R14 and R16 (not shown) lines have very nearby lying CO_2 lines that could diminish the quality of the measurements. *As the R12 line is more intensive and isolated it was selected for the quantitative measurements.*

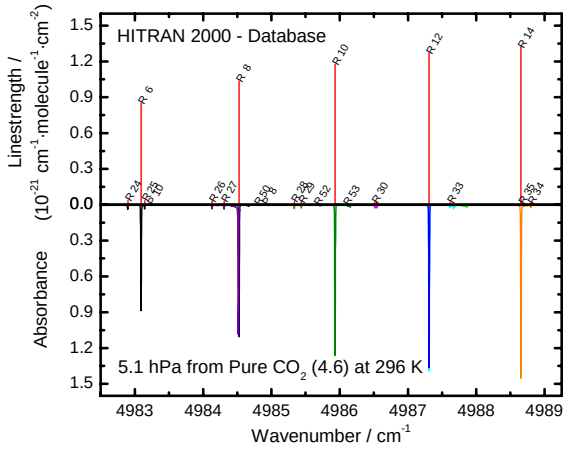

Figure 4.1: Tuning of CO_2 lines. All measurable CO_2 lines are shown. Top panel: calculated lines, bottom panel: measured lines. The depicted lines R6 to R14 correspond to the band $\nu_1+2\nu_2+\nu_3$. The other lines correspond to low intensive CO_2 adjacent transitions.

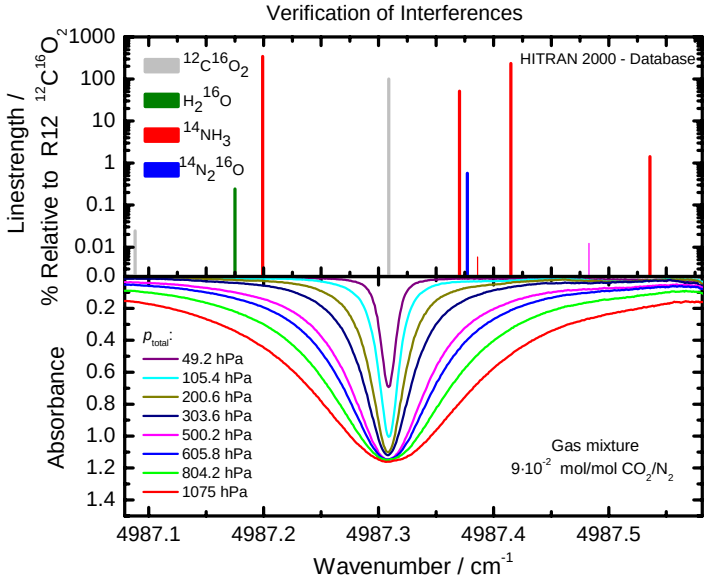

Figure 4.2: Measured line and possible interferences based on HITRAN Database for main vapor phase substances present in the atmosphere. The transition selected is the R12 line of the band $\nu_1+2\nu_2+\nu_3$ for the main isotope $^{12}C^{16}O_2$.

For an evaluation of the selectivity the data presented in Figure 4.2 were considered. The top panel of Figure 4.2 shows all the lines of common potential interferences of other substances found in atmospheric gas measurements within the laser sweep interval. The linestrengths are taken from [92]. Linestrengths are drawn relative to the selected R12 line. In case of the selected line, NH_3 could interfere at most because of its nearly 3 times larger linestrength. However, in typical applications concentrations of NH_3 and CO_2 are found in very different orders of magnitude. An example is the monitoring of NH_3 in bioreactor vent gases for the determination of potential space board air toxicity due to NH_3 production [11]. For this application a maximum

concentration of $5 \cdot 10^{-6}$ mol/mol NH_3 can constitute 1 % of the minimum concentration of CO_2 produced in such a system ($500 \cdot 10^{-6}$ mol/mol). If the linestrength is considered this results in a maximum of 3 % interference of NH_3 in the CO_2 measurements. N_2O and H_2O could be perceived as undetectable because of the low linestrengths.

The amount of isolation of the line depends also on test pressure (s. section 4.2) - as it is shown in the bottom panel of Figure 4.2 - and also on the absence of significant concentrations of other absorbing substances within the resolved spectrum of the measured species. However, potential interferences could often be eliminated -if significant- by measuring lines at Doppler-limited conditions. That is in the present study for $P_{total} < 20$ hPa [63].

4.2 Measurement Parameters

The test pressure influences sensitivity and selectivity. On one hand side selectivity is needed, which implies that the test pressure must be as small as possible. That is the pressure limit at which the line shape is Gaussian, where selectivity is maximized in the Doppler limited regime. On the other hand, sensitivity requires the detection or effective change of area under the absorption peak, which is as better as the pressure increases i. e. in the pressure broadening regime.

Regarding selectivity, the bottom panel of Figure 4.2 shows CO_2-spectra at different P_{total} from ~ 50 hPa to atmospheric pressure. At a pressure of ~ 500 hPa the line cannot be completely measured because the baseline comes not down to zero within the observed laser sweep interval. Thus, at higher pressures, x_{CO_2} could not be measured calibration-free anymore. The line width (FWHM) is ≤ 0.025 cm^{-1} for $P_{total} \leq 100$ hPa and ~ 0.04 cm^{-1} for $P_{total} > 200$ hPa. The interval between 50 and 200 hPa is that in which the absorbance maximum changes most significantly. Thus, it is the most sensitive one. Therefore, quantitative measurements were carried out at total pressure around 100 hPa.

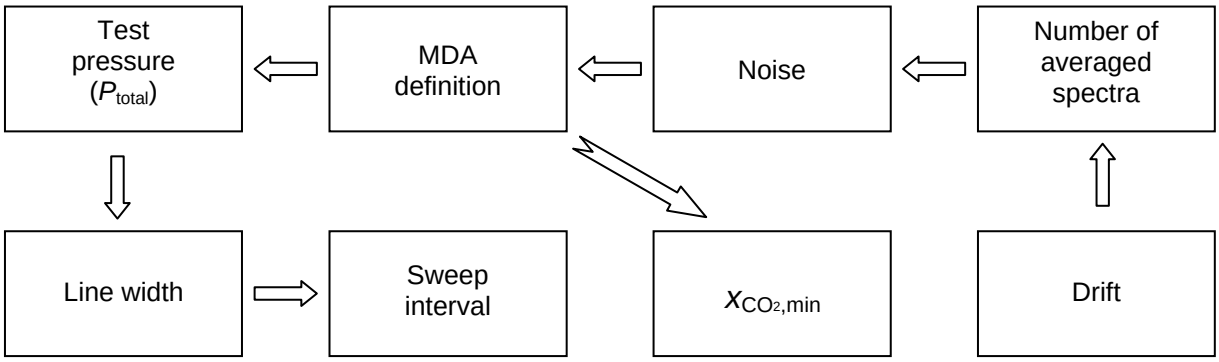

Figure 4.3: Dependence between measurement parameters.

Figure 4.3 sketches the relationship of the measurement parameters enabling high selectivity and sensitivity in TDLAS measurements. A sensitivity value is estimated considering the signal noise in absorbance units (minimum detectable absorbance: MDA) and its translation into amount of CO_2 fraction units ($x_{CO_2,min}$). In turn, noise depends on the number of averaged spectra (scans), in which averaging is limited, because signal, pressure and temperature instabilities or simply because of time

consumption. Noise cannot be infinitely reduced with averaging and the drift of the signals -i. e. of the zero absorbance value- plays also a role defining the number of spectra averaging. Tests of spectra averaging were carried out at 1, 10, 100 and 500 scans. The time for 500 scans was prohibitively large - 45 minutes for 10 replicates - with drifting signals. Results for 1 and 10 averaged scans were still too noisy. As a result, measurements with 100 averaged spectra (scans) - 15 minutes for 10 replicates - were found to be efficiently quick and rendered unbiased results.

Noise was estimated taking into account the sweep interval, more specific, the working interval [93] where the spectrum can be resolved. The noise can be calculated as the standard deviation of the baseline (initial intensity without absorption) in absorbance units or as the *maximum noise* (difference between maximum and minimum values). In this work, the standard deviation ($1 \cdot S$) of the baseline was used as noise definition for the minimum detectable absorbance (MDA). It has to be considered that the definition of the MDA affects its value [94]. Some authors mention a typical value for MDA in direct absorption of 10^{-4} [11] others remark that the published MDAs differ quite a lot in the way they are obtained [95]. Experience with this laser spectrometer showed that the limit of detection could vary for the same test conditions (e.g. oscillate from $3 \cdot 10^{-3}$ to $1 \cdot 10^{-4}$). The best MDA value found in this work was 10^{-4}. Details of the methodology for the calculation of the MDA in x_{CO_2} units are described in [11].

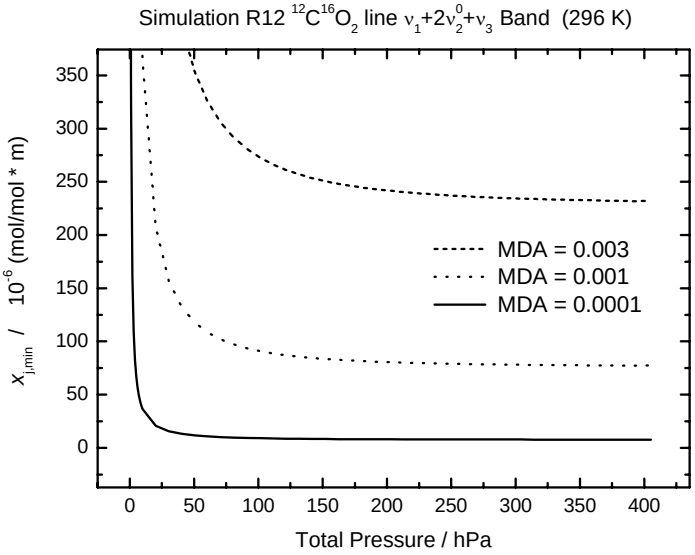

Figure 4.4: Sensitivity and optimal test pressure.

Based on the MDA calculation the optimal test pressure and the minimum detectable amount of CO_2 fraction $x_{j,min}$ was predicted such as shown in Figure 4.4. For example, for a MDA = $1 \cdot 10^{-3}$ with pressure of P_{total} > 100 hPa the $x_{j,min}$ remains constant. It means for higher pressures only an increase of the line width occurs and not of its maximum (the Lorentz profile is dominating the line shape); as a result selectivity will decrease. But at pressures < 100 hPa the $x_{j,min}$ starts to grow exponentially; then sensitivity is being lost. As a consequence, the 100 hPa (MDA = $1 \cdot 10^{-3}$) will produce the maximum sensitivity and selectivity. With the typical MDA values found in this work, the minimum x_{CO_2} can vary from ~ $10 \cdot 10^{-6}$

(MDA = $1 \cdot 10^{-4}$) to $250 \cdot 10^{-6}$ mol/mol·m (MDA = $3 \cdot 10^{-3}$). The optimum test pressure varies from ~ 50 (MDA = $1 \cdot 10^{-4}$) to 200 hPa (MDA = $3 \cdot 10^{-3}$). For this reason it is not possible to give a single conclusive optimal pressure. Thus, a test pressure of 100 hPa was confirmed.

Knowing the $x_{j,min}$, it was found that the results of x_{CO_2} could be biased if the atmospheric CO_2 (~ $380 \cdot 10^{-6}$ mol/mol) present in the optical bench -outside the absorption cell- of the spectrometer were not eliminated. Thus, ambient atmospheric CO_2 was purged out of the glass-fiber box covering the spectrometer (cover box in Figure 3.1) with a constant flow of dry nitrogen (5.0) at low overpressure (0.1 to 0.5 MPa).

As it was shown in Figure 4.3 the test pressure (P_{total}) affects the line width which has to be taken into account for the laser sweep interval needed to resolve the line. A test pressure of 100 hPa produces a line width (HWHM) of approximately 0.0125 cm^{-1} that is 32 times smaller than the sweep interval of 0.4 cm^{-1}. It complies totally the necessary interval to resolve a line having a Lorentz line shape, and as a consequence also that of a Voigt profile (s. section 2.2.3.2).

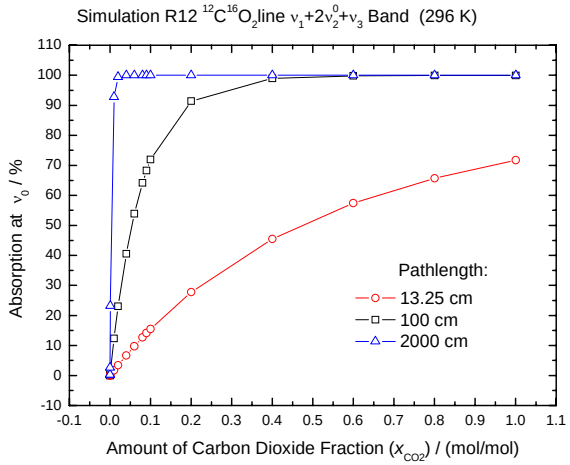

Figure 4.5: Simulated maximum absorption values at different pathlengths.

For the spectrometer, three gas absorption cells with different pathlengths were available. Figure 4.5 depicts the perceptual maximum absorption (1-T) at the center of the R12 line at P_{total} for different x_{CO_2} values. The 1 m length cell was selected because enables measure high signal to noise ratios at a useful x_{CO_2} interval between $1 \cdot 10^{-2}$ and $10 \cdot 10^{-2}$ mol/mol as it is shown in Figure 4.5. The signal to noise ratio was of the order of 100 to 700 (assuming a MDA =10^{-3}) for 10 to 70 % absorption respectively. This leads to absorbance values between 0.1 and 1.2. The interval of x_{CO_2} is useful for the quantification of vehicle-exhaust- and stack- emission applications. Also gas mixtures within this interval of x_{CO_2} are easily prepared by gravimetry. Thus, it is an optimal x_{CO_2} interval to probe the application of TDLAS as a calibration-free method. For proving the performance at extreme conditions of opacity, carbon dioxide in room air and CO_2/N_2 gas mixtures at higher concentration were selected as applications to prove the validity of the Beer-Lambert law under

these extreme conditions (~ 0.004 and 1.4 in absorbance units, respectively) and the performance of the method in applications (s. chapter 6).

4.3 Data Processing

Measurements could be acquired sequentially. An example of a sequential measurement is shown in Figure 4.6 including a measurement with and without absorption. Additionally the absorption spectrum of pure CO_2 is shown, which might be used to the control of the zero transmittance level. The current ramp applied to the laser at constant laser temperature is depicted in the top panel of Figure 4.6. The equivalence between sample point and time units can be observed.

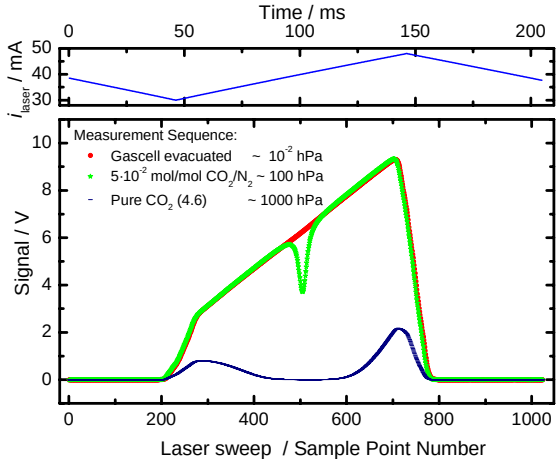

Figure 4.6: Example of a measurement sequence.

For the measurement of the absorbance according to (2.14) a two beam and a single beam method can be used. One beam measurements can be carried out by at least two sequential measurements: a measurement without absorption and a measurement with absorption. Two beam measurements can be carried out composing the ratio of the measurement signals with (D2) and without absorption (D1). Both, one and two measurement beam schemes have their own advantages and disadvantages.

For the single beam measurements only one detector is used. This avoids the possibility of a non equal behavior of different detectors or different amplification systems during detection. Single beam measurements allow controlling the zero value of transmittance if a chopper is used between the laser source and the detector (interval when the chopper is closed in Figure 4.7). However, they do not facilitate the control of incident intensity (baseline) changes due to possible fluctuations of the laser power or due to drifts of the detection system simultaneously with the absorption measurement, which would be of great relevance in absolute measurements. Contrary, two-beam ratio measurements do facilitate effective drift compensation. An additional advantage by these ratio measurements is the control of residual CO_2 that can be present in the optical bench.

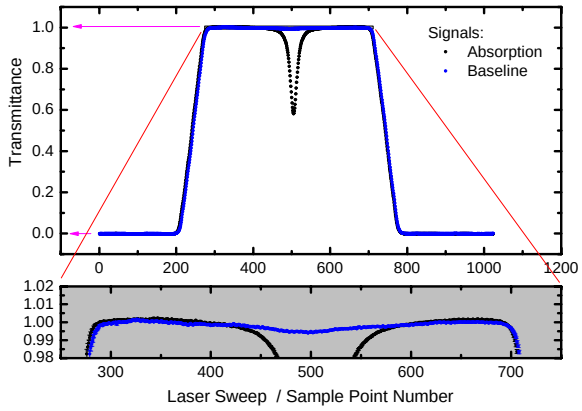

Figure 4.7: Control of transmittance stability. The transmittance value zero is controlled by the absence of laser light (chopper closed ~ 0-200 SP and ~ 800-1024 SP). The transmittance value one is controlled by adjusting the gain and the offset of detection in the measurement beams. This last is better shown in the bottom panel of the figure. In the bottom panel the baseline is curved due to the residual -after purge with N_2- atmospheric CO_2 absorption.

The measurements were carried out by means of two measurement beams. The key point of the two measurement beams ratio method was the control of the transmittance levels zero and one respectively. It is following described:

i) the two measurement beams were intensity-matched by help of the gain and the offset adjustment of the individual detector signals when no absorption was present,

ii) the logical transmittance-zero-level was defined by the physical signal of D2 by adjusting it zero when the chopper was closed by means of the offset of the D2-amplifier,

iii) the logical transmittance-one-level was adjusted by matching the signals of D1 and D2 by means of the gain and offset of the D1-amplifier.

The ratio of signals D2/D1 defining the transmittance levels zero and one can be observed in Figure 4.7.

The conversion of the digitized spectrum to the wavenumber scale was achieved by the known free spectral range of the Si-etalon in cm^{-1} (*FSR*) and the measured free spectral range in sample point units (*FSRSP*)

$$\tilde{\nu}/\mathrm{cm}^{-1} = r \cdot \tilde{\nu}/\mathrm{SP} \qquad (4.1),$$

where *r* is called the sweep rate. It is given by the ratio

$$r = \frac{FSR}{FSRSP} \qquad (4.2).$$

The *FSR* is a quantity that depends on the used frequency standard and it is also related to the used method for the determination of its value. For the determination of *FSR* the next two methods were used. Their uncertainty budgets are presented in Appendix A.

a) Calculation with a model: The model that describes the free spectral range of an etalon is

$$FSR = \frac{1}{2 \cdot n \cdot d} \tag{4.3}.$$

It is based on the length of the etalon *d* and the refractive index of the material *n*. In order to use the model to derive the *FSR* value of the Si-etalon, the length of the etalon was measured with a caliper, considering the respective changes due to the thermal expansion of silicon. The value of *n* was taken from a traceable source [53].

b) Measurement by FTIR: The Si-etalon transmission curve was measured using the same FTIR described in 3.1.1. The fringe separation (or *FSR*) can directly be read from the transmittance spectra. The resolution of the acquired data was 0.006 cm^{-1}. The limited resolution of the FTIR was the main uncertainty source as shown in the uncertainty budget presented in Appendix A. The respective FTIR-measured *FSR*-result appears as FTIR (TU-BS) in Figure 4.8.

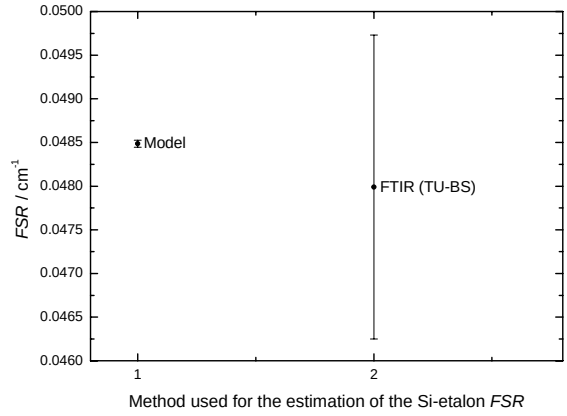

Figure 4.8: Si-etalon *FSR* results. The uncertainty bars indicate the standard uncertainty.

In Figure 4.8 the results of the determination of *FSR* for each method and their correspondent standard uncertainties are displayed. As it is shown, the results of the estimation of *FSR* are equivalent considering the larger uncertainty for the FTIR measurement. It has the consequence that both results have to be considered as valid. However, as it will be shown in chapter 6, it is possible to prove and to correct deviations of the measurement results which are much smaller than the estimated uncertainty on the basis of the *FSR* from FTIR and its large uncertainty. Therefore, it can be assumed that the uncertainty of *FSR* measured by FTIR is too large, although it was measured by means of a high resolution (0.006 cm^{-1}) instrument. On the other

hand the *FSR* uncertainty from the model seems to be slightly small. Measurements of *FSR* using the R12 and the neighboring R33 CO_2 absorption line lead to uncertainties 5 times higher. Unfortunately the absolute values of *FSR* could not be used here because they are conceived for a different wavelength interval.

The *FSRSP* value was determined from the digitized etalon signal measured by TDLAS. The estimation is conducted with the help of independent, two beam measurements. Measurements of *FSRSP* have to be done independently from the absorption measurements, because the reference beam (without etalon) has to be used for the prediction of the initial light intensity. The determination of *FSRSP* was achieved as the result of 6 independent measurements of the Si-etalon realized at 6 different days for room temperatures between 21.3 and 22.5°C.

The individual *FSRSP* values were obtained from an Airy function fit at the spectral position of the CO_2 line (450 -550 SP) within the laser sweep interval using two or three etalon fringes. Doing this, the Airy function fits the data more properly than using more than three etalon fringes. The standard deviation of the data accumulated during averaging was used as an instrumental weight in the Airy-fit performed with Origin®.

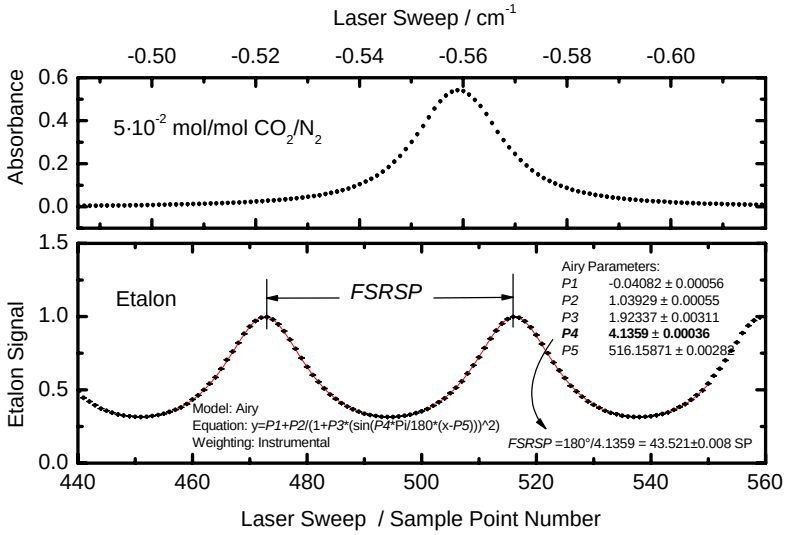

Figure 4.9: Digitized free spectral range *FSRSP* of the Si-etalon. The free spectral range of the etalon was used to convert digitized data to the wavenumber domain.

Each of the *FSRSP* values were obtained from the *P4* parameter as shown in the example of the bottom panel of Figure 4.9. The average value of the *FSRSP* obtained in this way was 43.487 ± 0.023 (k=1). The uncertainty is the standard deviation of the mean of the 6 étalon measurements. The value and the uncertainty of *r* depends on the values of *FSR* and *FSRSP*.

The Airy function is described by

$$y = P1 + P2 \cdot \frac{1}{1 + P3 \cdot \left[P4 \cdot \sin^2\left(x - P5\right)\right]} \qquad (4.4)$$

where *P1* to *P5* are the fit parameters [96]. An Airy fit is depicted in the bottom panel of Figure 4.9. From the Airy parameter *P4* the numerical value

$$FSRSP = \frac{\pi}{P4} \tag{4.5}$$

was calculated.

Because of the way in which a spectrum was constructed separated for the relative wavenumber scale (x-axis) and the absorbance (y-axis), the measurement equation (2.18) for the calculation of x_{CO_2} from TDLA measurements has to be rearranged to give the integral version of the combination of (2.18) and (2.21) [97]. The integral version separates the integration of the absorbance values $\alpha(SP)$ given by the Voigt profile fit from the SP-to-cm^{-1}-conversion by means of *r* [98]

$$x_j = \frac{r \cdot \int_{-\infty}^{+\infty} \alpha(SP)\mathrm{d}SP \cdot k_B \cdot T}{S_i(T) \cdot P_{total} \cdot L} \tag{4.6}.$$

This separation of $\alpha(SP)$ and *r* is quite important to facilitate uncertainties estimation. That is to avoid the use of a regression model, which can simultaneously consider uncertainties in both axes. In (4.6) the input quantities are referred to the respective measurement equations from chapters 2 and 4. The *r* value is calculated with (4.2), the Voigt profile area ($\int_{-\infty}^{+\infty} \alpha(SP)\mathrm{d}SP$) comes from (2.27), and the $S_i(T)$ is calculated with (2.20).

The calculation of the line area was done for the digitized spectrum by use of a Voigt-fit with Origin®. This Voigt fit is based on the non-linear Levenberg-Marquardt algorithm [82]. Important advantages of using the Voigt-fit are:

a) the correction of the zero value of the absorbance curve (offset),

b) the estimation of the uncertainty considering input uncertainties of the data by use of weighted regression,

c) the parameters of the fit can be maintained constant or vary.

The data were fitted setting the Gauss width as constant. This was based on the constant temperature maintained in the gas cell during a measurement. The Gauss width was calculated by use of the measured temperature according to (2.22).

In this work, the Voigt fit considered the y-axis variation of the spectrum within the averaging as a weighted regression. As variances of the digitized points change across the *SP* axis (especially around the kernel of the spectrum) a weighting based on the reciprocal variance is applied. Such a weighting method for a regression gives more importance to the data with less variability. Each replicate containing 100 averaged signal traces (scans) for each measurement beam has its associated standard deviation product of the averaging. A number of replicates is acquired (typically 10) for the same measurement conditions (pressure, temperature and gas

sample) and each replicate is separately fitted. The standard deviation is then taken as the standard uncertainty for each replicate, as a way of considering the correlation of the 100 scans within a replicate. The uncertainty of absorbance is considered by propagation of uncertainties from (2.14).

Figure 4.10 depicts a Voigt fit for one measurement and the parameters delivered by the fit. The uncertainty bars are the standard deviation of the absorbance. In the fit, y_0 is the baseline (or offset), x_c the line center, A the area, w_G the Gaussian line width, w_L the Lorentz line width. For the fit parameter: Chi2/DoF, Chi2 corresponds to the term mean sum of squares and DoF stands for degrees of freedom. The lower part of the graph presents a zoom at the baseline of the upper graph showing the data points with their standard deviation (uncertainty bars), the Voigt fit and its residuals. There, it is also possible to appreciate the noise or MDA (based on 1S) at 100 scans. This MDA is approximately $1 \cdot 10^{-3}$. It is also within typical MDA values found for direct absorption measurements [95]. The residuals of the fit are correlated around the kernel, probably as a result of collisional narrowing; indicating that the Voigt fit is unable to explain the line shape totally [98]. However, the difference between fit and data is less than $5 \cdot 10^{-3}$ at the kernel and about $2 \cdot 10^{-3}$ in the wings. This last value is only twice the value of the noise.

Any regression analysis has associated statistical suppositions on the properties of the residuals when the model is meant to fit the data appropriately: i) residuals have to have a normal distribution with a mean equals zero, ii) their variance should be constant and iii) residuals should not be correlated with each other. As a result, the observation of the residuals' behavior is a powerful tool for any kind of regression analysis.

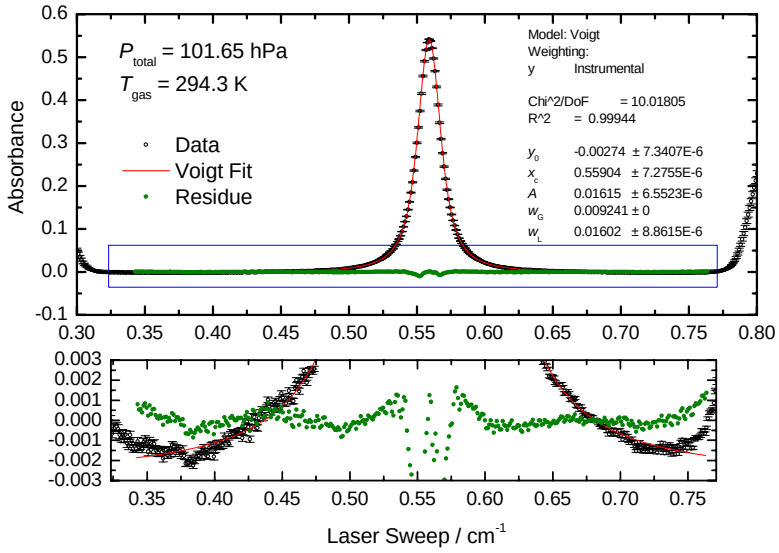

Figure 4.10: Typical Voigt profile fitted to the data. CO_2/N_2 gas mixture with $x_{CO_2} = 5 \cdot 10^{-2}$ mol·mol^{-1}.

Figure 4.11a depicts some examples of residuals of the respective Voigt fits for different x_{CO_2} values. The criteria that mean should equal zero is confirmed for the wings. However, it is not fulfilled at the center of the absorption peak. In the proximity

of the peak maximum an apparent “typical signature” of the Voigt profile residuals attributed to collisional narrowing was found [69]. An exception is the residual of the measurement with the lowest CO_2 concentration x_{CO_2} ($400 \cdot 10^{-6}$ mol/mol), where no “collisional narrowing influence” is observed such that the Voigt profile is well appropriate. Some structures of apparent fringes remain in the residuals. They come probably from reflections inside the optics. These effects are considered as not significant for this discussion. Therefore, for all the other measurements the residuals are correlated only around the kernel of the absorption. As a result the Voigt profile does not seem to be the very best model to describe the spectral line shape in any case. Nevertheless, the Voigt profile was used because it was proved that the influence of collisional narrowing is not significant for the measurement conditions as will be following discussed.

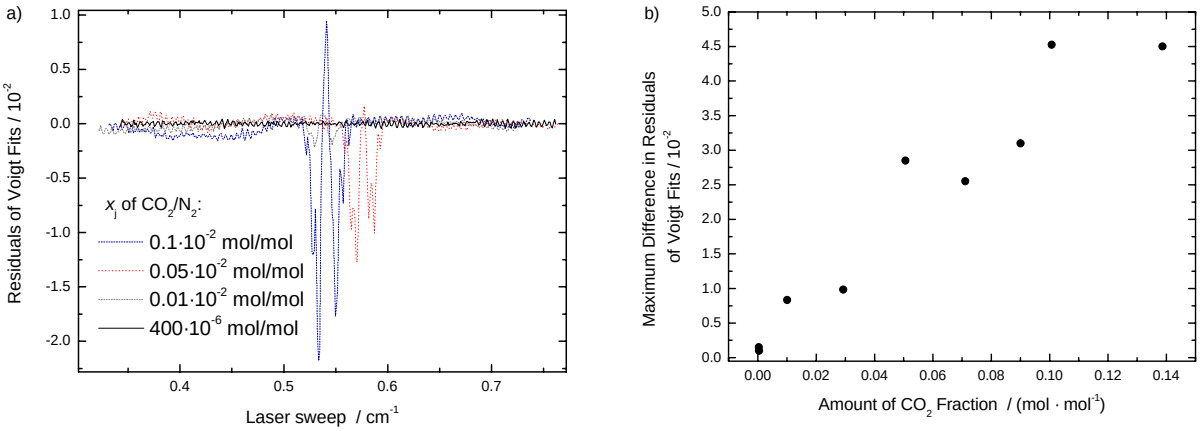

Figure 4.11: Residuals of Voigt-fits for different amount of CO_2 fraction measurements. P_{total} = 100 hPa. An increase of the residuals correlation with increased x_{CO_2} is observed. a) Residuals of Voigt fits at some x_{CO_2} values. b) Maximum difference in residuals: maximum residual value minus minimum residual value.

As a way of probing the efficiency of a fit, some authors have considered the relative difference in the residuals for varied line-profiles or varied concentrations [99]. The residuals for the interval of measured x_{CO_2} values can be observed in Figure 4.11a, where the y-axis scale is divided by a factor 10^2. Looking forward the maximum variability in the residuals (maximum residual value minus minimum residual value) Figure 4.11b has been constructed. In Figure 4.11b an increase of the maximum difference (or deviation) of the Voigt profile from the data with increasing x_{CO_2} values is evident. The *residuals* “see” together at least three effects: the frequency instability of the laser emission, the lack of complete purge of CO_2 in the optical bench and the collisional narrowing. Instabilities in the frequency of emission are thought to be manifested as an increase in the standard deviation (uncertainty) of averaged spectra around the kernel of the line. This effect is more evident for a higher absorption peak value because even for small changes of the ν_0 position in the *SP* scale - at constant *L* and P_{total} - the value of such uncertainty increases with the height of the absorbance maximum. Thus, the increase of the peak maximum with increasing x_{CO_2} is the reason for the linear correlation observed in Figure 4.11b. The lack of complete elimination of CO_2 present in the optical bench is manifested as a curved baseline in bottom panel of Figure 4.7 or more evidently in Figure 6.4. In these two figures, the not completely purged atmospheric CO_2 - especially evident for small values of x_{CO_2} -

can contribute also to the correlation of the residuals in the line center. This correlation can be misunderstood as an *apparently observed "collisional narrowing signature"*. However, collisional narrowing is predominant at lower pressures and it is not significant for this higher P_{total} (>1000 hPa) [69]. For CO_2 at room air concentration levels, the *differential calculation* allowed to eliminate totally the structure in the center of the line ($400 \cdot 10^{-6}$ mol/mol CO_2/N_2 in Figure 4.11a). Thus, it confirms the correlation of residuals due to remanent CO_2 and not as a result of the Dicke narrowing. Consequently it was concluded that the Voigt profile was suitable for the quantitative analysis.

Statements of literature - using the same scale of maximum difference in residuals (from maximum to minimum value) - showed discrepancies for defining an acceptable value for the maximum difference in residuals and comparing it with the results of Figure 4.11b. For CO 50 hPa it was found a $1.2 \cdot 10^{-2}$ difference in residuals. Additionally, a Galatry profile did not eliminate the called: "characteristic signature for collisional narrowing in the residual of a Voigt-fit [32, 99]" (see this signature e. g. in bottom graph of Figure 4.10), the investigated concentrations were in the interval from 0.1 to 0.75 volume fraction in nitrogen balance [32], elimination of the small amount of CO in air was not mentioned and also nothing was said about the stability of the laser. For $0.001 \cdot 10^{-2}$ mol/mol O_3 in air measurements at 20 hPa, the difference in residuals was $0.7 \cdot 10^{-2}$ for the Voigt profile [100]; when the Galatry profile was used the structure of collisional narrowing was eliminated and the difference was reduced to ~ $0.3 \cdot 10^{-2}$. This was also the case for a $300 \cdot 10^{-9}$ mol/mol ozone measurement, where the residuals go down to $0.1 \cdot 10^{-2}$. Such work had an extensive quality assurance of ozone in air mixtures generation and an active stability control of the laser emission frequency. A similar behavior of $1 \cdot 10^{-2}$ and $0.3 \cdot 10^{-2}$ in residuals differences (Voigt fit and Rautian or Galatry, respectively) are reported in [48] for mixtures of CH_4 in He balance at 20 hPa.

Avetisov and Kauranen [99] mentioned that the deviations of Voigt profiles from data are typically around $1 \cdot 10^{-2}$ when Doppler and collisional broadening have a similar magnitude. They also suggest that considering the collisional narrowing can reduce the lineprofile deviations to $0.2 \cdot 10^{-2}$ and lower. They arrived to this conclusion by modelling data with a Galatry profile, and found differences in residuals of $0.2 \cdot 10^{-2}$ for a Rautian-Sobelman profile fit and $6 \cdot 10^{-2}$ for a Voigt fit profile. These last values are in agreement with the relative residual values of Figure 4.11b. The authors conclude that the choice between a Rautian-Sobelman or Galatry profile is more a matter of convenience -except for very small or high mass ratios of collisional partners [48]- because the difference between them is normally smaller than "experimental precision".

Considering the results exposed in the last two paragraphs a criteria of acceptable deviation for the Voigt-residuals of $0.1 \cdot 10^{-2}$ to $0.3 \cdot 10^{-2}$ is justified. That is the value of the MDA. It was concluded that a Voigt profile properly fits the data when the residuals are of the order of the MDA. Such criteria fulfilled the limits of the differences for the residuals in the wings in Figure 4.11a or for fits of data in the absence of the correlated residuals (first data points Figure 4.11b around $400 \cdot 10^{-6}$ mol/mol CO_2). The correlations of residuals at higher concentrations do not produce unbiased results in the TDLAS-based x_{CO_2} values that will be presented in chapter 6.

4.4 Results

In chapter 2 it was highlighted that for realizing reliable TDLAS gas analysis without calibration of the substance being measured it is necessary to prove the generation of unbiased measurement results with respect to independent and accurate reference values, thus, the gravimetric values of reference gas mixtures were used for this purpose.

4.4.1 Absolute Performance

Gravimetrically prepared CO_2/N_2 gas mixtures with x_{CO_2} in the interval of 1 to $10 \cdot 10^{-2}$ mol/mol were analyzed applying TDLAS. The resultant TDLAS-based values were subsequently compared with their gravimetric counterparts. In the upper part of Figure 4.12 the laser-based values are plotted against the gravimetric ones. The underlying property of the laser-based values is the measured area of the respective absorption line, which was converted to x_{CO_2} with (4.6). The linear increase of the measured absorption area with increasing amount of CO_2 fractions (gravimetric values) seems to verify the applicability of the Lambert-Beer law in this concentration interval. But it also requires a slope 1 and a y-intercept 0. As it is shown in Figure 4.12, these two parameters (A and B) of the linear regression have not these values. This indicates that the TDLAS-based x_{CO_2} values are not reproducing the gravimetric x_{CO_2} values. In addition, the uncertainty of the intercept depicted in Figure 4.12 is smaller than its value, which is also an indication of a possible bias in the results. Visually, the residuals presented in the bottom part of Figure 4.12 do not seem to be correlated. They are randomly distributed. The mean equals zero and the variance is constant. Thus, a linear correspondence between the laser-based values of x_{CO_2} and the gravimetric values of x_{CO_2} can be conceded.

Having a linear fit that does not cross the origin and does not have a slope 1 confirmed the presence of additional effects that have to be considered in the calculation of the laser-based x_{CO_2} values.

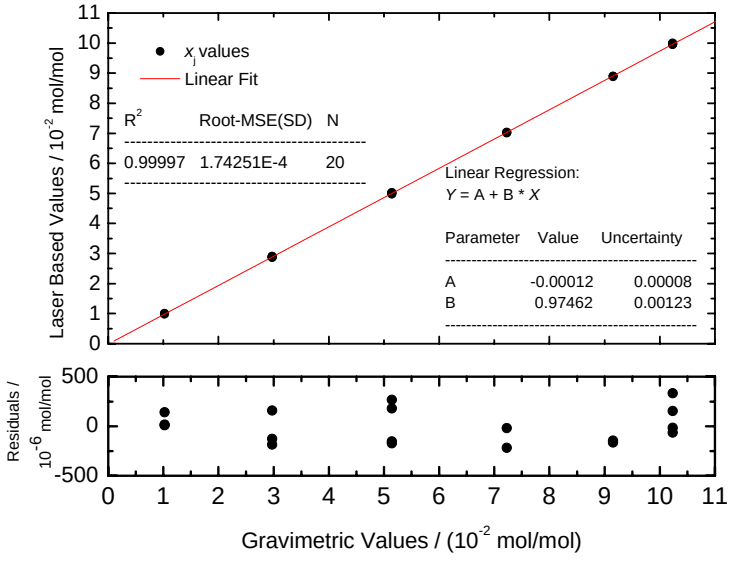

Figure 4.12: Linear regression for x_{CO_2} results.

For evaluating the quantitative difference between laser-based and gravimetric values of x_{CO_2} the relative bias (2.37) of the results was considered. Figure 4.13 presents the bias as a function of the gravimetric x_{CO_2}. A line centered at y=0 % shows the gravimetric values. The bias of the laser-based values with respect to the gravimetric values is of the order of -1.4 to -1.6 %. For a reliable comparison not only the x_{CO_2} values have to be considered, but also their correspondent uncertainties. Thus, a calculation of uncertainties is needed. Section 4.4.2 presents the uncertainty of $x_{Grav.}$ values and section 4.4.3 the uncertainty of x_{TDLAS} values.

The uncertainty bars for the gravimetric values in Figure 4.13 represent the expanded uncertainty (k=2). This uncertainty increases with decreasing amount of carbon dioxide fractions because the gas mixtures shown in this plot were prepared by a single dilution step of pure gases. The uncertainty bars of the laser based values contain only the reproducibility of the measurements (S_R). This reproducibility comprises 3 to 4 independent gas-cell fillings at different days. The reproducibility values include the repeatability values for each gas filling (measurement with a set of 9 to 10 replicates, each having 100 averaged spectra), whose uncertainties are expanded as will be explained in section 4.4.3. The reproducibility values span from $S_R = \pm 0.02$ to ± 0.9 %. In average, the reproducibility is of an order of approximately $S_R = \pm 0.3$ %. In general, it is smaller for bigger amount of CO_2 fraction values. This tendency is because of the constancy of optical pathlength and total test pressure used here. That results in smaller absorbance area values for smaller x_{CO_2} and in an relative increase of noise.

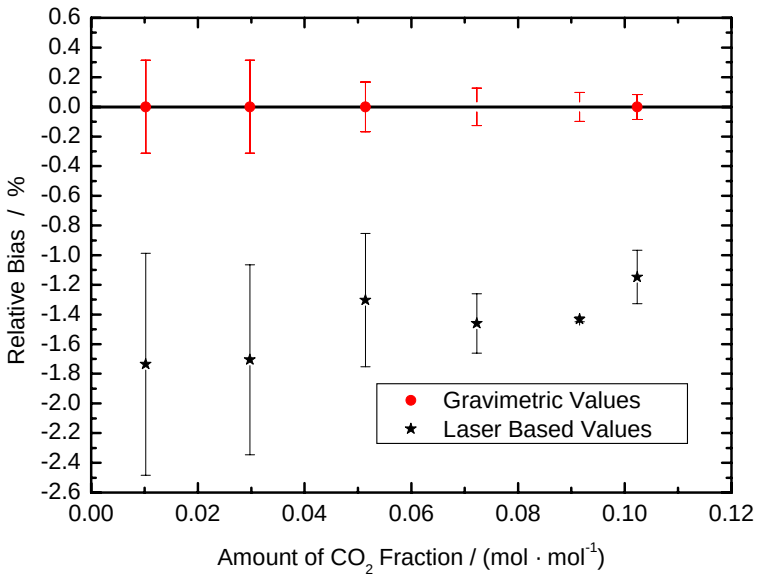

Figure 4.13: Absolute performance for analysis of carbon dioxide. Difference of the laser-based x_{CO_2} values from the gravimetric ones. The laser-based x_{CO_2} are presented as their relative bias according to (2.37).

The expanded uncertainty of the TDLAS-based x_{CO_2} measurement results (not shown in Figure 4.13) varies depending on the reproducibility. For the most reproduceable x_{TDLAS} value ($S_R = \pm 0.02$ % for $x_{CO_2} \sim 0.09 \cdot 10^{-2}$ mol/mol) the uncertainty is U_r (x_{CO_2}) = ± 3.8 % (k=2). The relative apparent bias of -1.4 % of the x_{TDLAS} result is more than 30 % of the ± 3.7 % uncertainty. As a result, this *apparent bias* is

significant [101]. The estimation of measurement uncertainties presented in 4.4.3 will show that the main uncertainty contribution is that of the linestrength. The respective value for the linestrength and its uncertainty taken for the results of Figure 4.13 were those of the HITRAN database, whose reliability and level of confidence is not exactly known. Thus, it was necessary to determine traceable results of linestrengths (s. chapter 5) in order to improve x_{TDLAS} results.

4.4.2 Uncertainty Budgets of Gravimetric Gas Mixtures

The uncertainty of static gas mixtures has been extensively studied for high accuracy *substitution weighing* in *comparator balances* and in *two-pan balances* [87, 91, 102]. In many cases, such investigations include the effect of correlation between the input quantities [103, 91]. This correlation was shown to be not significant. For the amount of substance interval of a few 10^{-2} mol/mol, the uncertainty of these mixtures is normally limited by the weighted mass of parent gases. Three main uncertainty sources are identified: the uncertainty of the purity of the parent gases, the uncertainty of the weighing process and the uncertainty of the molar masses [87]. Among them, with the high purity gases available, only the weighing was significant for the mixtures prepared here. The uncertainties of the weight of the gases have two additional components, which could change also the values of the weight of each gas component: the air buoyancy correction and the residual pressure in the sphere. As the residual pressure is of the magnitude order of 0.1 Pa, the correction is only of 1 μg, being a no significant uncertainty source. For the estimation of the air buoyancy correction in *single pan direct reading balances* some studies available were used [104, 105]. The densities of gases were taken from [106] and the density of stainless steel from [91]. The density of air was calculated with the equation taken from [87]. For air buoyancy, it was found that the correction in mass varies from 0.2 to 0.4 mg for the binary mixtures prepared here. This variation depends on the suppositions used for the mean density of the stainless steel sphere, the valve and the gas component, when they are not available as accurate measurements. With these values, the uncertainty can increase by a factor of 2. For the uncertainty of the weighing was taken a pooled standard uncertainty of 0.5 mg considering: non-linearity, calibration, repeatability, readability, zero-reading and excentricity of the balance.

The procedure for the determination of the amount of carbon dioxide fraction by gravimetry ($x_{Grav.}$) was explained in section 3.3. The measurement equation is (2.36) [87]. This equation was used for the calculation of the uncertainty budget. The most important influence quantities are those of the weighing, which was already mentioned as typical of these gas mixtures. The main uncertainty sources of $x_{Grav.}$ are presented in Table 4.2 for an example of a nominal $5 \cdot 10^{-2}$ mol/mol CO_2/N_2 gas mixture. Table 4.1 describes the meaning of the quantities given in Table 4.2. The complete uncertainty budget is given in Appendix A.

Table 4.1: Main quantities contributing to the uncertainty of gravimetric x_{CO2}.

Quantity	Unit	Definition
x_{CO2}	mol/mol	Amount of CO_2 fraction
m_1	g	Mass for sphere + parent gas 1: CO_2
m_0	g	Mass for empty sphere
m_2	g	Mass for sphere + parent gas 1: CO_2 and 2: N_2

Table 4.2: Main uncertainty sources for gravimetric x_{CO_2}.

Quantity	Value	Standard Uncertainty	Probability Distribution	Degrees of Freedom	Sensitivity Coefficient	Uncertainty Contribution	Index *
m_1	879.6357 g	$500 \cdot 10^{-6}$ g	Normal	50	0.10	$50 \cdot 10^{-6}$ mol/mol	53.9 %
m_0	879.1040 g	$500 \cdot 10^{-6}$ g	Normal	50	-0.092	$-46 \cdot 10^{-6}$ mol/mol	45.8 %
m_2	885.8790 g	$500 \cdot 10^{-6}$ g	Normal	50	$-7.8 \cdot 10^{-3}$	$-3.9 \cdot 10^{-6}$ mol/mol	0.3 %
x_{CO_2}	0.051421 mol/mol	$67.8 \cdot 10^{-6}$ mol/mol	t-assumed	100	**U_r (x_{CO_2}) = 0.26 %**	**(k = 2)**	

***** The different contribution to the combined uncertainty of the masses is due to the given "natural weighing" of (2.36) given by the first derivative of the quantity, i. e. the sensitivity coefficient. The mass m_1 is the most important due to the little amount of the CO_2 mass added to the sphere. The mass m_2 is not the second because it is the balance gas, i. e. the N_2 mass added was much larger. Thus, the most important contribution to the uncertainty is the little amount of mass of CO_2, and it is given by the difference m_1 - m_0.

4.4.3 Uncertainty Budgets of Amount of Substance Fraction by TDLAS

The contribution of the input quantities in (4.6) to the combined uncertainty of x_{CO_2} measured by TDLAS is presented in the column "Index" of Table 4.3. The "Index"

Table 4.3: Uncertainty budget of x_{CO_2} by TDLAS with *FSR* from FTIR measurements.

Quantity	Value	Standard Uncertainty	Probability Distribution	Degrees of Freedom	Sensitivity Coefficient	Uncertainty Contribution	Index
L	100.000 cm	0.289 cm	Rectangular	∞	$-890 \cdot 10^{-6}$	$-260 \cdot 10^{-6}$ mol/mol	0.5 %
T	295.450 K	0.200 K	Normal	50	$570 \cdot 10^{-6}$	$110 \cdot 10^{-6}$ mol/mol	0.1 %
P_{total}	101.000 hPa	0.300 hPa	Normal	50	$-890 \cdot 10^{-6}$	$-270 \cdot 10^{-6}$ mol/mol	0.5 %
*FSR**	0.04799 cm^{-1}	$1.74 \cdot 10^{-3}$ cm^{-1}	Normal	50	1.9	$3.2 \cdot 10^{-3}$ mol/mol	79.0 %
FSRSP	43.4870 SP	0.0230 SP	Normal	5	$-2.1 \cdot 10^{-3}$	$-47 \cdot 10^{-6}$ mol/mol	0.0 %
Area	25.7518 SP	0.0164 SP	Normal	50	$3.5 \cdot 10^{-3}$	$57 \cdot 10^{-6}$ mol/mol	0.0 %
$S_i(T_0)$	$1.2730 \cdot 10^{-21}$ cm	$22.5 \cdot 10^{-24}$ cm	Normal	50	$-70 \cdot 10^{18}$	$-1.6 \cdot 10^{-3}$ mol/mol	18.8 %
Q_{T0}	33.408 Arbitrary	0.100 Arbitrary	Normal	50	$-2.7 \cdot 10^{-3}$	$-270 \cdot 10^{-6}$ mol/mol	0.5 %
Q_T	33.2066 Arbitrary	0.0996 Arbitrary	Normal	50	$2.7 \cdot 10^{-3}$	$270 \cdot 10^{-6}$ mol/mol	0.5 %
x_{CO_2}	0.0895 mol/mol	$3.65 \cdot 10^{-3}$ mol/mol	*t* - assumed	75	**U_r (x_{CO_2}) = 8.2 %**	**(k = 2)**	

***** The value and uncertainty of the *FSR* is taken from a FTIR - measurement (s. 4.3). It is the reason of the relatively large uncertainty.

shows that the main influence quantity is the *FSR* contributing with 79.0 % to the combined uncertainty. The second most important influence quantity is the $S_i(T_0)$ having a contribution of 18.8 % to the combined uncertainty. The used linestrength

was that of the HITRAN database [92]. For this calculation the *FSR* from FTIR was taken, which is the reason of the relative large uncertainty 8.2 %. If the *FSR* is taken from the model (4.3) the uncertainty is much lower 3.7 % and the linestrength is the main influence quantity with a contribution of 89.1 %. The last results are shown in Table 4.4.

In Tables 4.3 and 4.4, the value of *r* from (4.6) is displayed as its components *FSR* and *FSRSP* from (4.2). The $S_i(T)$ value from (4.6) has been already replaced with the quantities of (2.20). The Voigt profile area uncertainty was determined from the combination of variances in- and between-replicates of measurement. The uncertainty of the area is that of the reproducibility combination. This reproducibility combination is following explained. Tables 4.3 and 4.4 give only the main uncertainty sources. A detailed explanation of the uncertainty budgets is given in Appendix A.

Table 4.4: Uncertainty budget of x_{CO_2} by TDLAS with the *FSR* given by (4.3).

Quantity	Value	Standard Uncertainty	Probability Distribution	Degrees of Freedom	Sensitivity Coefficient	Uncertainty Contribution	Index
L	100.000 cm	0.289 cm	Rectangular	∞	$-900\cdot10^{-6}$	$-260\cdot10^{-6}$ mol/mol	2.4 %
T	295.450 K	0.200 K	Normal	50	$580\cdot10^{-6}$	$120\cdot10^{-6}$ mol/mol	0.5 %
P_{total}	101.000 hPa	0.300 hPa	Normal	50	$-900\cdot10^{-6}$	$-270\cdot10^{-6}$ mol/mol	2.5 %
FSR	0.048486 cm^{-1}	$38.8\cdot10^{-6}$ cm^{-1}	Normal	50	1.9	$72\cdot10^{-6}$ mol/mol	0.2 %
FSRSP	43.4870 SP	0.0230 SP	Normal	5	$-2.1\cdot10^{-3}$	$-48\cdot10^{-6}$ mol/mol	0.1 %
Area	25.7518 SP	0.0164 SP	Normal	50	$3.5\cdot10^{-3}$	$58\cdot10^{-6}$ mol/mol	0.1 %
$S_i(T_o)$	$1.273\cdot10^{-21}$ cm	$22.5\cdot10^{-24}$ cm	Normal	50	$-71\cdot10^{18}$	$-1.6\cdot10^{-3}$ mol/mol	89.1 %
Q_{To}	33.408 Arbitrary	0.100 Arbitrary	Normal	50	$-2.7\cdot10^{-3}$	$-270\cdot10^{-6}$ mol/mol	2.6 %
Q_T	33.2066 Arbitrary	0.0996 Arbitrary	Normal	50	$2.7\cdot10^{-3}$	$270\cdot10^{-6}$ mol/mol	2.6 %
x_{CO_2}	0.0904 mol/mol	$1.69\cdot10^{-3}$ mol/mol	t-assumed	62	**U_r (x_{CO_2}) = 3.7 % (k = 2)**		

As an example, the relative deviation from the mean of 10 measured replicates of line areas is plotted in Figure 4.14 together with the standard deviation of the single values and their respective repeatability. In this figure, the uncertainty bars of the single values represent the relative uncertainties (*S*) of the integrated area delivered by the Voigt-fit. The uncertainty bars of the mean value represent the repeatability (S_r) of the ten replicates. The repeatability of the measurement in Figure 4.14 is S_r = 0.17 % for the x_{CO_2} ~ $5\cdot10^{-2}$ mol·mol^{-1}; however, the repeatability varies from S_r = 0.1 to 0.9 % for x_{CO_2} ~$10\cdot10^{-2}$ to $1\cdot10^{-2}$ mol·mol^{-1} respectively. The Voigt-fit area uncertainty included a correlation estimation within the 100 averaged scans for each single value, assuming the input uncertainties of the data in y-axis in absorbance units as the standard deviation. This supposition is thought to be a reasonable approximation, because the correlation contribution of scans to the uncertainty of absorbance will increase with the number of averaging spectra (as the standard deviation does relative to the standard deviation of the mean); thus, using the

standard deviation of the mean at this stage would underestimate the uncertainty due to correlation of the scans. Moreover, the method [107] of combining the variability within- and between-replicates needs as input parameter the standard deviation within replicates - that is the uncertainty of the Voigt Fit -, but not the standard deviation of the mean.

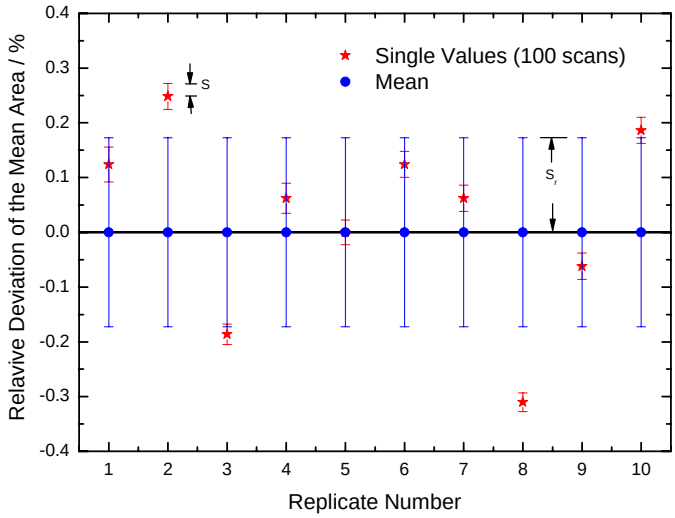

Figure 4.14: Replicates of TDLAS measurements. Example of a $5{\cdot}10^{-2}$ mol/mol CO_2/N_2 gas mixture. The uncertainty bars of the single values represent the relative uncertainties of the integrated area of the Voigt-fit (S). The uncertainty bars of the mean value shows the relative repeatability (S_r) for the 10 measured replicates.

The control of the stability of the transmittance levels zero and one avoided the necessity of drift corrections between replicates (s. section 4.3). Corrections of the drift would be needed if the results of the measured area (or x_{CO_2}) replicates were not randomly distributed. The absence of drift can be appreciated in Figure 4.14, where the depicted individual replica values (single values) show no trend, indicating a random behavior. This absence of drift is also manifested in Figures 6.2 and 6.6.

In Figure 4.14, the values of the relative uncertainties of areas (S = 0.05 %) compared with that of the repeatability of areas (S_r = 0.17 %) are of different orders of magnitude. When the method of combining the uncertainties to find the S_r value of [107] is used, then the main contribution to the uncertainty will come from the variation between single values -specifically from the standard deviation of the replicates- and not from the variation within single values. In order to estimate a more reliable value of area or x_{CO_2} if the variability between replicates is larger than that within replicates -having averaged a considerable number of scans: here 100-, it will be recommended to measure more replicates (such as the ten used here).

5 Measurement of Linestrengths

An additional determination of the CO_2 linestrength was carried out because the uncertainty of the so far used HITRAN value provided the main contribution to the uncertainty of the resulting x_{CO_2}. This was also done because the uncertainties in HITRAN are not -until now- informatively claimed. Thus, they are not full GUM [46] compatible. The purpose of such experimental determination was to get a reliable-accurate value of the linestrength. Moreover, the determined value and the uncertainty of linestrength could modify its contribution to the uncertainty of x_{CO_2}.

Several characteristics differentiate the determination of the linestrength of CO_2 from that of the amount of CO_2 fraction. The most important already highlighted in section 3.2 is that the CO_2 molecules have to be isolated. This is achieved by measuring pure CO_2 gas at P_{total} corresponding to the Doppler line width limit. Because the pressures were in practice less than 2 hPa, it was necessary to use proper facilities to measure this pressure levels accurately. Thus, the measurements of linestrengths had to be carried out in the vacuum facilities of the PTB-Berlin in a special designed TDLA-Spectrometer.

This TDLA-Spectrometer allowed to perform linestrength measurements using certain measurement procedures (s. 5.1) and data processing schemes (s. 5.2), that differed from those applied for the measurements of amount of CO_2 fractions.

As the main problem with the available literature linestrength values is their reliability -i. e. traceability of the values- it was necessary not only to measure a reliable value of linestrength, but also an accurate one. Thus, to minimize systematic errors in the determination of the linestrength and to improve its accuracy, the measurements of linestrengths were performed at different pressures P_{total} and for varied pathlengths L. The determination of a traceable pathlength in a Herriott cell is not a trivial task and systematic errors in this determination can affect the linestrength results. It was the main reason for measuring linestrengths at different L. P_{total} had to be varied in order to have a useful dispersion of the measurement results for the linestrength determination by a linear fit of the measured line areas (s. 5.3).

The measurement procedure and the data processing were done according to [85]. The discussion of the experimental results shall be restricted to the selected CO_2 transition for this thesis: the R12 line of the $\nu_1+2\nu_2+\nu_3$ absorption band.

5.1 Measurement Procedure

The spectrometer configuration was already described in 3.2. The laser was operated as described in 3.1.1.

The procedure of linestrength measurements was conducted in a specific sequence of 4 measurements. First, the gas cell was evacuated and a number of averaged spectra (scans) were saved; second, the cell was filled with pure CO_2 to a certain pressure and the absorption signal of CO_2 was measured; third, an optically thick spectrum of pure CO_2 was measured; and fourth, the cell was evacuated and measured again. A specific name for each measurement in the sequence was given as presented in Table 5.1. These names will be used for the description of the data processing in 5.2. Each saved data set within the measurement contained: the

signals of the 3 *measurement beams* (*reference*-, *sample*- and *frequency-marker-beam*), the laser current modulation data, and those values from temperature and pressure measured during the averaging of the spectra. A data set for each *measurement beam* consisted of 2500 digitized sample points, which resolved the spectrum with a digitized-point resolution of the order of ~ $1 \cdot 10^{-5}$ cm^{-1}. Each digitized point was the result of the averaging of 70 scans in 30 s.

Table 5.1: Given names for each measurement in sequence based on the opacity of the measured gas.

Type of measurement	Description
Zero-absorption	Gas cell evacuated
Partial-absorption	Gas cell + sample
Total-absorption	Gas cell + optically thick sample
Zero-absorption-control	Gas cell evacuated

5.2 Data Processing

The data processing used for the measurement of linestrengths differed from the measurement of amount of CO_2 fraction. Table 5.2 shall be helpful for the understanding of the individual measurement types and for the respective signals used for the data processing. That is, how the signals coming from the measurement beams were utilized.

Table 5.2: Use of the measured signals in the sequence of measurement.

Signal of the Beam:	**Type of Measurement**			
	Zero-absorption	Partial-absorption	Total-absorption	Zero-absorption-control
Reference	Calibration curve for I_0	I_0 for sample beam		
Sample		Absorbance curve and $T = 1$	$T = 0$	Stability of Zero-absorption
Frequency		cm^{-1} – scale conversion		

Note. The use of the measured signals coming from the respective measurement beam is written by the notes in the cells. The signals of beam with cells in grey were not needed for the calculation of the linestrength.

a) A totally different control of the stability of the values 0 and 1 of transmittance was used. That is not only two measurement beams were simultaneously measured and divided as in the amount of CO_2 fraction determination. Instead three measurement beams were available in the Berlin-TDLA-spectrometer. They were simultaneously measured following the sequence of Table 5.1.

For the control of the transmittance 1 value (Table 5.2), the reproduction of the initial intensity (I_0) of the *sample beam* based on that of the *reference beam* was utilized as following described. A calibration curve for the I_0 of the *sample beam* signal versus the I_0 of the *reference beam* signal -both in the *zero-absorption measurement*- was used to calculate the I_0 for the *sample beam* in the *partial-absorption measurement* (Table 5.2). With help of this $\hat{I}_0$ calculation and the reference beam signal of the partial absorption measurement the drift of the 1 transmittance value was controlled. The resulting $\hat{I}_0$ curve was compared with the wings of the measured *sample beam* signal of the *partial-absorption measurement* in the wings of the line. The wing values are used to determine the zero value of absorbance (transmittance value 1). The

stability of the calibration curve during the time needed for the whole measurement sequence was verified by comparison using data of the *partial-absorption* (Figure 5.1), and also of the *zero-absorption-control measurements* (Figure 5.5) -later described-. The difference in residuals - I minus the $\hat{I}_0$ of the *sample beam* signal in a *partial-absorption measurement* - can be observed in Figure 5.1. In this figure, the structure of residuals in the wings is of the order of $3 \cdot 10^{-3}$, which is approximately the MDA by direct absorption spectroscopy [95].

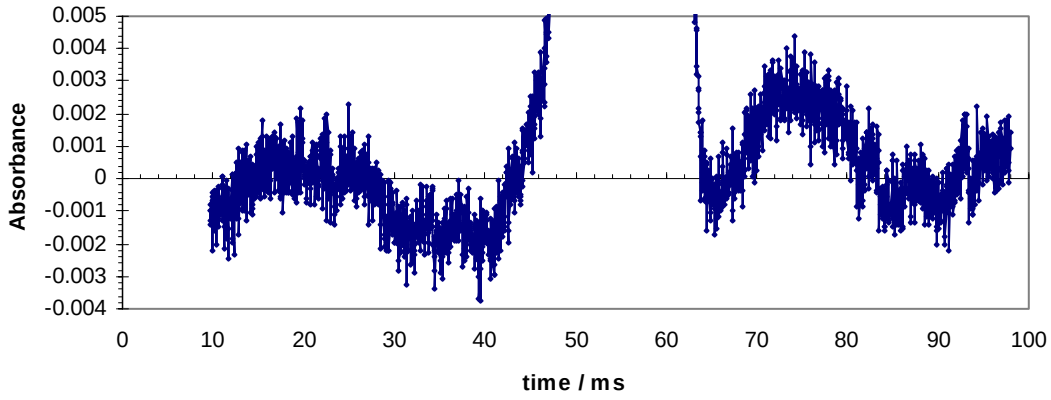

Figure 5.1: Verification of zero absorbance value. The residuals of the difference of I minus the calculated I_0 (or $\hat{I}_0$) of the *sample beam* signal in a *partial-absorption measurement* are plotted.

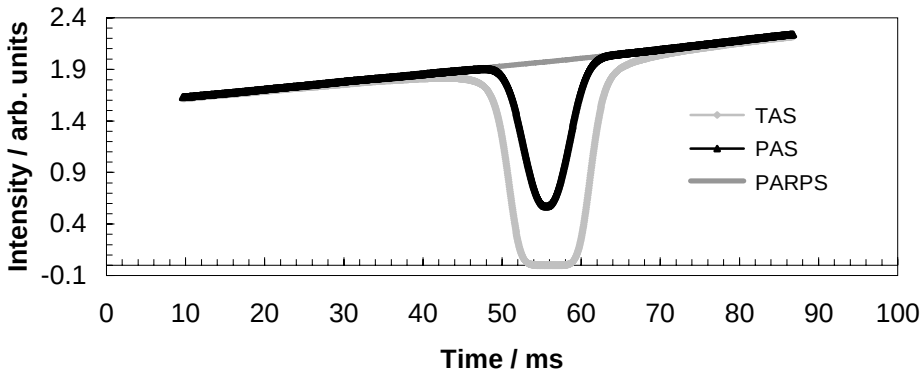

Figure 5.2: Sample beam signals for correction of transmittance values. Where: TAS = total-absorption signal, PAS = partial-absorption signal, PARPS = partial-absorption calculated $\hat{I}_0$ signal.

For the transmittance 0 value the 100 % absorption value (or intensity offset) of the total absorption measurements was used. This 100 % absorption of the *sample beam* signal of the *total-absorption measurement* was used for the estimation of the *zero-signal value* (Table 5.2). The values of the *sample beam* signal of the *partial-absorption measurement* I and the *predicted sample beam* signal $\hat{I}_0$ were corrected for the intensity offset I_{offset} derived from the 100 % absorption. Figure 5.2 shows the

signals of a total-, a partial- and a calculated $\hat{I}_0$ measurement with the I_{offset} already corrected by

$$T = \frac{I - I_{\text{offset}}}{\hat{I}_0 - I_{\text{offset}}} \tag{5.1}.$$

The transmittance scale was also corrected for the linearity of the detectors according to measurements realized in [85].

b) The replicates of averaged scans -that is the *sample beam* signals of the *partial-absorption measurements*- were added ensuring that the individual line maxima were located at the same position within the digitized time window. After that, a mean spectrum of the replicates was calculated. The reason for the displacement of the replicate's maxima in an absorption spectrum was already discussed in section 4.3. The resulting mean spectrum of the replicates is shown in the upper panel of Figure 5.3. The bottom panel of Figure 5.3 depicts the standard uncertainty of the absorbance. The uncertainty of the absorbance values was in the wings of the order of the MDA, but in the kernel larger and correlated as a product of the possible slight instability of laser emission frequency.

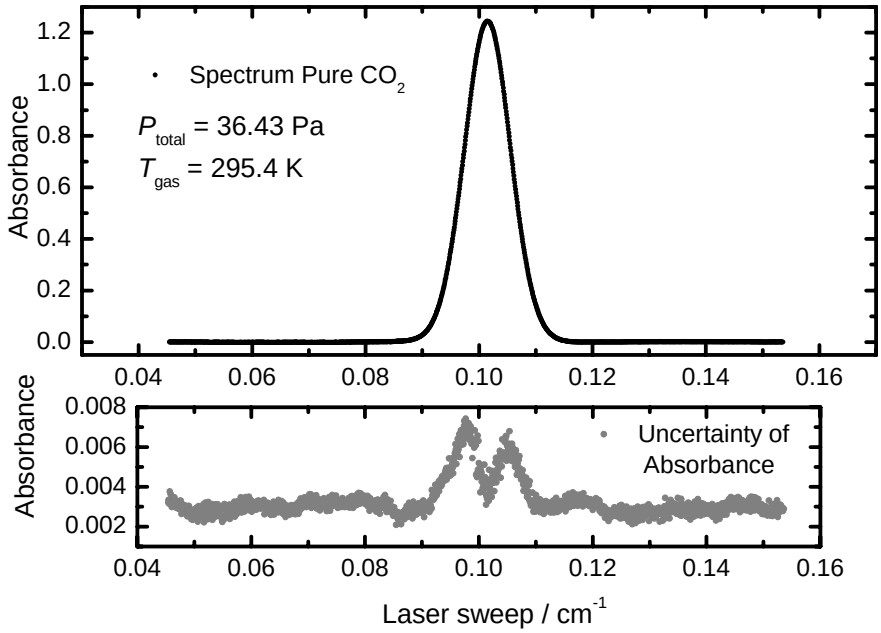

Figure 5.3: Averaged spectrum for a linestrength measurement. The upper graph is an example of the good resolved spectra of a replicate. The bottom graph is the uncertainty of absorbance for the averaged scans in a replicate.

c) No assumption of the constancy of the sweep rate was made. As the frequency-marker beam was simultaneously measured with the spectra, the conversion of digitized data from time to wavenumber scale was individually determined for each digitized time segment by the respective couple of etalon fringes. In this way the

variation of the fringes separation within the whole digitization time window was accounted for.

For this, the *frequency-marker beam* signal of the *partial-absorption measurement* was used (Table 5.2). A parabolic-fit with the same number of digitized points at each side of an etalon fringe maximum -or constructive interference- was used for the estimation of a more accurate value of the etalon fringe position. Each segment of the relative wavenumber scale was corrected by the difference between two consecutive etalon fringe positions (an example of etalon fringes can be seen in Figure 3.4). Figure 5.4 shows the increase of the sweep rate within the digitization time window. The uncertainty bars represent the standard uncertainty. Further details for the calculation of the wavenumber scale are given in [85].

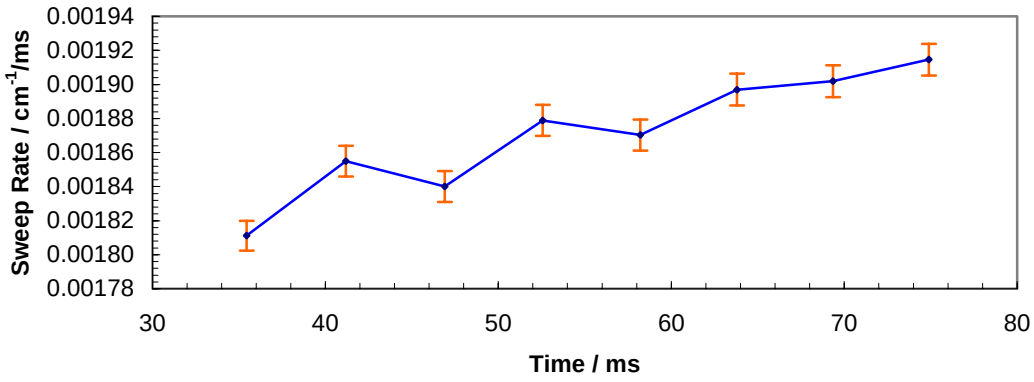

Figure 5.4: Sweep rate variation. The time is representing the position within the time window of one laser sweep. The first value of the sweep rate corresponds to the difference between the first and the second etalon fringes. The subsequent sweep rate values were the consecutive differences between the etalon fringes.

d) Direct integration of the area under the absorption peak -it means no use of any line shape fit-. If a line shape fit shall not be used then the zero value of the absorbance, i. e. the *baseline*, will be very important for the estimation of an unbiased area of the absorption line. This was achieved by maintaining a zero value of absorbance with the procedure described in a). As it was mentioned in a), the reference signal and the wings of the “good resolved spectra” were used to determine the zero value of absorbance. For the used test pressures -from 36 to 136 Pa- a number of 9 Doppler-widths (FWHM) from each side of the line center was considered to give a complete resolved lineshape for the Doppler broadening lines [63, 108]. The tested pressure interval was limited by the line broadening in the high pressure regime and in the lower regime by the uncertainty of the pressure measured with the CDG. Such uncertainty is for pressures > 30 Pa smaller than 0.2 %, but for pressures from 30 to 1 Pa increases gradually from 0.2 % to 3 %, respectively.

The whole measured absorption line was segmented by rectangles with a height given by the measured absorbance value and a width of the wavenumber step corresponding to the respective time step of the digitization. The subsequent integration was performed by summarizing the areas of all rectangles. This direct integration of the area was realized according to [85]. Each digitized point was used with its uncertainty in y-axis and the uncertainty in x-axis separately. In this way the uncertainty of the area considered the uncertainties in both axes.

The signal of the *sample beam* of the *zero-absorption-control measurement* (Table 5.2) re-verifies the applicability of the calibration curve used for the generation of the *sample beam* incident power of the *partial-absorption measurement*. In Figure 5.5 the residuals $-I$ of the *sample beam* of a *zero-absorption measurement* minus the $\hat{I}_0$ of the *sample beam* signal in the respective *partial-absorption measurement*- can be observed along the whole sweep interval, showing again a value near to the MDA of $3 \cdot 10^{-3}$. When the area under these residuals was integrated, it was < $1 \cdot 10^{-4}$ cm^{-1}. The uncertainty of the area was found between the maximum values of $2 \cdot 10^{-5}$ cm^{-1} and $3 \cdot 10^{-4}$ cm^{-1} for an underestimated and an overestimated uncertainty approach [85]. The first approach considered the replicates as independent, the second as totally correlated, i. e. $r(x_i, x_j) = 1$ in (2.30).

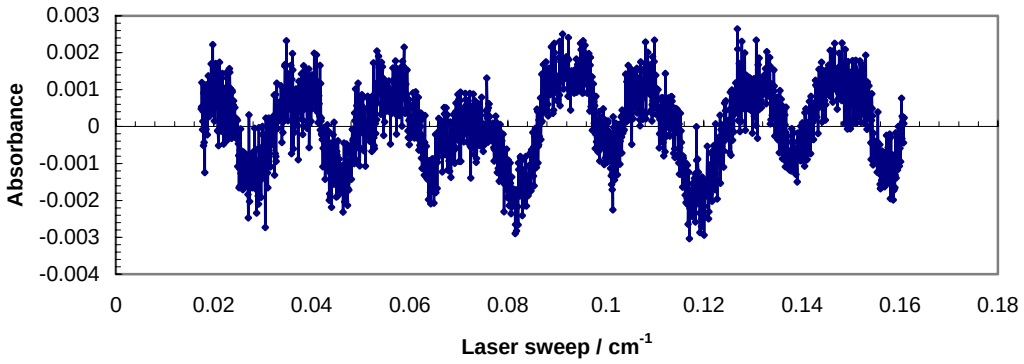

Figure 5.5: *Zero-control measurement* for the *sample beam.* The residuals of the difference of the I of the *sample beam* signal of a *zero-absorption measurement* minus the $\hat{I}_0$ of the *sample beam* signal in a *partial-absorption measurement* are plotted.

e) As the temperature and the pressure readings during measurements were automated, the uncertainties of these two quantities were diminished and the reliability of these measurements is higher compared to the same quantities for the measurements of amount of CO_2 fractions.

5.3 Linestrength Results

The resulting value of the R12 linestrength was based on 28 independent measurements at 6 different pathlengths of the Herriott cell and different pressures. The guide for the expression of uncertainty [46] recommends a variation of the influence quantities - when possible - for a better knowledge of their influence. With independent measurements it is meant a new filling of the Herriott cell with pure CO_2 gas samples for each sequence of measurement carried out according to section 5.1.

The experimentally determined line area values deliver respective figures for the linestrength, calculated according to (2.15) with the parallel measured pressure and gas temperature. Details of the pressure and temperature measurements for the 28 measurement sequences used to evaluate the R12 linestrength are given in [85]. The calculated individual linestrength values and their assigned uncertainties are summarized in Table 5.3.

Table 5.3 : Results of linestrength for individual measurements.

#	S_i / 10^{-21} *	$u(S_i)$ / 10^{-24} *	#	S_i / 10^{-21} *	$u(S_i)$ / 10^{-24} *	#	S_i / 10^{-21} *	$u(S_i)$ / 10^{-24} *	#	S_i / 10^{-21} *	$u(S_i)$ / 10^{-24} *
1	1.2426	2.4	**8**	1.2546	2.5	**15**	1.2852	2.4	**22**	1.2487	3.7
2	1.2642	8.7	**9**	1.2426	8.8	**16**	1.2531	2.6	**23**	1.2545	3.0
3	1.2633	6.3	**10**	1.2527	6.0	**17**	1.2482	4.5	**24**	1.2603	7.0
4	1.2560	6.5	**11**	1.2517	8.3	**18**	1.2562	5.2	**25**	1.2596	7.7
5	1.2600	6.8	**12**	1.2549	7.4	**19**	1.2641	8.9	**26**	1.2592	7.4
6	1.2626	7.2	**13**	1.2793	9.3	**20**	1.2457	6.2	**27**	1.2656	11
7	1.2558	3.3	**14**	1.2658	8.3	**21**	1.2516	3.3	**28**	1.2715	11
Mean Value: $1.2582 \cdot 10^{-21}$ $cm^{-1} \cdot molecule^{-1} \cdot cm^2$, Uncertainty: $0.0119 \cdot 10^{-21}$ $cm^{-1} \cdot molecule^{-1} \cdot cm^2$											

* in $cm^{-1} \cdot molecule^{-1} \cdot cm^2$

The respective mean value of

$$\overline{S}_i(T_0) = 12582 \cdot 10^{-21} \mathrm{cm}^{-1} \cdot \mathrm{molecule}^{-1} \cdot \mathrm{cm}^2$$

and its uncertainty *

$$u\left(\overline{S}_i(T_0)\right) = 0.0119 \cdot 10^{-21} \mathrm{cm}^{-1} \cdot \mathrm{molecule}^{-1} \cdot \mathrm{cm}^2$$

can be compared with the result of a linear regression analysis carried out for the determined line areas versus the product of molecular density n and the optic pathlength L. Rearranging (2.15) leads to

$$Area = S_i(T) \cdot n(p,T) \cdot L \tag{5.2}$$

which could also be read as a linear equation

$$Y = A + B \cdot X \tag{5.3}$$

with the slope

$$B = S_i(T)$$

and the intercept

$$A = 0$$

Measurements at different L and P_{total} gave the opportunity to define the linestrength in terms of the slope of the linear fit. This definition of the measurand S_i was important, because the definition of the measurand itself affects its value [46]. In other words, it is not the same to calculate linestrengths from the average of the 28 measurements or determining the linestrength from the slope of a linear fit where systematic errors of the influence quantities can be compensated. Because of this compensation the result of the linear regression analysis is seen to be the more reliable one. The linear fit of the measured areas for the respective product $n \cdot L$ is presented in Figure 5.6.

* This uncertainty considered the variabiliy in- and between- measurements, in the 70 scans for each individual measurement and between the 28 replicates, respectively. The combination of the uncertainty was calculated according to [107].

The slope evaluation method of the linear regression analysis delivers a value of

$1.2549 \cdot 10^{-21}$ $cm^{-1} \cdot molecule^{-1} \cdot cm^2$

for the linestrength $S_i(T_0)$ and of

$\pm 0.0072 \cdot 10^{-21}$ $cm^{-1} \cdot molecule^{-1} \cdot cm^2$

for the standard uncertainty. The uncertainty in Figure 5.6 for S_i (B value) is smaller than its total uncertainty, because the uncertainty of non-linearity of detectors is not yet combined. The uncertainties in this figure are the uncertainties of the model having already considered all other combined uncertainties. Uncertainties in both axes have been considered according to [85]. The advantage of using a linear fit for the calculation of S_i is the elimination of possible systematic errors coming mainly from the measurement of *L* and *Area* [63, 85, 109].

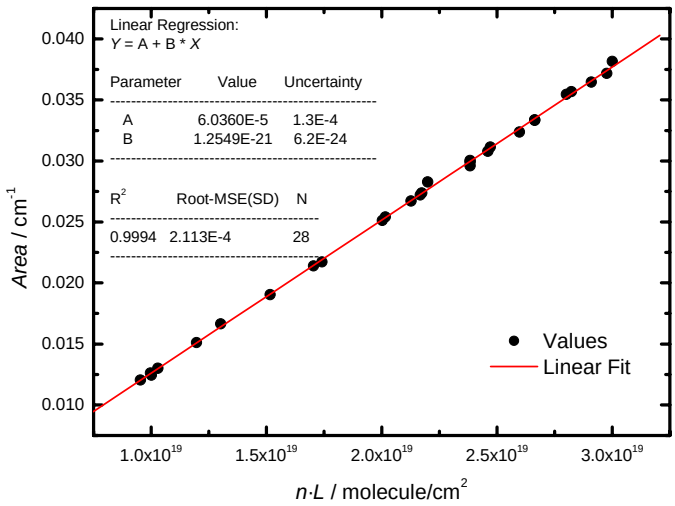

Figure 5.6: Calculation of linestrength for the R12-Line. The linestrength is determined from the slope of a linear fit of the line area versus the product of the molecular density and the optic pathlength. The fit parameters are depicted.

A characteristic of the linear fit in Figure 5.6 is that the uncertainty of the intercept is larger than its value, therefore, the intercept value can be considered as not significant. It is not zero because the *zero-absorption-control measurement* predicts the smallest value of area being of this order of magnitude, giving it the physical meaning of noise present in the *zero-absorption measurements*.

Both results of the linestrengths are concordant within their uncertainties. They have a relative standard uncertainty of 0.94 and 0.57 % respectively. They differ only by 0.32 % from each other. Table 5.4 compares the results of both methods. The respective values delivered by HITRAN [92] have also been incorporated in the last column, showing that the experimental results of the PTB-TDLAS approach deviate from HITRAN by -1.2 and -1.4 % respectively.

Table 5.4: Comparison of R12 line strength results.

Parameter	Direct	Slope	HITRAN [92]
$S_i(T_0)$ / 10^{-21} cm^{-1}·$molecule^{-1}$·cm^2	1.2589	1.2549	1.273
$u_r(S_i(T_0))$ / %	0.94	0.57	2.04 *
% Deviation from HITRAN	-1.2	-1.4	0

* For details about the uncertainty refers to Appendix A or table 4.3

Coming back to the calibration-free measurement of amount of CO_2 fraction x_{CO_2} one must conclude that the apparent bias (see section 4.4.1) of the TDLAS-based x_{CO_2} values with respect to the gravimetric references lies exactly in the range of the TDLAS-based linestrength deviation for the slope method from the HITRAN figure.

5.4 Uncertainty Budget of Linestrength Measurements

Because the uncertainty of the linestrength measurements were evaluated from a linear regression it was not processed by the GUM workbench® software, but by a specific program developed in [85]. When the measurement equation includes only products or quotients of input quantities (second rule of [110]) the uncertainty contribution of each quantity can be evaluated by its respective relative uncertainty. This approach is also full GUM compatible.

Table 5.5: Influence quantities of linestrength measurements.

#	*Area* / cm^{-1}	u_r(*Area*) / %	u(*Area*-α)/ $u(\nu)$ / cm^{-1}	$\alpha(\nu_0)$	*L* / cm	u_r(*L*) / %	*p* / Pa	u_r(*p*) / %	*T* / K	u_r(*T*) / %
1	0.01244	0.17	1.7	1.18	718.3	0.14	54.40	0.03	296.703	0.020
2	0.01205	0.14	1.2	1.28	718.3	0.14	58.75	0.03	296.666	0.012
3	0.01512	0.16	1.1	1.48	718.3	0.14	68.30	0.03	296.683	0.017
4	0.01903	0.16	1.2	1.86	718.3	0.14	86.49	0.03	296.678	0.015
5	0.03003	0.14	0.8	2.92	718.3	0.14	136.00	0.03	296.665	0.012
6	0.01300	0.13	0.2	2.74	1116.5	0.09	80.53	0.03	295.860	0.012
7	0.02721	0.17	0.1	3.59	1116.5	0.09	106.53	0.03	295.904	0.012
8	0.02990	0.13	0.3	3.04	1516.1	0.07	66.31	0.03	295.726	0.012
9	0.02961	0.15	0.3	3.68	1516.1	0.07	80.22	0.03	295.694	0.012
10	0.03337	0.14	0.3	2.49	1516.1	0.07	53.97	0.03	295.675	0.012
11	0.03334	0.16	0.3	2.69	1015.7	0.10	87.13	0.03	295.581	0.012
12	0.02139	0.15	0.2	2.96	1015.7	0.10	95.85	0.03	295.608	0.012
13	0.01665	0.11	0.2	1.25	718.3	0.14	56.99	0.03	295.957	0.012
14	0.01261	0.19	1.0	2.11	1116.5	0.01	62.35	0.17	295.542	0.012
15	0.02826	0.09	15.5	1.65	1116.5	0.09	47.59	0.08	295.483	0.014
16	0.03645	0.19	1.3	1.24	1116.5	0.01	36.43	0.08	295.440	0.012
17	0.02173	0.16	0.8	2.91	1015.7	0.10	95.83	0.03	295.612	0.012
18	0.02673	0.16	0.6	3.27	1015.7	0.10	107.12	0.03	295.589	0.012
19	0.03569	0.15	0.7	3.26	1015.7	0.10	107.11	0.03	295.586	0.014
20	0.03236	0.17	0.6	2.17	1314.8	0.08	54.07	0.03	295.559	0.012
21	0.03079	0.16	0.5	2.66	1314.8	0.08	66.09	0.03	295.574	0.012
22	0.03717	0.17	0.5	3.22	1314.8	0.08	80.70	0.03	295.596	0.012
23	0.02512	0.15	0.8	3.54	1314.8	0.08	87.70	0.03	295.578	0.012
24	0.02540	0.18	0.9	2.69	1614.5	0.07	55.37	0.03	297.701	0.042
25	0.03113	0.17	0.9	3.03	1614.5	0.07	62.97	0.03	297.688	0.012
26	0.02737	0.18	1.1	3.48	1614.5	0.07	71.38	0.03	297.693	0.013
27	0.03546	0.17	1.1	3.71	1614.5	0.07	76.45	0.03	297.700	0.013
28	0.03815	0.18	0.8	2.50	1614.5	0.07	51.36	0.03	297.733	0.016

Table 5.5 presents the influence quantities for the linestrength governed by (5.2), or equations (2.15) and (2.16). In this table u_r are the relative standard uncertainties. All other uncertainties given in the table are standard uncertainties.

The analysis of the uncertainty contributions from the quantities in Table 5.5 is as follows:

a) For the product $n \cdot L$ -used as independent variable in Figure 5.6- the relative uncertainty of length $u_r(L)$ is more significant than that of n. This is evident because n is calculated from (2.16) and the u_r's of p and T are lower than that of L. In the same sense, the limiting quantity for the estimation of n is the $u_r(p)$. The reason that L is the main uncertainty source is the lack of knowledge and reproducibility of the optical pathlength for the change of the reflections in the Herriott cell,

b) When $u_r(Area)$ is compared with $u_r(L)$ the accuracy is limited by the area uncertainty in most cases. Only in measurement # 13 the accuracy is limited by the uncertainty of length,

c) The area accuracy is mostly limited by the contribution of the absorbance uncertainty $\{u(Area\text{-}\alpha)\}$ instead of the frequency scale uncertainty contribution $\{u(\nu)\}$. This is due to the lack of areas repeatability during averaging. When the uncertainty contribution of the frequency was larger than that of the area $\{u(Area\text{-}\alpha)/u(\nu) < 1\}$ it was due to the lack of stability of the open confocal etalon during averaging.

The relative standard uncertainty of the linestrength $S_i(T_0)$ is 0.57 %. As the relative uncertainties of the input quantities were of the order of 0.2 % and lower, the main uncertainty contribution to the $u(S_i(T_0))$ was originated by the linear regression model. That was produced by the dispersion of measurements around the linear regression.

6 Improvement of the Absolute Performance and Applications

This chapter presents in section 6.1 the results of amount of CO_2 fraction x_{CO_2} measurement already presented in section 4.4.1 but reprocessed with use of the new value for the R(12) line strength discussed in the previous chapter. After that, two sections evidence the use of the method in a couple of potential applications. Section 6.2 shows results for a multi-component certified gas mixture and section 6.3 deals with CO_2 measurements in room air. Section 6.4 summarizes the uncertainty of the x_{CO_2} measured by TDLAS. Section 6.5 explores the limits for applications of TDLAS as a calibration free method for measurements of x_{CO_2} and section 6.6 gives some recommendations for future work.

6.1 Improvement of the Absolute Performance

Using the measured value $S_i = 1.2549 \cdot 10^{-21}$ $cm^{-1} \cdot molecule^{-1} \cdot cm^2$ (see chapter 5) the data presented in section 4.4.1 (Figure 4.13) have been reprocessed. The resulting deviation of the new TDLAS-based x_{CO_2} values are plotted in Figure 6.1 as relative bias with respect to the gravimetric reference against the gravimetric x_{CO_2} values. The apparent bias of laser based x_{CO_2} results is of the order of 0.4 % and lower [97]. Figure 4.13 exhibited a maximum bias of -1.6 %, however, this apparent bias exists not more with the improved linestrength in Figure 6.1. In Figures 4.13 and 6.1 the uncertainty bars are representing only the uncertainty component of the reproducibility of the measurements and not the total uncertainty, which will be dealt with in section 6.4.

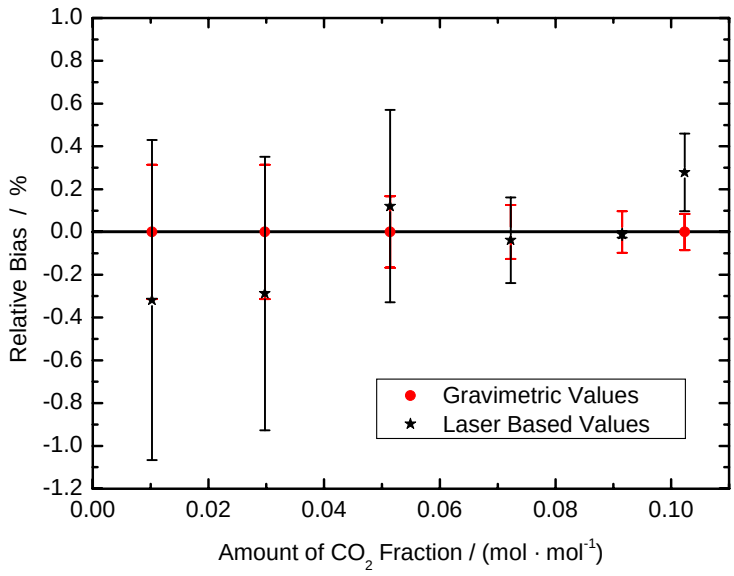

Figure 6.1: Absolute performance for analysis of carbon dioxide. The measured TDLAS-based x_{CO_2} values are compared with their gravimetric counterparts. Values are compared by use of the relative bias (2.37). The uncertainty bars of the gravimetric values are the expanded uncertainty (k=2). The uncertainty bars of the laser based values represent exclusively the reproducibility S_R of the tests.

6.2 Measurements of a Certified Vehicle Exhaust Emission Gas Mixture

The performance of the method was further proved at higher opacity values, i. e. at higher x_{CO_2} values in a more complex matrix: namely in a multi-component gas mixture. An important application of TDLAS could be seen as a certification technique for reference materials, in this case of reference gas mixtures. This application was proved for commercially certified amount of substance values with $x_{CO_2} = 14.1 \cdot 10^{-2}$ mol/mol, $x_{CO} = 5.04 \cdot 10^{-3}$ mol/mol and $x_{Propane} = 197 \cdot 10^{-6}$ mol/mol in N_2 balance. If the method is working properly no interference is expected, especially not with CO, which is the problem in some commercial NDIRs [111]. As predicted in section 4.1, no feature of interference from other substances was present in the absorption spectrum.

Figure 6.2 depicts the result of x_{CO_2} measurements of the multi-component gas mixture. The relative bias of the laser-based x_{CO_2} values with respect to the commercially certified value is presented. The individual values represent the replicates of the TDLAS measurement. The uncertainty bars for the mean of the TDLAS-based values show a repeatability of ± 0.23 %. The repeatability figure was obtained as described in section 4.4.3. The difference between the certified and the TDLAS-based mean value is -0.55 %. This means an agreement of both values considering the uncertainty of the certified value ± 1 % (k=2). Thus, TDLAS has the potential to be used as a calibration-free method in vehicle exhaust emission applications and also as a possible certification method of reference materials.

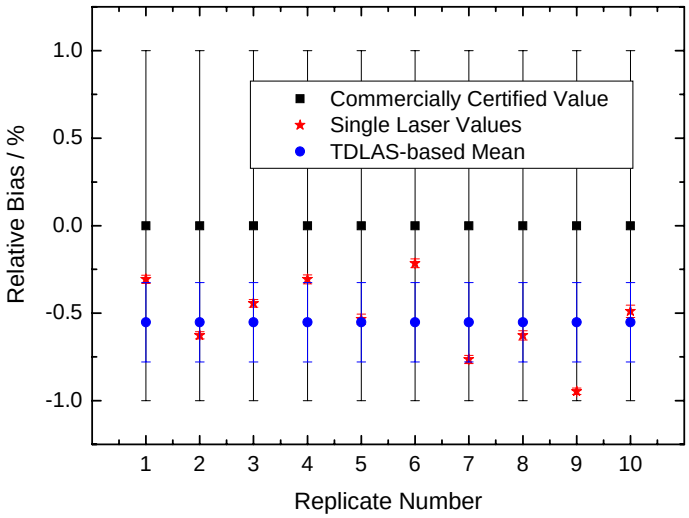

Figure 6.2: Multi-component gas mixture for vehicle exhaust emissions application. The measured TDLAS-based x_{CO_2} values are compared with the commercially certified value. Values are compared in terms of the relative bias. The relative apparent bias of the TDLAS-based mean value with respect to the commercially certified value is -0.55 %. The uncertainty bar of the commercially certified value is the expanded uncertainty of ± 1 % (k=2). The uncertainty bars of the individual laser values represent only the area uncertainty of the Voigt fit. The uncertainty bar of the mean value is the repeatability of the test S_r = 0.23 %.

6.3 Measurements of Carbon Dioxide in Room Air

The performance of the method was also proved at lower opacity conditions, i. e. for x_{CO_2} values in trace levels. Among trace levels, an application is the monitoring of room air quality or in atmosphere. The amount of CO_2 in room air was measured as an unknown sample concentration of CO_2. The effectivity of the method at this level of concentration was controlled with a synthetic gas mixture of CO_2 in N_2. The room air was sampled from the laboratory atmosphere by evacuating the gas cell from atmospheric pressure to a total pressure of 100 hPa. For control, a gravimetric gas mixture with $x_{CO_2} = 400 \cdot 10^{-6}$ mol/mol was prepared as described in section 3.3.

Having a gas absorption cell of constant pathlength the main problem of measuring these atmospheric trace levels of CO_2 is the detection scheme to be used. For the determination of x_{CO_2} in room air a slightly different calculation method was used. It was based on a modification of the *differential absorption* detection technique [112]. The differential spectrum (Figure 6.3 and 6.4) was the result of the subtraction -already in absorbance units- of the measured spectrum with the CO_2 absorption minus the measured spectrum without CO_2 in the gas cell (baseline subtraction). This differential absorption was used because the maximum of the CO_2 absorbance peak was very weak (of the order of < 0.009). With this very low opacity the residual absorption of the CO_2 outside the gas absorption cell was not anymore non-significant. The elimination of the residual CO_2 -even present after purging with pure N_2 (see Figure 4.7) was successfully carried out by the described method. Figures 6.3 and 6.4 depict examples of 100-scans CO_2 spectra for the synthetic-mixture (control) and the room-air sample, respectively. The relatively small values of absorbance allowed to discover the influence of the residual CO_2 in the optical bench at these low sample concentrations. This residual CO_2 is observed in both Figures 6.3 and 6.4 as a curved baseline. The differential spectrum of the absorption minus baseline eliminates the structure. However, for conducting the differential measurements it is important to get a stable baseline for deducting it from the spectrum with the CO_2 sample peak. For example, Figure 6.3 shows a baseline with a larger offset with respect to the measurement with the CO_2 peak than Figure 6.4, where the baseline without CO_2 and the baseline with the CO_2 peak coincide well. Each differential spectrum includes the combination of the uncertainties by the subtraction of the spectrum with CO_2 absorption minus the baseline. The uncertainty bars of the measured spectra in both plots are representing the standard deviation of the averaged spectra. A Voigt fit for the differential spectrum, including its residuals is also depicted in Figure 6.4. The correlation of the residuals has disappeared in all these measurements when the differential correction was applied as was previously discussed in section 4.3.

Such *differential absorption* calculation could be applied to measurements having values of $x_{CO_2} > 1 \cdot 10^{-2}$ mol/mol, but as the line area is much larger than that of a low opacity measurement (i. e. here $x_{CO_2} = 400 \cdot 10^{-6}$ mol/mol), the effect in the improvement of the unbiased TDLAS-based x_{CO_2} results given in Figure 6.1 would not be significant.

The results of both measurements: CO_2 in air (sample) and CO_2 in N_2 (control) are given in Figure 6.5 in amount of carbon dioxide fraction units and in Figure 6.6 in relative units. In Figure 6.5 the expanded uncertainty (U) of the TDLAS-based x_{CO_2}

values is presented for the measurement in air, this value is also presented in the relative units (U_r = 3.3 %) of Figure 6.6a.

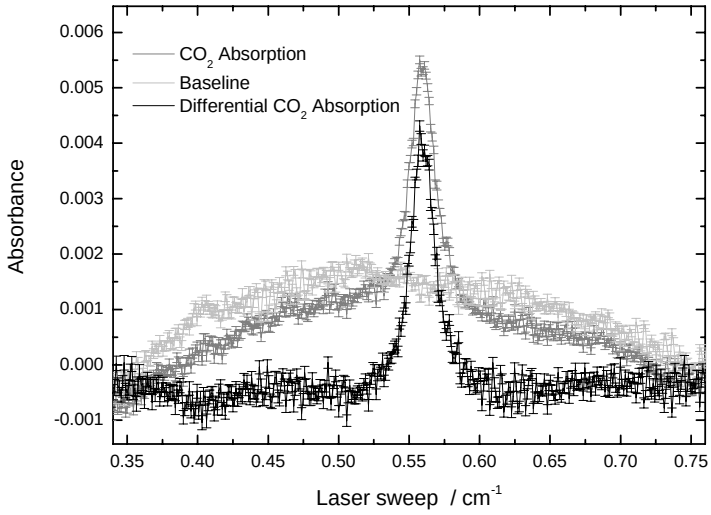

Figure 6.3: Example of differential absorption for a gravimetric $400 \cdot 10^{-6}$ mol/mol CO_2 in N_2 gas mixture. Sequential measurements of the baseline (without the gas mixture in the gas absorption cell) and the CO_2 absorption are depicted. The differential CO_2 absorption is the difference of the CO_2 absorption minus the baseline.

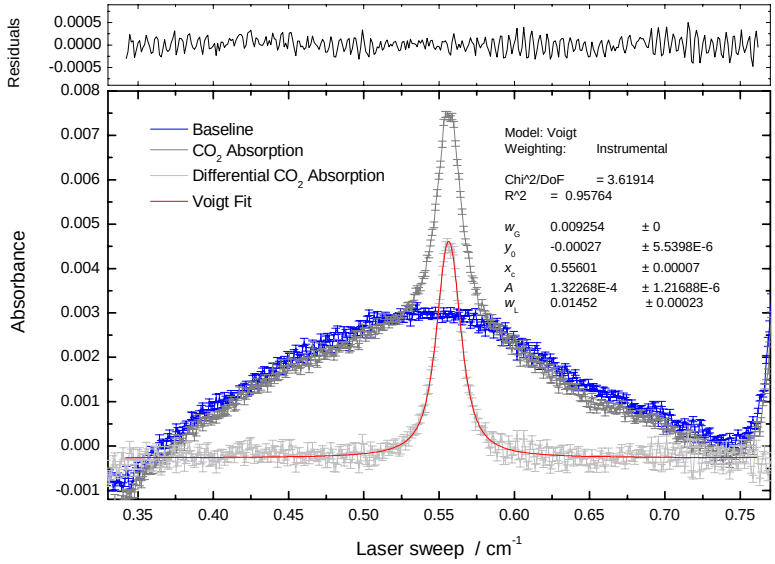

Figure 6.4: Example of differential absorption for CO_2 in room air. Sequential measurements of the baseline (without the air sample in the gas absorption cell) and the CO_2 absorption are depicted. The differential CO_2 absorption is the difference of the CO_2 absorption minus the baseline. A Voigt fit, its parameters as well as the residuals of the fit are shown.

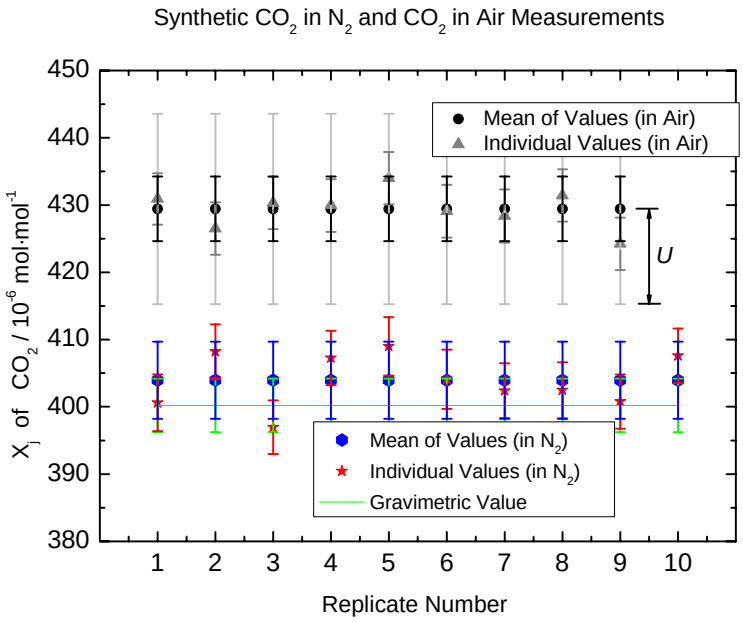

Figure 6.5: x_{CO_2} at room air concentration levels.

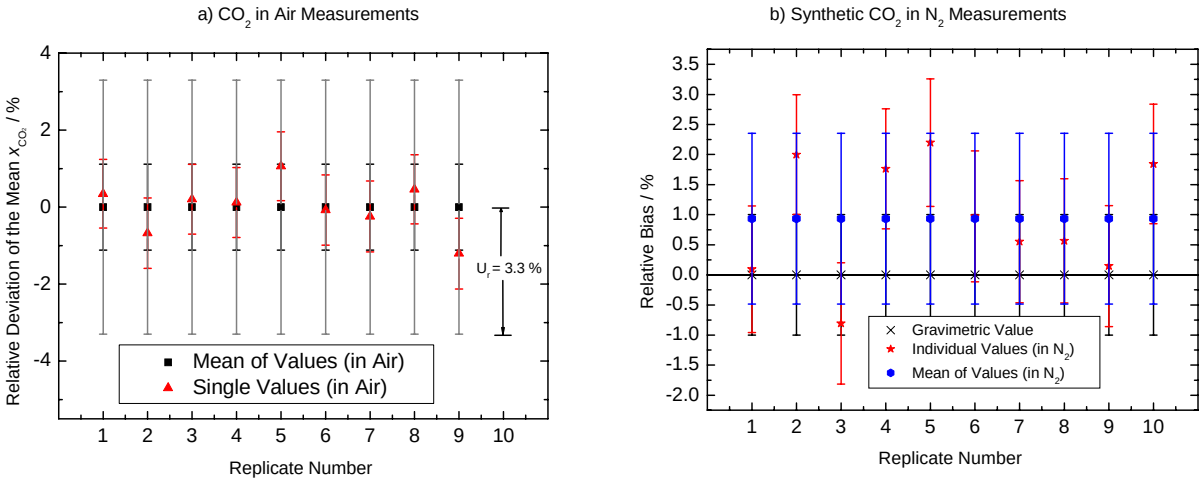

Figure 6.6: Relative x_{CO_2} at room concentration levels. a) CO_2 in air measurements. b) Synthetic CO_2 in N_2 measurements.

The relative units in Figure 6.6 allow to compare the results. Comparing Figure 6.6 a) and b) having similar magnitudes of x_{CO_2}, the repeatability represented by the uncertainty bars of the mean values is ± 1.1 % and ± 1.4 % for CO_2 in air and in nitrogen, respectively. Repeatability was obtained as described in section 4.4.3. The uncertainty bars of the single values are the uncertainties of the Voigt-fitted area with an order of magnitude of ± 0.9 to ± 1 % for CO_2 in air and in nitrogen, respectively. As the repeatabilities and the uncertainties of the Voigt-fitted area have a similar

order of magnitude, the uncertainty contribution introduced by the Voigt fit is more significant compared to the results for $x_{CO_2} > 1 \cdot 10^{-2}$ mol/mol (see e.g. Figure 4.14). Thus, considering the uncertainties between- and within- replicates, as was done in this work (see 4.4.3), it is very important for getting reliable results at low opacities. For the synthetic gas mixture in Figure 6.6 b) the relative bias of the TDLAS-based x_{CO_2} was about 0.93 %. It is smaller than the repeatability S_r of the TDLAS measurements. Also, TDLAS-based x_{CO_2} mean value and the gravimetric value agree considering that this relative bias is lower than ± 1 % uncertainty of the gravimetric x_{CO_2} depicted in Figure 6.6 b).

As it can be appreciated in Figures 6.2 and 4.14, the variability between single values (replicates) was larger than the uncertainty within each replicate, in other words, the main contribution to the repeatability is resulting from the variability between single values of line areas and not from the respective contribution introduced by the Voigt-fitted areas. As was already mentioned for Figure 6.6, the variability of the method (± 1.2 to ± 1.4 %) was of similar order as within the variability of replicates (± 0.9 to ± 1.1 %). Results of the repeatability for the measurements of CO_2 in room air suggested that the variability within the replicate almost explain the total variability of the measurements. It means that the measurement value of the area is more noise limited than drift limited. The reason of the different contribution of between- and within-variability in this plots was the smaller area of the absorption peak -it was a consequence of the smaller absorbance for lower x_{CO_2} values- (Figures 6.3 and 6.4) when compared with areas of larger x_{CO_2} values (Figure 4.10). The global value for repeatability and reproducibility varies depending on the area of the absorption peak from ± 0.1 to ± 0.9 %. It can be concluded from the measurements that the reproducibility of the method was better than 0.9 % for the interval of x_{CO_2} from $400 \cdot 10^{-6}$ to $14 \cdot 10^{-2}$ mol/mol validated in this work.

6.4 Uncertainty Budgets of TDLAS

Table 4.4 in section 4.4.3 gave an example of the uncertainty budget of a TDLAS-analyzed CO_2 gas mixture. The main influence quantity, the linestrength, was improved with its traceable measurement presented in chapter 5. Using this new $S_i(T_0)$ value, the uncertainty budget for the example of Table 4.4 is now given in Table 6.1. In this table it is shown that the uncertainty has been improved from 3.7 % (Table 4.3) to 1.7 % (Table 6.1). Not only the uncertainty but also the apparent bias was diminished with this improved linestrength value, i. e. as mentioned in section 6.1 from -1.6 % to an amount of the size of the uncertainty of the gravimetric reference values < |± 0.4 %|. This successful correction factor was possible although the deviations were within the uncertainty of the measurement result of 3.7 %. Therefore, a conclusion can be drawn that the uncertainty estimated on the basis of the *FSR* from FTIR measurements is too large (s. 4.3). Thus, the *FSR* calculated with (4.3) was only subsequently used. The final and valid uncertainty budget of this calculation is given in Table 6.1. The main influence quantity still corresponds to the measured linestrength. The contribution of the *FSR* is not anymore significant. In addition if the uncertainty of the *FSR* were slightly larger its contribution to the combined uncertainty would not be significant any more. The contribution of the influence quantities is more balanced, that is, more than only one or two influence quantities contributes significantly to the combined uncertainty.

Table 6.1: Uncertainty budget of x_{CO_2} by TDLAS using a reliable linestrength value.

Quantity	Value	Standard Uncertainty	Probability Distribution	Degrees of Freedom	Sensitivity Coefficient	Uncertainty Contribution	Index
L	100.000 cm	0.289 cm	Rectangular	∞	$-920\cdot10^{-6}$	$-260\cdot10^{-6}$ mol/mol	11.7 %
T	295.450 K	0.200 K	Normal	50	$580\cdot10^{-6}$	$120\cdot10^{-6}$ mol/mol	2.3 %
P_{total}	101.000 hPa	0.300 hPa	Normal	50	$-910\cdot10^{-6}$	$-270\cdot10^{-6}$ mol/mol	12.4 %
FSR	0.048486 cm^{-1}	$38.8\cdot10^{-6}$ cm^{-1}	Normal	50	1.9	$73\cdot10^{-6}$ mol/mol	0.9 %
FSRSP	43.4870 SP	0.0230 SP	Normal	5	$-2.1\cdot10^{-3}$	$-48\cdot10^{-6}$ mol/mol	0.4 %
Area	25.7518 SP	0.0164 SP	Normal	50	$3.6\cdot10^{-3}$	$58\cdot10^{-6}$ mol/mol	0.6 %
$S_i(T_o)$	$1.2549\cdot10^{-21}$ cm	$7.20\cdot10^{-24}$ cm	Normal	50	$-73\cdot10^{18}$	$-530\cdot10^{-6}$ mol/mol	46.4 %
Q_{To}	33.408 Arbitrary	0.100 Arbitrary	Normal	50	$-2.7\cdot10^{-3}$	$-280\cdot10^{-6}$ mol/mol	12.7 %
Q_T	33.2066 Arbitrary	0.0996 Arbitrary	Normal	50	$2.8\cdot10^{-3}$	$280\cdot10^{-6}$ mol/mol	12.7 %
x_{CO2}	0.09170 mol/mol	$773\cdot10^{-6}$ mol/mol	t-assumed	190	**U_r (x_{CO_2}) = 1.7 % (k = 2)**		

Using the same *FSR* given by (4.3) and the linestrength $S_i(T_0) = 1.2549\cdot10^{-21}$ $cm^{-1}\cdot molecule^{-1}\cdot cm^2$, uncertainty budgets for the whole interval of CO_2 gas mixtures measured by the free-of-calibration TDLAS method were calculated. Their results are presented in Table 6.2.

Table 6.2: Most significant uncertainty sources for TDLAS.

Quantity	X_{CO_2} (TDLAS) / (mol/mol) :	$408\cdot10^{-6}$	$1.018\cdot10^{-2}$	$5.121\cdot10^{-2}$	$10.27\cdot10^{-2}$	$14.23\cdot10^{-2}$
	Standard Uncertainty	**Index (% of contribution to the combined uncertainty)**				
L	Constant	3.0 %	8.2 %	11.0 %	11.4 %	8.0 %
T	Constant	0.6 %	1.6 %	2.2 %	2.2 %	1.6 %
P_{total} *	Constant	3.3 %	9.0 %	11.8 %	12.2 %	34.1 %
FSR	Constant	0.9 %	2.5 %	3.4 %	3.5 %	2.4 %
FSRSP	Constant	0.1 %	0.3 %	0.4 %	0.4 %	0.3 %
Area	relative grow with decrease of X_{CO_2}	73.4 %	28.0 %	3.9 %	0.8 %	4.9 %
$S_i(T_o)$	Constant	12.0 %	32.5 %	43.5 %	45.0 %	31.5 %
Q_{To}	Constant	3.3 %	8.9 %	11.9 %	12.3 %	8.6 %
Q_T	Constant	3.3 %	8.9 %	11.9 %	12.3 %	8.6 %
Relative Expanded Uncertainty U_r (x_{CO_2}) with (k = 2)		**3.3 %**	**2.0 %**	**1.7 %**	**1.7 %**	**2.0 %**

* For $x_{CO_2} = 14.23\cdot10^{-2}$ mol/mol, P_{total} was not 100 but 50 hPa

Table 6.2 shows the evolution of the most significant uncertainty sources with the change of amount of carbon dioxide fraction. At levels of good signal to noise ratio (from x_{CO_2} = 1 to $14 \cdot 10^{-2}$ mol/mol, see e. g. Figure 4.5), the main uncertainty source is still the linestrength -excluding the $x_{CO_2} = 14 \cdot 10^{-2}$ mol/mol gas mixture, for which the main uncertainty source was P_{total}-. At these x_{CO_2} values the expanded uncertainty was $\leq$ 2.0 %. But at lower signal to noise ratio (CO_2 in air measurements) the main uncertainty source becomes the area under the fit. For this x_{CO_2} value the uncertainty increased to 3.3 %. From these results it is concluded that the accuracy -given the constant *L*- is controlled at higher x_{CO_2} values by the linestrength and at trace levels it is limited by noise. Improvements of noise are possible with the use of larger optical pathlengths, leading to higher signal to noise ratios.

The highlighted cells in Table 6.2 show the influence quantities with a significant contribution to the combined x_{CO_2} uncertainties. Balanced uncertainty budgets were obtained for $x_{CO_2} > 1 \cdot 10^{-2}$ mol/mol.

6.5 Limits of Application of TDLAS as a calibration-free method

TDLAS as a calibration-free method in the sense of the present study requires the application of single-line spectroscopy [113]. This means that the molecule should have an infrared line-spectrum which is resolvable at the Doppler limit, which in practice includes most of the molecules with up to five atoms [14]. Some of the larger molecules may also be covered by this technique [14].

The method is especially useful for in situ trace gas analysis because of its large sensitivity and selectivity [14]. For sensitivity and selectivity reasons the application could be limited to the operation in vacuum at reduced pressures.

The spectral interval where the integration of the single line can be performed has to cover the total area under the absorption peak. If this is not fulfilled, negative systematic bias is expected to be found.

Operation temperatures are limited to intervals of temperatures where the uncertainty of the partition function is not prohibitively large. For temperatures from 70 to 415 K the uncertainty of the partition function is smaller that 0.1 %. For higher temperatures, such as combustion temperatures, deviations are expected in the partition function, e. g. as was described for CO_2 in section 2.1.4. If these deviations are not taken into account it can be an additional source of bias in the results.

An additional limitation of the TDLAS as a calibration-free method in gas analysis is the validity of the measurement equation, which is discussed in the next section.

6.5.1 Scope of the Validity of the Measurement Equation

In the description of the Beer-Lambert law in section 2.2.1 the suppositions for the application of the equations were highlighted in italics. Taking advantage of the laser properties and use of a narrow linewidth tunable diode laser, the criteria of *parallel beam (*directionality) and *monochromaticity* can be fulfilled. For gas analysis the restriction of *small optical depths* and *weekly absorbing media* is in some way overcome. *Homogeneity of the absorbing material* or the precondition of a uniform absorbing medium is satisfied by use of gas mixtures independently prepared and

appropriately handled (premixed). This last happened in laboratory conditions; in field measurements caution should be provided.

Thermodynamic equilibrium in temperature was assured in this work by conditioning the gas mixtures to the room temperature of at least one day previous to any analysis. This is normal practice in gas metrology (e. g. for the certification of static gas mixtures). But for example, in case of extractive sampling at higher temperatures than the gas cell, the temperature equilibrium has to be considered.

The Beer-Lambert law for gaseous samples in the form of (2.18) is applicable only for *ideal gases*. This criterion is met for diluted gas concentrations in a matrix of an ideal gas, which brings a larger potential of this technique to the trace levels of concentration. Additionally, the operation of the gas cell at vacuum conditions renders lower deviations of the ideal gas behavior. The non-ideal behavior of the gas sample can be treated by its respective uncertainty considerations, e. g. from those of the standards [106, 114]. However, for the calculation of the compressibility factor for a real gas state equation the knowledge of the composition of the gas mixtures is needed. This situation can limit the consideration of real gases to binary mixtures, or necessitate the measurement of the sample composition by other techniques.

Deviations from the Beer-Lambert law are normally discussed in literature in terms of *non-linear* behavior of the absorbance with respect to the amount concentration, but for gas phase instead of amount concentration, amount of substance fraction is the preferred quantity to express results of measurements. Moreover, linearity limitations of the Lambert-Beer law could apply in cases when the peak maximum is used for quantification, but for an isolated line the discussion has to consider the integral absorbance. In addition, any non linear detector response would cause deviations in the transmittance (consequently also in absorbance) at different levels of opacity. Thus, in such cases, a calibration of detectors or a calibration of the transmittance scale should be considered. The linearity and subsequent the necessity of such calibration could be probed plotting the integral absorbance (area under the peak in question) -or other useful influence quantity of the Beer-Lambert law- versus amount of substance fraction. If a calibration of the transmittance scale were used the non linearity could be corrected.

The application of (2.18) may suffer from the following problems due to both *limitations of instrumentation* and to *chemical factors* [115].

Within *instrumental limitations* are: (a) the stray radiations reaching the detector (reflected within the instrument), (b) the power fluctuations of the radiation source and detector amplification system, and (c) the sensitivity changes of the detector. However, a double beam spectrometer tends to cancel out most of the random causes of deviation [115], like those from (b) and (c). By this reason a laser spectrometer using two measurement beams might be of superior design for calibration-free measurements.

Chemical factors arise from the nature of the gas sample. Among them are:

(a) Scattering of light due to particulates in the sample. Scattering can be considered as insignificant in *moderate concentrations* since the quality of gases are certainly

free of dust particles, but it could be not the case for in situ measurements, where filtering of samples in some applications would be needed,

(b) Adsorption or reaction of the sample with the internal walls of the cell, dissociation of the substance, change of composition by chemical reactions, shifts in chemical equilibrium as a function of concentration need to be considered. Some of these effects are especially important to be considered for reactive or corrosive substances. A realistic solution for the wall effect is the passivation of the gas cell or/and selection of more universal compatible materials for gas cells -e. g. extruded aluminium-.

(c) Deviations in absorption coefficients at high concentrations due to electrostatic interactions between molecules in close proximity could be more problematic for analyzing strongly polar substances (not for CO_2) or charged substances.

6.6 Recommendations for Future Work

Possible future potentials of the TDLAS technique in gas analysis recommended to research are:

a) to confirm the potentials of accurate isotopic ratio analysis and with this, the possibility of TDLAS like that of the potential primary method of isotopic dilution mass spectrometry (IDMS) [35,83], which could be called isotope dilution laser spectroscopy (IDLS) to prove the potential of the method as a candidate primary ratio method directly applied (direct traceability for field measurements).

b) to evaluate the limits of spectra averaging by use of the Allan variance [47]. This would allow confirm some good reproducibilities of 0.01 % for the technique reported in [24]. To know the limits of spectra averaging automation of the data processing by each individual scan is needed.

c) to extent the measurement procedure developed in this thesis to other gas species, especially to non stable or reactive gas species and to lower trace levels of concentrations for in situ applications and confirmation of the direct traceability concept without precedents in gas analysis. Passivation technique experiences developed in gas specialty industries and use of better gasket materials for gas-cells can make these measurements possible.

d) to prove the potential of the technique for purity gas analysis.

e) to use stable frequency standards in a third measurement beam is recommended for the evaluation of the frequency scale stability of the TDLAS spectrometer.

f) to check the possibility to use the presented method for routine instruments. Here the advantage of calibration-free measurements could lead to basic improvements concerning the

- measurement accuracy (SI traceable results) and reliability

- maintenance (no need of calibration with test gases) and cost.

The extension of the spectrometer to other laser sources including QCLs and external cavity diode lasers could be of advantage. The first will render lower detection limits due to the more sensitive MIR wavelength range and the second a cheaper alternative to near infrared DFB-lasers [117]. With the use of lasers having a larger tuning range it would be possible to measure more lines simultaneously.

A deeper knowledge of the limits of the technique, especially of the reproducibility and the trueness will allow the prediction of more accurate fundamental spectroscopic parameters: broadening coefficients and linestrengths, and of potential fit-for-intended use applications. More accurate fundamental spectroscopic parameters would render in the future possible free of calibration measurements of not only amount of substance, but also of temperature and pressure, that would save costs in peripheral measurement instruments like pressure and temperature sensors.

7 Conclusions

The aim of this work was to investigate the potential of tunable diode laser absorption spectroscopy (TDLAS) in traceable calibration-free measurements of amount of substance fractions x_j. As an example, carbon dioxide was selected to probe the calibration-free performance of the method in the frame of metrology including traceability and uncertainty analysis of amount of carbon dioxide fraction x_{CO_2}. This method is based on the Beer-Lambert law. All significant input quantities and correction factors that generate the TDLAS-based x_{CO_2} results were considered. The respective measurement equation with all the input quantities expressed in SI-units (directly traceable to SI units) was used for the TDLAS-based determination of x_{CO_2}.

In order to improve the uncertainty of the TDLAS-based results of amount of CO_2 fraction and to establish the traceability of the result a traceable linestrength value of the R12 line of the $\nu_1+2\nu_2+\nu_3$ band of CO_2 had to be measured. It produced a result of $1.2549 \cdot 10^{-21}$ $cm^{-1} \cdot molecule^{-1} \cdot cm^2$ with an expanded uncertainty of 1.1 % (k=2), whose value is -1.4 % lower but in agreement within the uncertainty (2 to 5 %) given in the HITRAN database [92] for this line. The lower uncertainty of the measured linestrength represents an improvement in accuracy and reliability compared to that of HITRAN database.

In order to prove the absence of bias in the improved TDLAS-based x_{CO_2} results, gravimetric values of x_{CO_2} were used and compared with their respective TDLAS-measured x_{CO_2} results in the interval of $1 \cdot 10^{-2}$ to $10 \cdot 10^{-2}$ mol/mol. This comparison showed concordance and a *non significant* or *apparent bias* of $< |\pm 0.4\ \%|$ giving the expanded uncertainty of the TDLAS-based x_{CO_2} values of < 2 % (k=2). Based on these achieved uncertainties, it is thought that the proved TDLAS method is *fit-to-intended-use* in the direct traceability scheme for field applications in gas analysis. The large traceability chains using reference materials would effectively be reduced by the application of such a method. It could be useful, e. g. in the monitoring of CO_2 emissions in different combustion processes, including stack and automotive exhaust emission tests.

The performance of the TDLAS method was probed in two applications at extreme opacity conditions for confirming the validity of the measurement equation: the measurement of x_{CO_2} in a commercially certified multi-component gas mixture used for the calibration of vehicle exhaust emissions sensors and in CO_2 measurements in room air. For the multi-component gas mixture the *apparent bias* was -0.55 %, which was concordant within the uncertainty of the certified value $\pm$ 1 % (k=2) and the bias was not significant within the uncertainty of 2 % (k=2) of the TDLAS-based x_{CO_2} value. Thus, TDLAS has the potential to be used as a calibration-free method in vehicle exhaust emission applications and has also the potential to be used as a possible certification method of reference materials. For the CO_2 measurements in room air a synthetic gravimetric gas mixture of CO_2 was also prepared. The *apparent bias* of the TDLAS-based x_{CO_2} was +0.93 %. It was also concordant with the 1 % (k=2) uncertainty of the gravimetric x_{CO_2} and the bias was also not significant considering the uncertainty of TDLAS-based x_{CO_2} value 3.3 % (k=2). The uncertainty of the CO_2 measurements in room air could be improved by use of larger pathlengths (i. e. higher signal to noise ratios) and by considering the recommendations given in chapter 6 to improve the reproducibility of results.

By the first time it was shown a GUM-compliant, *transparent* and complete uncertainty budget of calibration-free amount of carbon dioxide fraction measurements by TDLAS. The uncertainty budgets fulfilled *state of the art* and internationally recognized metrological principles, including establishment of traceability of the measurement results to the SI system of units. The uncertainty budgets evidenced the importance to show adherence to the complete uncertainty estimation philosophy of the GUM. That is, considering all influence quantities and corrections factors that substantially contribute to the uncertainty, having complete and transparent uncertainty budgets, and reporting informative uncertainties of measurement results.

The TDLAS-based method developed in this work is a method without precedent among the existing methods in gas analysis and gas metrology for calibration-free performance or direct traceability better called: *potential primary method directly applied*. For this kind of methods the uncertainty has not to be necessarily as low as that of a primary method based on the also larger uncertainties achieved for field measurements using the large traditional traceability chains. The calibration-free TDLAS method is of fundamental importance in the concepts of Metrology in Chemistry. That is the establishment of the direct traceability of amount of substance fraction measurements. Thus, the international comparability of calibration-free measurement results performed by TDLAS can be established. It opens also the potential of equivalent measurement procedures to be developed for TDLAS instruments and to be *fit-to-intended-use* applied in the market of gas analysis. This is especially important in fields where a chemical reference gas specie (e. g. reference material) does not exist until now, especially for *in situ* measurements of reactive and non-stable compounds.

References

1. Cooper D. E., Martinelli R. U., et al., Measurement of $^{12}CO_2$:$^{13}CO_2$ ratios for medical diagnostics with 1.6 μm distributed-feedback semiconductor diode lasers, Applied Optics, Vol. 32, No. 33, 6227-6731 (1993)

2. Bowling David R., Sargent Steve D., Tanner Bert D., Ehleringer James E., Tunable diode laser absorption spectroscopy for stable isotope studies of ecosystem- atmospheric CO_2 exchange, Agricultural and Forest Meteorology 118, 1-19 (2003)

3. McManus J. B., Zahniser M. S, et al., Infrared laser spectrometer with balanced detection for measurement of isotopic ratios of carbon gases, Spectrochimica Acta Part A, 58, 2465-2479 (2002)

4. Uehara K., Yamamoto K. et al., Site-selective nitrogen isotopic ratio measurements of nitrous oxide using 2 μm diode lasers, Spectrochimica Acta Part A, 59, 957-962 (2003)

5. Gharavi M. and Buckley S. G., Single diode laser sensor for wide-range H_2O temperature measurements, Applied Spectroscopy, Vol. 58, No. 4, 468-473 (2004)

6. Lack M., Winter F., et al., Spektroskopischer Einsatz neuer langwelliger (bis 2 μm) Diodenlaser (VCSEL) für schwierige Bedingungen, Technisches Messen, 70, 294-305 (2003)

7. ISO guide 35: Certification of reference materials - General and statistical principles, 2nd ed., ISO, Geneva (1989)

8. Ebert V., Gasanalyse mit Nahinfrarot-Diodenlasern, Technisches Messen, 68, 9, 363-364 (2001)

9. news in http://optics.org/

10. Wielgosz R. I., CCQM primary methods symposium: how far does the light shine?, Accred. Qual. Assur., 6, 329-331 (2001)

11. Webber M. E., Diode laser measurements of NH_3 and CO_2 for combustion and bioreactor applications, Dissertation, Stanford University, USA (2001)

12. Besson J. P., Schilt S. et al., Sub-ppm multi gas sensing based on photoacoustic spectroscopy using DFB laser diodes, VDI- Berichte Nr. 1863, 4. Konferenz über Optische Analysenmesstechnik in Industrie und Umwelt, 189 - 196 (2004)

13. Kleine D., Hochempfindlicher Spurennachweis mit Cavity Ring-Down Spektroskopie im sichtbaren und infraroten Spektralbereich, Dissertation, Heinrich-Heine Universität Düsseldorf (2001)

14. Werle P., A review of the recent advances in semiconductor laser-based gas monitors, Spectrochimica Acta Part A, 54, 197-236 (1998)

15. Roller C., Khosrow N., et al., Nitric oxide breath testing by tunable-diode laser absorption spectroscopy: application in monitoring respiratory inflammation, Applied Optics, Vol. 41, No. 28, 6227-6731 (2002)

16. Henningsen J., Measurement of free SO_2 in wine with a 7.4-µm difference frequency spectrometer, Appl. Phys. B, 76, 451-456 (2003)

17. Berezin A., Bugoslavskii Yu., et al., Measurement of ethanol concentration with near infrared diode lasers, 2nd International conference on tunable diode laser spectroscopy (1998)

18. Ebert V., Fernholz T., et al., Diodenlaserbasierte, probennahmefreie Multikomponenten-Gasanalyse in einem 1000 MW_{th}-Gaskraftwerk, Technisches Messen, 68, 9, 406-414 (2001)

19. Mihalcea R. M., Baer D. S., et al., Diode laser sensor for measurements of CO, CO_2 and CH_4 in combustion flows, Applied Optics, Vol. 36, No. 33, 8745-7852 (1997)

20. Ankerhold G. and Buchtal R., Einsatz von Diodenlaserspektroskopie für die industrielle Gasmesstechnik, Technisches Messen, 68, 9, 415-423 (2001)

21. Linnerud I., Kaspersen P., et al., Gas monitoring in the process industry using diode laser spectroscopy, Appl. Phys. B, 67, 297-305 (1998)

22. Nelson D. D., Zahniser M. S, et al., A tunable diode laser system for the remote sensing of on-road vehicle, Appl. Phys. B, 67, 433–441 (1998)

23. Ebert V., Giesemann C., et al., Simultaner CH_4/H_2O-In-Situ-Nachweis in der Stratosphäre mittels hochauflösender Diodenlaserabsorptionsspektroskopie, VDI- Berichte Nr. 1863, 4. Konferenz über Optische Analysenmesstechnik in Industrie und Umwelt, 149 - 154 (2004)

24. Werle P., Slemr F., et al., Near- and mid-infrared laser-optical sensors for gas analysis, Optics and Lasers in Engineering, 37, 101-114 (2002)

25. Barrass S., Gérard Y., et al., Near-infrared diode laser spectrometer for the remote sensing of vehicle emissions, Spectrochimica Acta Part A, 60, 3353-3360 (2004)

26. Durry G., Amarouche N., In situ sensing of the middle atmosphere with balloonborne near-infrared laser diodes, Spectrochimica Acta Part A, 60, 3371-3379 (2004)

27. Ebert V., Extractive and In-situ detection of gases by diode laser based absorption spectroscopy in near infrared, 3rd gas analysis symposium & exhibition, Amsterdam, The Netherlands (2004)

28. Webber M. E., Kim S., et al., In *situ* combustion measurements of CO_2 by use of a distributed-feedback diode-laser sensor near 2.0 μm, Applied Optics, Vol. 40, No. 6, 821-828 (2001)

29. Mihalcea R. M., Webber M. E., et al., Diode laser absorption measurements of CO_2, H_20, N_2O, and NH_3 near 2.0 μm, Applied Physics B, 67, 283-288 (1998)

30. Sassi M. P., Zucco M., et al., Accurate gas mixture concentration measurements without the use of reference gases, SPIE, Vol. 4829, 907-909 (2003)

31. Henningsen J. and Simonsen H., Quantitative wavelength-modulation spectroscopy without certified gas mixtures, Appl. Phys. B, 70, 627-633 (2000)

32. Henningsen J., Simonsen H., et al., The 0 → 3 overtone band of CO: precise linestrengths and broadening parameters, Journal of Molec. Spec., 193, 354-362 (1999)

33. ISO/IEC 17025, General requirements for the competence of testing and calibration laboratories, ISO, Geneva (1999)

34. ISO 9001 Quality management systems - Requirements, ISO, Geneva (2000)

35. Milton Martin, NPL, National metrology system programme for quantum metrology, public release version, Project 3.5 High-accuracy traceable analysis by IDMS, United Kingdom, 90-94 (2001)

36. Alink A., The first key comparison of primary standard gas mixtures, Metrologia, 37, 35-49 (2000)

37. Van der Veen A. M. H., Pilot comparison CCQM-P41: Greenhouse gases, confidential report to participants, Delft (2003)

38. Milton M. J. T. and Quinn T. J., Primary methods for the measurement of amount of substance, Metrologia, 38, 289-296 (2001)

39. De Bièvre P., The key elements of traceability in chemical measurement: agreed or still under debate?, Accred. Qual. Assur., 5, 423-428 (2000)

40. Richter W. and Dube G., Measurement standards and the general problem of reference points in chemical analysis, Metrologia, 34, 13-18 (1997)

41. Ellison S. R. L., King B., et al., EURACHEM/CITAC guide, Traceability in chemical measurement, (2003)

42. U. S. Environmental Protection Agency, EPA traceability protocol for the assay and certification of gaseous calibration standards, EPA-600/R-97/121(1997), free available in http://www.epa.gov/ttn/emc/news.html

43. NIST, Chemical Science and Technology Laboratory, page 16 and 24, Annual report federal year (2004)

44. Haerri H. P., Eine neue Methode fuer die Spurenmessung von Gasen, metINFO, Vol. 10, No. 3, 10-15 (2003)

45. Rothman L.S., Jacquemart D., et al., The HITRAN 2004 molecular spectroscopic database, J. Quant. Spectrosc. Radiat. Transfer, Vol. 96, 139–204 (2005)

46. BIPM, IEC, ISO, IFCC, IUPAC, IUPAP and OIML, Guide to the expression of uncertainty in measurement, first edition (1993)

47. Werle P., Mücke R., et al., The limits of signal averaging in atmospheric trace-gas monitoring by tunable diode-laser absorption spectroscopy (TDLAS), Appl. Phys. B, 57, 131-139 (1993)

48. Lepère M., Line profile study with tunable diode lasers, Spectrochimica Acta A, 60, 3249-3258 (2004)

49. Duggan P., Sinclair P. M., et al., Testing lineshape models: measurements for υ = 1-0 CO broadened by He and Ar, Journal of Molec. Spec., 186, 90-98 (1997)

50. Kovalevsky J., The consequences of the mutual recognition of measurement standards for international metrology, Accred. Qual. Assur., 5, 409-413 (2000)

51. Kaarls R. and Quinn T. J., The comité consultative pour la quantité de matière: a brief review of its origin and present activities, Metrologia, 34, 1-5 (1997)

52. http://msl.irl.cri.nz/si-units/chemical/metrology.html

53. Kaplan S. G. and Hanssen L. M., Silicon as a standard material for infrared reflectance and transmittance from 2 to 5 μm. Infrared Physics &Technology, 43, 389-396 (2002)

54. Van Deijck W., Accreditation: worth of the trouble?, Accred. Qual. Assur. 1, 197-200 (1996)

55. Khristenko S.V., Maslov A.I., and Shevelko V.P.. Molecules and their spectroscopic properties. Springer-Verlag (1998)

56. Herzberg G., Molecular spectra and molecular structure II: Infrared and raman spectra of polyatomic molecules, Krieger Publishing Company, Reprint edition (1991)

57. Rothman L. S., Rinsland C. P., et al., The HITRAN molecular spectroscopic database and HAWKS (HITRAN atmospheric workstation): 1996 edition, J. Quant. Spectrosc. Radiat. Transfer, Vol. 60, No. 5, pp. 665-710 (1998)

58. Rothman L. S. and Young L. D. G., Infrared energy levels and intensities of carbon dioxide – II, J. Quant. Spectrosc. Radiat. Transfer, Vol. 25, 505–524 (1981)

59. Gamache R. R, Hawkins R. L., and Rothman L. S., Total internal partition sums in the temperature range 70-3000 K: atmospheric linear molecules, Journal of Molec. Spectros. 142, 205-219 (1990)

60. Wattson R. B. and Rothman L. S., Direct numerical diagonalization: wave of the future, JQSRT, Vol. 48, 5/6. 763-780 (1992)

61. Rothman L. S., R. L. Hawkins, et al., Energy levels, intensities, and linewidths of atmospheric carbon dioxide bands, JQSRT 48, 5/6. 537-566 (1992)

62. Nelder J. A. and Mead R., A simplex method for function minimization, Comput. J., 7, 308-131 (1965)

63. Maki A. G. and Wells J. S., NIST Special Publication 821, US Department of Commerce (1991)

64. Humlicek J., Optimized computation of the Voigt and complex probability functions, J. Quant. Spectrosc. Radiat. Transfer, Vol. 27, No. 4, 437-444 (1982)

65. Whiting E. E., An empirical approximation to the Voigt profile, J. Quant. Spectrosc. Radiat. Transfer, Vol. 8, 1379-1384 (1968)

66. Roston G. D. and Obaid F.S., Exact analytical formula for Voigt spectral line profile, J. Quant. Spectrosc. Radiat. Transfer, Vol. 94, 255-263 (2005)

67. Di Rocco H. O., Exact expression of the Voigt profile function, J. Quant. Spectrosc. Radiat. Transfer, Vol. 92, 231-237 (2005)

68. Luque J. M., Calzada M. D., et al., A new procedure for obtaining the Voigt function dependent upon the complex error function, J. Quant. Spectrosc. Radiat. Transfer, Vol. 92, 151-161 (2005)

69. Varguesse P. L. and Hanson R. K., Collisional narrowing effects on spectral line shapes measured at high resolution, Applied Optics, 23, 14, 2376-2385 (1984)

70. Guenzler H., Akkreditierung und Qualitätssicherung in der Analytischen Chemie, Springer-Verlag (1994)

71. http://www.bipm.fr/en/committees/cc/ccqm/

72. De Bièrve, Report on the first meeting of the Consultative Committee (to CIPM/BIPM) on Amount of Substance, BIPM, Paris, 19-21 April 1995 , Accred. Qual. Assur., 1, 37-39 (1996)

73. Kaarls R. and Quinn T., The Comité Consultatif pour la Quantité de Matière: a brief review of its origin and present activities, Metrologia, 34,1-5 (1997)

74. BIPM, IEC, IFCC, ISO, IUPAC, IUPAP and OIML, International vocabulary of basic and general terms in Metrology (VIM), DIN, second edition (1994)

75. Chu P. M., Guenther F.R., Rhoderick G. C., and Lafferty W. J., The NIST quantitative infrared database, J. Res. Nat. Inst. Stand. Technol., 104, 1, 59-81(1999)

76. http://www.irmm.jrc.be/html/activities/isotopic_measurements/isotopic_measurements.htm

77. http://www.bipm.fr/en/scientific/chem/gas_metrology/

78. Quinn T.J., Primary methods of measurement and primary standards, Metrologia 34, 61-65 (1997)

79. Taylor P., Kipphardt H., De Bièvre P., The definition of primary method of measurement (PMM) of the 'highest metrological quality': a challenge in understanding and communication, Accred. Qual. Assur. 6,103-106 (2001)

80. Milton M. J. T., Marschal A., Frequently-asked questions about primary methods of measurement, Accred Qual Assur, 6,270-271(2001)

81. De Bièvre P., Apt timing for described measurement procedures (DMP) of primary methods of measurement (PMM), Accred Qual Assur, 3, 481(1998)

82. Otto M., Chemometrics, Wiley-VCH (1999)

83. Verkouteren R. M. and Dorko W. D., High-accuracy gas analysis via isotope dilution mass spectrometry: carbon dioxide in air, Anal. Chem., 61, 2416-2422 (1989)

84. ISO 5725-1 Accuracy (trueness and precision) of measurement methods and results – part 1: general principles and definitions (1994)

85. Padilla V. G. J., Investigation of TDLAS for its application as primary standard for partial pressure measurements, Dissertation TU-Berlin (2005)

86. Lanzinger E., Jousten K., et al., Partial pressure measurement by means of infrared laser absorption spectroscopy, Vacuum, 51, 1, 47-51 (1998)

87. ISO 6142: Preparation of calibration gas mixtures – gravimetric method (2001)

88. D. Schiel, K. Röhker, Highly accurate gas chromatographic analysis of reference gases for use in vehicle emission measurements, Fresenius J Anal Chem, 357, 619-623 (1997)

89. The BIPM Key Comparison Data Base, http://kcdb.bipm.fr/appendixC/default.asp

90. CMC Abteilung 3 der PTB, lfd. Nr. 12, http://www.ptb.de/de/org/3/_index.htm

91. Alink A. and van der Veen M. H., Uncertainty calculations for the preparation of primary gas mixtures, Metrologia, 37, 641-650 (2000)

92. Rothman L.S., Barbe A., et al., The HITRAN molecular spectroscopic database: edition of 2000 including updates through 2001 , J. Quant. Spectrosc. Radiat. Transfer, Vol. 82, 5–44 (2003)

93. De Bièvre P., Boettger D., et al., EURACHEM guide, The fitness for purpose of analytical methods: a laboratory guide to method validation and related topics (2003)

94. Hogan, Specialty gas analysis, chapter 8, Wiley VCH, (1997)

95. Werle P. W., Mazzingui P., et al., Signal processing and calibration procedures for in-situ diode laser absorption spectroscopy, Spectrochimica Acta Part A, 60, 1685-1705 (2004)

96. Lanziger E., Partialdruckbestimmung von Kohlenmonoxid im Hochvakuum mittels Infrarot-Absorptionsspektroskopie unter Verwendung einer Vielfachreflexionszelle nach Herriott, Dissertation Universität Hannover (1997)

97. Werhahn O., Koelliker D. J., Schiel D, Kalibrationsfreie Bestimmung von Stoffmengenanteilen – Potenziale für Quantenkaskadenlaser in der Gasanalytik, Technisches Messen, 72, 6, 396-405 (2005)

98. Koelliker D. J., Werhahn O., Schiel D., Absolute measurements of amount of substance fraction by laser spectroscopy, DPG-Tagung, Berlin (2005)

99. Avetisov V. G. and Kauranen P., Two-tone frequency-modulation spectroscopy for quantitative measurements of gaseous species: theoretical, numerical, and experimental investigation of line shapes, Applied Optics, 35, 24, 4705-4723 (1996)

100. Dufour G., Valentin A., et al., Concentration measurements of ozone in the 1200-300 ppbv range: an intercomparison between the BNM ultraviolet standards and infrared methods, Spectrochimica Acta Part A, 60, 3345-3352 (2004)

101. Maroto A. Boqué R. et al., Should non-significant bias be included in the uncertainty budget ?, Accred. Qual. Assur.,7, 90-94 (2002)

102. Milton M., Holland P., et al., Sources of uncertainty in the gravimetric preparation of a binary gas standard on a twin-pan balance, NPL Report COEM 60 April (2001)

103. Milton M., Woods P., et al., Uncertainty reduction due to correlation effects in weighing during the preparation of gas standards, Metrologia, 39, 97-99 (2002)

104. Schoonover R. M. and Jones F. E., Air buoyancy correction in high-accuracy weighing on analytical balances, Anal. Chem., 53, 900-902 (1981)

105. Kehl K. G., Weirauch K, et al., The influence of variations in atmospheric pressure on the uncertainty budget of weighing results, Analyst, 125, 959-962 (2000)

106. DIN 1871, Gasförmige Brennstoffe und sonstige Gase – Dichte und andere volumetrische Größen (1999)

107. ISO 5725, Part 1 and Part 2, Accuracy (trueness and precision) of measurement methods and results (1994)

108. Korb C. L., Hunt R. H., et al., Measurements of line strengths at low pressures application to the 2-0 band of CO, J. Chem. Phys., 48, 4252-4260 (1968)

109. Corsi C., D'Amato F., et al., High-resolution measurements of line intensity, broadening and shift of CO2 around 2 μm, Eur. Phys. J. D, 6, 327-332 (1999)

110. Ellison S. L. R., Rosslein M., et al., Eurachem – CITAC guide, Quantifying uncertainty in analytical measurements, second edition (2000)

111. NIST, Chemical Science and Technology Laboratory, page 137 and 138, Annual report federal year (2002)

112. Durry G. and Megie G., Atmospheric CH_4 and H_2O monitoring with near-infrared InGaAs laser diodes by the SDLA, a balloonborne spectrometer for tropospheric and stratospheric in situ measurements, Applied Optics, Vol. 38, No. 36 (1999)

113. Heinlein C., Gas analysis with tunable diode laser in demanding process environments, VDI- Berichte Nr. 1863, 4. Konferenz über Optische Analysenmesstechnik in Industrie und Umwelt, 217-219 (2004)

114. DIN 51896, Zusammensetzungsgrößen, Realgasfaktor, Teil 1 & 2 (1991)

115. Peckson R. L. and Shields L. D., Modern methods of chemical analysis, Wiley (1968)

116. Hildebrandt L., Kompakte External-Cavity-Dioden-Laser für die industrielle Messtechnik, Technisches Messen, 68, 9, 374-379 (2001)

117. González M. H., Incertidumbre en la calibración de calibradores tipo vernier, Rev 1/CENAM, free in http://www.cenam.mx/publicaciones/gratuitas/ (2001)

118. E. D. Palik, Handbook of Optical Constants of Solids, Academic, Orlando, Fl., p. 566 and 569 (1985)

119. Jaroslav F. and Allen P. B., Thermal expansion and grueneisen parameters of amorphous silicon: a realistic model calculation, Phys. Rev. Lett., 79, 10, 1885-1888 (1997)

120. Fried A., Sams R., Dorko W., et al., Determination of nitrogen dioxide in air compressed gas mixtures by quantitative tunable diode laser absorption spectrometry and chemiluminescence detection, Analytical Chemistry, 60, 5, 384-403 (1988)

Dedication

Sag mir was ist bloß um uns geschehen!

Du scheints mir auf einmal völlig fremd zu sein

Warum geht's mir nicht mehr gut?... Ist es egal geworden was mit uns passiert?

Wo wills du hin, ich kann dich kaum noch sehen... Ich hab' geglaubt wir könnten echt alles ertragen...

Und jetzt wird es Still um uns... Denn wir stehen hier im Regen haben uns nichts mehr zu geben

Und es ist besser wenn du gehts...

Denn es ist Zeit sich ein zu gestehen es nicht geht...

Es gibt nichts mehr zu reden... Ist es besser aufzugeben...

Und es verdichtet sich die Stille über uns. Ich verstehe kein Word mehr aus deinem Mund...

Haben wir zuviel versucht. Warum konnten wir es nicht ahnen?

Es wird nicht leicht alles einzusehen

Und so wie's ist so geht's nicht weiter. Das Ende ist schon lang geschrieben. Und das war unsre

Silbermond

Para la reina de mi castillo…

Para mi Lady Di, mi madre Teresa y el Papa Juan Pablo II…

Para todos y para uno de ellos: mi mamá…

Yo? … recibí dos títulos de postgrado…Y ella? dos cánceres, uno por cada título…

El primero lo superó con bravura y nos hizo 11 años más inmensamente felices…

El segundo?… La llevó al cielo en el año de Juan Pablo, junto a la madre Teresa y Lady Di…

Se fué con una sonrisa, me cuentan, yo no nunca la pude ver… Nunca la vi enferma, sino sana…

Se fué con la misma esperanza que con el primer postgrado: que volviera a casa…

Y por segunda vez se cumplirá…

Más la segunda vez ella tuvo una mejor recompensa, no verme a mi… sino ver a Dios…

Nació una reina, una santa, una misericordiosa y la mejor mamá...

Josefina Delgado Tovar de Koelliker

21-09-1931 – 10-10-2005

Acknowledgments

There are a lot of people that I would like to thank, who help me to make this thesis possible.

First of all, I am obligated to Dr. Detlef Schiel, who gave me the opportunity to come to the PTB, he supported me infinitely not only scientifically but also personally. Without all the enthusiasm and kindness of my Doktorvater Prof. Dr. K. H. Gericke, this work would have not been possible, thank you for accept me as en external doctor student and support the metrological ideas of my research. Thanks to Prof. Dr. Peter Ulbig and to Prof. Dr. U. Engelhardt for the help, kindness and efficient work during the revision of my thesis.

I would like to thank all the sponsors of my fellowships in different times of my studies: CENAM, CONACYT, DAAD and PTB. Also to the German BMBF and PTB that supported the QUANSYS project. I especially recognize the big effort of the Mexican government for the invested resources through CONACYT. Its counterpart in Germany the DAAD, highlighting Ms. Stefanie Buechl and the Lateinamerika-Nord-Abteilung of the DAAD do a magnificent job for the Mexican students in Germany.

My fellowship of CONACYT would have not been possible without my recommenders my boss: Dr. Yoshito Mitani N., Director of Metrology of Materials of CENAM; and the heads of the institutions where I were formed: Dr. Alberto Bustani A., principal of the ITESM Monterrey Campus; and M. S. David Trigueros C., in those days principal of the ITC.

From CENAM, I am in debt with all my colleagues and the management staff of the company, who help me with all the needs for my research in Germany. Especially, I would like to thank our general director Dr. Hector Nava Jaimes and Dr. Yoshito Mitani N. for giving me the chance to improve myself and for allowing me to continue in service of the Mexican society. Thanks for the support to all the directive staff: the members of the scientific development program of CENAM, the SIDEPRO. I should mention many other colleagues who helped, but the list would be so large.

From the PTB thanks to all the group of Metrology in Chemistry and Division 3, especially for all the colleagues of Dr. Schiel's inorganic chemistry group. They not only do a great job there, they also took the time to help me enormously. Thank you for the patience, remarkably at the beginning of my stay in Germany helping me to find a good start and a nice working environment. Dr. D. Schiel and Dr. O. Werhahn guide me and gave me infinitely support during my thesis, remarkably to improve the final version of my thesis. This thesis would have not been succeed without the help of both of them. Thank you to Dr. K. Jousten and Dr. Gerardo Padilla from the PTB-Institute Berlin for the excellent cooperation in the QUASYS project. The chapter 5 of this research would not exists without them. In general, thanks to all the PTB staff, especially to the scientists involved in gas metrology measurements. Thanks also to all the NMIs who helped me answering my questions, especially to the staff from BAM, NIST and NMi.

From the TU Braunschweig thanks also to Dr. Christof Maul for the laser characterization measurements by FTIR.

At the end I would like to mention those that I personally considered vital during my research in Germany and in my life.

From the PTB, I personally feel deeply obligated and thankful to Dr. Olav Werhahn for all the infinite help, cooperation and suggestions. He always tried to do the best for our work. I learn with Olav not only good physics, he also showed me how to think easier and right. He woke up my desire to do a better job in science. I also learnt from him many practical things for life with all his amazing suggestions, including of course friendly conversations in German language that I enjoyed. With the time I learnt the most important thing: to see him more as a friend as a colleague. He has done so much for me, thank you Olav: you know better how intensively you help me, how difficult was it for you and me, and also you know that I needed such help. I have to write it down in German: „er war wie ein Doktorvater, ein Vater, meine deutsche Familie, ein Kumpel, aber auch ein Kindermädchen“. It was, it is and it will be an honor for me the work with you. I am in debt with you for all my life. It is my deeply desire, I will become the scientist you deserve for all the effort that you, Dr. Schiel, Dr. Güttler and the PTB have invested in my person.

For all the friends who always send me greetings and e-mails thank you. They gave me energy to survive all these beautiful, but also very difficult years. Thank you to Diana V., Raul P., Alejandro O., Araceli G., Alexander S., Raquel A., Lucy A., Emma C., and Monica S. Not least, thank you to all my friends and colleagues from CENAM. Also for all my best friends of Goethe Institute, especially: Aiko T., Alain R., Patricia, Barbara L., Yukari, Marco P., and all the other so important friends I met from Germany, Japan, China, Korea, Vietnam, Turkey, France, Spain, USA, etcetera. Also thank you to Dr. Florencia Ardón who gave many suggestions for my thesis.

Finally thank you to my amazing great family: you are the most important in my life. They waited patiently at home, but we were, we are and will be always together. I did all of this for you and mainly for my mom, but God wanted a better award for her.

All the good of this thesis is dedicated to my parents because also all the good that I could be, is because of them.

Appendix A

Uncertainty Budgets

Uncertainty of the Si-Etalon's Free Spectral Range calculated by (4.3)

By use of the equation (4.3): FSR= 1 / (2 * *n* * *d*) where n is the index of refraction and d the length of the ètalon, the free spectral range was determined by the measurement of the physical length of the ètalon. From a calliper calibration example of length [117], it was shown that the uncertainties of the Abbe effect, the repeatability, the resolution and the reading error by parallelism could be significant length uncertainties. The contribution of the expansion coefficient of Si [118] is not significant for the uncertainty of d. In [53] it was found that the uncertainty of *n* is concordant with the published values until 0.002. Data for *n* where taken from [119]. The dependence of n with wavelength variations -within the laser sweep- and with temperature variations are not significant.

Model Equation:

d = Abbe + Parall + Res + S;
*FSR = 1 / (2 * n * d);*

List of Quantities:

Quantity	Unit	Definition
FSR	cm-1	uncertainty of the Free spectral range of the etalon
n		Index of refraction of Silicium
d	cm	length of the ètalon measured with a calliper
Abbe	cm	Abbe error of the calliper
Parall	cm	Error of parallel reading
Res	cm	Resolution of the calliper
S	cm	Repeatability of length measurement

FSR:
Result

n:
Type B normal distribution
Value: 3.4489
Expanded Uncertainty: 0.002
Coverage Factor: 1

d:
Interim Result

Abbe:
Type B normal distribution
Value: 0 cm
Expanded Uncertainty: 0.0006 cm
Coverage Factor: 1

Parall:
Type B normal distribution
Value: 0 cm
Expanded Uncertainty: 0.0006 cm
Coverage Factor: 1

Res:
Type B normal distribution
Value: 0 cm
Expanded Uncertainty: 0.0014 cm

Coverage Factor: 1

S:
Type B normal distribution
Value: 2.99 cm
Expanded Uncertainty: 0.0000001 cm
Coverage Factor: 1

Uncertainty Budget:

Quantity	Value	Standard Uncertainty	Degrees of Freedom	Sensitivity Coefficient	Uncertainty Contribution	Index
n	3.44890	$2.00 \cdot 10^{-3}$	50	-0.014	$-28 \cdot 10^{-6}$ cm-1	52.9 %
d	2.99000 cm	$1.64 \cdot 10^{-3}$ cm				
Abbe	0.0 cm	$600 \cdot 10^{-6}$ cm	50	-0.016	$-9.7 \cdot 10^{-6}$ cm-1	6.3 %
Parall	0.0 cm	$600 \cdot 10^{-6}$ cm	50	-0.016	$-9.7 \cdot 10^{-6}$ cm-1	6.3 %
Res	0.0 cm	$1.40 \cdot 10^{-3}$ cm	50	-0.016	$-23 \cdot 10^{-6}$ cm-1	34.5 %
S	2.990000000 cm	$100 \cdot 10^{-9}$ cm	50	-0.016	$-1.6 \cdot 10^{-9}$ cm-1	0.0 %
FSR	0.048486 cm-1	$38.7 \cdot 10^{-6}$ cm-1	120			

Result:
Quantity: FSR
Value: 0.048486 cm-1
Relative Expanded Uncertainty: ±0.16 %
Coverage Factor: 2.0
Coverage: t-table 95%

Uncertainty of the Free Spectral Range measured by FTIR

An Airy function was used for fitting the spectra of ètalon measurements by FTIR. Two uncertainty sources were used for the estimation of the FSR measurement uncertainty:
- the Airy-function-fit parameter *P4* in (4.4).
- the resolution of the FTIR. The resolution of the FTIR was 0.006 cm^{-1}

In this way the free spectral range uncertainty of the 29.9 cm Si ètalon was obtained.
NOTE.-
The value of the standard deviation of the directly read etalon fringes' maxima method and that of the Airy Function Fit used to get the free spectral range are concordant within the standard deviation (0.001 cm^{-1}) and consequently concordant within the uncertainty of measurement.

Model Equation:
FSR= *Smodel* + *Res;*

List of Quantities:

Quantity	Unit	Definition
Res	cm-1	Influence of limited FTIR resolution
FSR	cm-1	uncertainty of the Free spectral range of the ètalon
Smodel	cm-1	Standard deviation of the FSR for the Airy function

Res:
Type B rectangular distribution
Value: 0 cm-1

Halfwidth of Limits: 0.003 cm-1

FSR:
Result

Smodel:
Type B normal distribution
Value: 0.04799 cm-1
Expanded Uncertainty: 0.00015 cm-1
Coverage Factor: 1

Uncertainty Budget:

Quantity	Value	Standard Uncertainty	Degrees of Freedom	Sensitivity Coefficient	Uncertainty Contribution	Index
Res	0.0 cm-1	$1.73 \cdot 10^{-3}$ cm-1	∞	1.0	$1.7 \cdot 10^{-3}$ cm-1	99.3 %
Smodel	0.047990 cm-1	$150 \cdot 10^{-6}$ cm-1	50	1.0	$150 \cdot 10^{-6}$ cm-1	0.7 %
FSR	0.0480 cm-1	$1.74 \cdot 10^{-3}$ cm-1	∞			

Result:
Quantity: FSR
Value: 0.0480 cm-1
Expanded Uncertainty: $\pm 3.5 \cdot 10^{-3}$ cm-1
Coverage Factor: 2.0
Coverage: t-table 95%

Uncertainty of the Gravimetric Amount of Carbon Dioxide Fraction

Example for a $5 \cdot 10^{-2}$ mol/mol CO_2/N_2 gas mixture (Table 4.1 and 4.2)

Model Equation:
$M_{O2}=2*M_O$; $M_{H2O}=2*M_H+M_O$; $M_{N2}=2*M_N$; $M_{CH4}=4*M_H+M_O$;

$M_{H2}=2*M_H$; $M_{CO}=M_C+M_O$; $M_{CO2}=M_C+2*M_O$;

$m_{CO2}=(m_1-m_0)$;

$m_{N2}=(m_2-m_1)$;

$M_A= x_{O2A}*M_{O2}+x_{H2OA}*M_{H2O}+x_{N2A}*M_{N2}+x_{CH4A}*M_{CH4}+x_{H2A}*M_{H2}+x_{COA}*M_{CO}+x_{CO2A}*M_{CO2}$;

$M_B= x_{O2B}*M_{O2}+x_{H2OB}*M_{H2O}+x_{N2B}*M_{N2}+x_{CH4B}*M_{CH4}+x_{COB}*M_{CO}+x_{CO2B}*M_{CO2}$;

$x_{CO2} = (m_{CO2}*x_{CO2A}/M_A+m_{N2}*x_{CO2B}/M_B)/(m_{CO2}/M_A+m_{N2}/M_B)$

List of Quantities:

Quantity	Unit	Definition
x_{CO2}	mol/mol	Amount of CO_2 fraction
m_{CO2}	g	Mass of the pure CO_2 parent gas
x_{CO2A}	mol/mol	Amount of CO_2 fraction in the parent gas A: CO_2
M_A	g/mol	Average molar mass of the parent gas A: CO_2
m_{N2}	g	Mass of the pure N_2 parent gas

Quantity	Unit	Definition
M_B	g/mol	Average molar mass of the parent gas B: N_2
x_{CO2B}	mol/mol	Amount of CO_2 fraction in the parent gas B: N_2
x_{O2A}	mol/mol	Amount of O_2 fraction in the parent gas A: CO_2
M_{O2}	g/mol	molar mass of O_2
x_{H2OA}	mol/mol	Amount of H_2O fraction in the parent gas A: CO_2
M_{H2O}	g/mol	molar mass of H_2O
x_{N2A}	mol/mol	Amount of N_2 fraction in the parent gas A: CO_2
M_{N2}	g/mol	molar mass of N_2
x_{CH4A}	mol/mol	Amount of CH_4 fraction in the parent gas A: CO_2
M_{CH4}	g/mol	molar mass of CH_4
x_{H2A}	mol/mol	Amount of H_2 fraction in the parent gas A: CO_2
M_{H2}	g/mol	molar mass of H_2
x_{COA}	mol/mol	Amount of CO fraction in the parent gas A: CO_2
M_{CO}	g/mol	molar mass of CO
M_{CO2}	g/mol	molar mass of CO_2
x_{O2B}	mol/mol	Amount of O_2 fraction in the parent gas B: N_2
x_{H2OB}	mol/mol	Amount of H_2O fraction in the parent gas B: N_2
x_{N2B}	mol/mol	Amount of N_2 fraction in the parent gas B: N_2
x_{CH4B}	mol/mol	Amount of CH_4 fraction in the parent gas B: N_2
x_{COB}	mol/mol	Amount of CO fraction in the parent gas B: N_2
m_1	g	Mass for sphere + parent gas 1: CO_2
m_0	g	Mass for empty sphere
m_2	g	Mass for sphere + parent gas 1: CO_2 and 2: N_2
M_O	g/mol	molar mass of O
M_H	g/mol	molar mass of H
M_N	g/mol	molar mass of N
M_C	g/mol	molar mass of C

x_{CO2}:
Result

m_{CO2}:
Interim Result

x_{CO2A}:
Type B t-distribution
Value: 0.99996 mol/mol
Standard Uncertainty: 0.000003 mol/mol
Degrees of Freedom: 100

M_A:
Interim Result

m_{N2}:
Interim Result

M_B:
Interim Result

x_{CO2B}:
Type B rectangular distribution
Value: 0.00000025 mol/mol
Halfwidth of Limits: 50 %
x_{O2A}:
Type B rectangular distribution
Value: 0.0000029 mol/mol
Halfwidth of Limits: 50 %

M_{O2}:
Interim Result

x_{H2OA}:
Type B rectangular distribution
Value: 0.000005 mol/mol
Halfwidth of Limits: 50 %

M_{H2O}:
Interim Result

x_{N2A}:
Type B rectangular distribution
Value: 0.0000035 mol/mol
Halfwidth of Limits: 50 %

M_{N2}:
Interim Result

x_{CH4A}:
Type B rectangular distribution
Value: 0.0000019 mol/mol
Halfwidth of Limits: 50 %

M_{CH4}:
Interim Result

x_{H2A}:
Type B rectangular distribution
Value: 0.0000001 mol/mol
Halfwidth of Limits: 50 %

M_{H2}:
Interim Result

x_{COA}:
Type B rectangular distribution
Value: 0.0000005 mol/mol
Halfwidth of Limits: 50 %

M_{CO}:
Interim Result

M_{CO2}:
Interim Result

x_{O2B}:
Type B rectangular distribution
Value: 0.000003 mol/mol
Halfwidth of Limits: 50 %

x_{H2OB}:
Type B rectangular distribution
Value: 0.000002 mol/mol
Halfwidth of Limits: 50 %

x_{N2B}:
Type B t-distribution
Value: 0.999994 mol/mol
Standard Uncertainty: 0.0000011 mol/mol
Degrees of Freedom: 100

x_{CH4B}:
Type B rectangular distribution
Value: 0.0000005 mol/mol
Halfwidth of Limits: 50 %

x_{COB}:
Type B rectangular distribution
Value: 0.00000025 mol/mol
Halfwidth of Limits: 50 %

m_1:
Type A summarized
Value: 879.6357 g
Standard Uncertainty: 0.0005 g
Degrees of Freedom: 50

m_0:
Type A summarized
Value: 879.1040 g
Standard Uncertainty: 0.0005 g
Degrees of Freedom: 50

m_2:
Type A summarized
Value: 885.8790 g
Standard Uncertainty: 0.0005 g
Degrees of Freedom: 50

M_O:
Import
Filename: Molecular-mass.smu
Quantity: M_O

M_H:
Import
Filename: Molecular-mass.smu
Quantity: M_H

M_N:
Import
Filename: Molecular-mass.smu
Quantity: M_N

M_C:
Import
Filename: Molecular-mass.smu
Quantity: M_C

Uncertainty Budget:

Quantity	Value	Standard Uncertainty	Degrees of Freedom	Sensitivity Coefficient	Uncertainty Contribution	Index
m_{CO2}	0.531700 g	$707 \cdot 10^{-6}$ g				
x_{CO2A}	0.99996000 mol/mol	$3.00 \cdot 10^{-6}$ mol/mol	100	$2.6 \cdot 10^{-3}$	$7.9 \cdot 10^{-9}$ mol/mol	0.0 %
M_A	44.00807 g/mol	$1.01 \cdot 10^{-3}$ g/mol				
m_{N2}	6.243300 g	$707 \cdot 10^{-6}$ g				
M_B	28.013472 g/mol	$146 \cdot 10^{-6}$ g/mol				
x_{CO2B}	$250.0 \cdot 10^{-9}$ mol/mol	$72.2 \cdot 10^{-9}$ mol/mol	∞	1.0	$74 \cdot 10^{-9}$ mol/mol	0.0 %
x_{O2A}	$2.900 \cdot 10^{-6}$ mol/mol	$837 \cdot 10^{-9}$ mol/mol	∞	-0.035	$-30 \cdot 10^{-9}$ mol/mol	0.0 %
M_{O2}	31.998800 g/mol	$600 \cdot 10^{-6}$ g/mol				
x_{H2OA}	$5.00 \cdot 10^{-6}$ mol/mol	$1.44 \cdot 10^{-6}$ mol/mol	∞	-0.020	$-29 \cdot 10^{-9}$ mol/mol	0.0 %
M_{H2O}	18.015280 g/mol	$331 \cdot 10^{-6}$ g/mol				
x_{N2A}	$3.50 \cdot 10^{-6}$ mol/mol	$1.01 \cdot 10^{-6}$ mol/mol	∞	-0.031	$-31 \cdot 10^{-9}$ mol/mol	0.0 %
M_{N2}	28.013480 g/mol	$140 \cdot 10^{-6}$ g/mol				
x_{CH4A}	$1.900 \cdot 10^{-6}$ mol/mol	$548 \cdot 10^{-9}$ mol/mol	∞	-0.022	$-12 \cdot 10^{-9}$ mol/mol	0.0 %
M_{CH4}	20.031160 g/mol	$410 \cdot 10^{-6}$ g/mol				
x_{H2A}	$100.0 \cdot 10^{-9}$ mol/mol	$28.9 \cdot 10^{-9}$ mol/mol	∞	$-2.2 \cdot 10^{-3}$	$-64 \cdot 10^{-12}$ mol/mol	0.0 %
M_{H2}	2.015880 g/mol	$140 \cdot 10^{-6}$ g/mol				
x_{COA}	$500 \cdot 10^{-9}$ mol/mol	$144 \cdot 10^{-9}$ mol/mol	∞	-0.031	$-4.5 \cdot 10^{-9}$ mol/mol	0.0 %
M_{CO}	28.010100 g/mol	$854 \cdot 10^{-6}$ g/mol				
M_{CO2}	44.00950 g/mol	$1.00 \cdot 10^{-3}$ g/mol				
x_{O2B}	$3.000 \cdot 10^{-6}$ mol/mol	$866 \cdot 10^{-9}$ mol/mol	∞	0.056	$48 \cdot 10^{-9}$ mol/mol	0.0 %
x_{H2OB}	$2.000 \cdot 10^{-6}$ mol/mol	$577 \cdot 10^{-9}$ mol/mol	∞	0.031	$18 \cdot 10^{-9}$ mol/mol	0.0 %
x_{N2B}	0.99999400 mol/mol	$1.10 \cdot 10^{-6}$ mol/mol	100	0.049	$54 \cdot 10^{-9}$ mol/mol	0.0 %
x_{CH4B}	$500 \cdot 10^{-9}$ mol/mol	$144 \cdot 10^{-9}$ mol/mol	∞	0.035	$5.0 \cdot 10^{-9}$ mol/mol	0.0 %
x_{COB}	$250.0 \cdot 10^{-9}$ mol/mol	$72.2 \cdot 10^{-9}$ mol/mol	∞	0.049	$3.5 \cdot 10^{-9}$ mol/mol	0.0 %
m_1	879.635700 g	$500 \cdot 10^{-6}$ g	50	0.10	$50 \cdot 10^{-6}$ mol/mol	53.9 %
m_0	879.104000 g	$500 \cdot 10^{-6}$ g	50	-0.092	$-46 \cdot 10^{-6}$	45.8 %

Quantity	Value	Standard Uncertainty	Degrees of Freedom	Sensitivity Coefficient	Uncertainty Contribution	Index
					mol/mol	
m_2	885.879000 g	$500 \cdot 10^{-6}$ g	50	$-7.8 \cdot 10^{-3}$	$-3.9 \cdot 10^{-6}$ mol/mol	0.3 %
M_O	15.9994 g/mol	$300 \cdot 10^{-6}$ g/mol	50	$-2.2 \cdot 10^{-3}$	$-660 \cdot 10^{-9}$ mol/mol	0.0 %
M_H	1.00794 g/mol	$70.0 \cdot 10^{-6}$ g/mol	50	0.0	0.0 mol/mol	0.0 %
M_N	14.00674 g/mol	$70.0 \cdot 10^{-6}$ g/mol	50	$3.5 \cdot 10^{-3}$	$240 \cdot 10^{-9}$ mol/mol	0.0 %
M_C	12.0107 g/mol	$800 \cdot 10^{-6}$ g/mol	50	$-1.1 \cdot 10^{-3}$	$-890 \cdot 10^{-9}$ mol/mol	0.0 %
x_{CO2}	0.051421 mol/mol	$67.8 \cdot 10^{-6}$ mol/mol	100			

Result:

Quantity: x_{CO2}
Value: 0.05142 mol/mol
Relative Expanded Uncertainty: ±0.26 %
Coverage Factor: 2.0
Coverage: t-table 95%

Uncertainty of the amount of CO_2 fraction measured by direct absorption spectroscopy

Example for a $9 \cdot 10^{-2}$ mol/mol CO_2/N_2 gas mixture (Table 4.3)

S_T from HITRAN and *FSR* from FTIR measurements

Model Equation:

$S_T=S_{To}*(Q_{To}/Q_T)*exp(-h*c*E/k_B*(1/T-1/T_0))*(1-exp(-h*c*\nu_0/(k_B*T)))/(1-exp(-h*c*\nu_0/(k_B*T_0)));$

x_{CO2} = FSR/FSR*SP*Area*10^6*k_B*T/(S_T*P_{total}*10^2* L);

List of Quantities:

Quantity	Unit	Definition
S_T	cm	Line strength at temperature T
L	cm	Cell Pathlegth
k_B	J/K	Boltzmann constant
T	K	Temperature in Gascell
P_{total}	hPa	Total-Pressure in Gascell
x_{CO2}	mol/mol	Amount of substance fraction of CO_2
FSR	cm^{-1}	Free spectral range (FSR) of a Si - etalon
FSRSP	SP #	FSR of a Si - etalon in SP # digitalized by the adquisition card
Area	SP #	Area under the Voigt profile
S_{To}	cm	Linestrength for norm temperature To = 296 K
T_0	K	Norm temperature

Quantity	Unit	Definition
h	J s	Planck constant
c	m/s	Ligth speed in vacuum
E	cm-1	Lower state energy
ν_0	cm^{-1}	linecenter
Q_{To}	Arbitrary	internal partition sum for temperature To
Q_T	Arbitrary	internal partition sum for temperature T

S_T:
Interim Result

L:
Type B rectangular distribution
Value: 100 cm
Halfwidth of Limits: 0.5 cm

1 cm expanded uncertainty, not informative type B uncertainty source gives 0.5 cm

k_B:
Type B normal distribution
Value: $1.3806505 \cdot 10^{-23}$ J/K
Expanded Uncertainty: $0.0000024 \cdot 10^{-23}$ J/K
Coverage Factor: 1

Value 1.380 6505 x 10-23 J K-1
Standard uncertainty 0.000 0024 x 10-23 J K-1
Relative standard uncertainty 1.8 x 10-6
From: CODATA Internationally recommended values of the Fundamental Physical constants, NIST(2000)

T:
Type B normal distribution
Value: 295.45 K
Expanded Uncertainty: 0.2 K
Coverage Factor: 1

+/- 0.1 C accuracy specification
< 0.1 C repeatability and stability

P_{total}:
Type B normal distribution
Value: 101.0 hPa
Expanded Uncertainty: 0.3 hPa
Coverage Factor: 1

+/- 0.2 hPa uncertainty of calibration around 100 hPa
+/- 0.2 hPa maximum variability, typically 0.1 hPa

x_{CO2}:
Result

FSR:
Type B normal distribution
Value: 0.04799 cm^{-1}
Expanded Uncertainty: 0.00174 cm^{-1}
Coverage Factor: 1

FSRSP:
Type A summarized
Value: 43.487 SP #
Standard Uncertainty: 0.023 SP #
Degrees of Freedom: 5

Area:
Type B normal distribution
Value: 25.751811 SP #
Expanded Uncertainty: 0.016399 SP #
Coverage Factor: 1

The uncertainty includes the repeatability of areas combining the uncertainty from Voigt function and that of the variability between 9 replicates with 100 scans for each one.
relative uncertainty = 0.064 %
Area/cm^{-1} / r_{sweep}/(cm^{-1}/SP) = 0.02843/0.001104 = 25.751811 SP
u(Area)/cm^{-1} / r_{sweep}/(cm^{-1}/SP) = 0.0000181046/0.001104 = 0.016399 SP

S_{To}:
Type B normal distribution
Value: $1.273 \cdot 10^{-21}$ cm
Expanded Uncertainty: $0.045 \cdot 10^{-21}$ cm
Coverage Factor: 2

3.5 % is the half of the relative uncertainty values (2 to 5 %)

T_0:
Constant
Value: 296 K

h:
Type B normal distribution
Value: $6.6260693 \cdot 10^{-34}$ J s
Expanded Uncertainty: $0.0000011 \cdot 10^{-34}$ J s
Coverage Factor: 1

Value 6.626 0693 x 10-34 J s
Standard uncertainty 0.000 0011 x 10-34 J s
Relative standard uncertainty 1.7 x 10-7
From: CODATA Internationally recommended values of the Fundamental Physical constants, NIST(2000)

c:
Constant
Value: 299792458 m/s

Value 299 792 458 m s-1
From: CODATA Internationally recommended values of the Fundamental Physical constants, NIST(2000)

E:
Constant
Value: 60.8709 cm-1

ν_0:
Type B normal distribution
Value: 4987.3087 cm^{-1}
Expanded Uncertainty: 0.0040 cm^{-1}
Coverage Factor: 1

0.001 cm^{-1} for u(ν_0) form HITRAN and 0.003 cm^{-1} from the possible line shift of ν_0

Q_{To}:
Type B normal distribution
Value: 33.4082828864 Arbitrary
Expanded Uncertainty: 0.3 %
Coverage Factor: 1

Q_T:
Type B normal distribution
Value: 33.2066 Arbitrary
Expanded Uncertainty: 0.3 %
Coverage Factor: 1

Uncertainty Budget:

Quantity	Value	Standard Uncertainty	Degrees of Freedom	Sensitivity Coefficient	Uncertainty Contribution	Index
S_T	$1.2828 \cdot 10^{-21}$ cm	$23.3 \cdot 10^{-24}$ cm				
L	100.000 cm	0.289 cm	∞	$-890 \cdot 10^{-6}$	$-260 \cdot 10^{-6}$ mol/mol	0.5 %
k_B	$13.8065050 \cdot 10^{-24}$ J/K	$24.0 \cdot 10^{-30}$ J/K	50	$6.5 \cdot 10^{21}$	$160 \cdot 10^{-9}$ mol/mol	0.0 %
T	295.450 K	0.200 K	50	$570 \cdot 10^{-6}$	$110 \cdot 10^{-6}$ mol/mol	0.1 %
P_{total}	101.000 hPa	0.300 hPa	50	$-890 \cdot 10^{-6}$	$-270 \cdot 10^{-6}$ mol/mol	0.5 %
FSR	0.04799 cm^{-1}	$1.74 \cdot 10^{-3}$ cm^{-1}	50	1.9	$3.2 \cdot 10^{-3}$ mol/mol	79.0 %
FSRSP	43.4870 SP #	0.0230 SP #	5	$-2.1 \cdot 10^{-3}$	$-47 \cdot 10^{-6}$ mol/mol	0.0 %
Area	25.7518 SP #	0.0164 SP #	50	$3.5 \cdot 10^{-3}$	$57 \cdot 10^{-6}$ mol/mol	0.0 %
S_{To}	$1.2730 \cdot 10^{-21}$ cm	$22.5 \cdot 10^{-24}$ cm	50	$-70 \cdot 10^{18}$	$-1.6 \cdot 10^{-3}$ mol/mol	18.8 %
T_0	296.0 K					
h	$662.606930 \cdot 10^{-36}$ J s	$110 \cdot 10^{-42}$ J s	50	$29 \cdot 10^{27}$	$3.2 \cdot 10^{-12}$ mol/mol	0.0 %
c	$299.792458 \cdot 10^{6}$ m/s					
E	60.8709 cm-1					
ν_0	4987.30870 cm^{-1}	$4.00 \cdot 10^{-3}$ cm^{-1}	50	0.0	0.0 mol/mol	0.0 %
Q_{To}	33.408 Arbitrary	0.100 Arbitrary	50	$-2.7 \cdot 10^{-3}$	$-270 \cdot 10^{-6}$ mol/mol	0.5 %
Q_T	33.2066 Arbitrary	0.0996 Arbitrary	50	$2.7 \cdot 10^{-3}$	$270 \cdot 10^{-6}$ mol/mol	0.5 %
x_{CO2}	0.0895 mol/mol	$3.65 \cdot 10^{-3}$ mol/mol	75			

Result:
Quantity: x_{CO2}
Value: 0.0895 mol/mol

Relative Expanded Uncertainty: ±8.2 %
Coverage Factor: 1.0
Coverage: manual

Example for a $9 \cdot 10^{-2}$ mol/mol CO_2/N_2 gas mixture (Table 4.4)

S_T from HITRAN and *FSR* from (4.3)

Model Equation:

$S_T=S_{To}*(Q_{To}/Q_T)*exp(-h*c*E/k_B*(1/T-1/T_0))*(1-exp(-h*c*\nu_0/(k_B*T)))/(1-exp(-h*c*\nu_0/(k_B*T_0)));$

$x_{CO2} = FSR/FSRSP*Area*10\text{^}6*k_B*T/(S_T*p_{total}*10\text{^}2* L);$

List of Quantities:

Quantity	Unit	Definition
S_T	cm	Line strength at temperature T
L	cm	Cell Pathlegth
k_B	J/K	Boltzmann constant
T	K	Temperature in Gascell
p_{total}	hPa	Total-Pressure in Gascell
x_{CO2}	mol/mol	Amount of substance fraction of CO_2
FSR	cm^{-1}	Free spectral range (FSR) of a Si - etalon
FSRSP	SP #	FSR of a Si - etalon in SP # digitalized by the adquisition card
Area	SP #	Area under the Voigt profile
S_{To}	cm	Linestrength for norm temperature To = 296 K
T_0	K	Norm temperature
h	J s	Planck constant
c	m/s	Ligth speed in vacuum
E	cm-1	Lower state energy
ν_0	cm^{-1}	linecenter
Q_{To}	Arbitrary	internal partition sum for temperature To
Q_T	Arbitrary	internal partition sum for temperature T

S_T:
Interim Result

L:
Type B rectangular distribution
Value: 100 cm
Halfwidth of Limits: 0.5 cm

1 cm expanded uncertainty, not informative type B uncertainty source gives 0.5 cm

k_B:
Type B normal distribution
Value: $1.3806505 \cdot 10^{-23}$ J/K
Expanded Uncertainty: $0.0000024 \cdot 10^{-23}$ J/K
Coverage Factor: 1

Value 1.380 6505 x 10-23 J K-1

Standard uncertainty 0.000 0024 x 10-23 J K-1
Relative standard uncertainty 1.8 x 10-6
From: CODATA Internationally recommended values of the Fundamental Physical constants, NIST(2000)

T:
Type B normal distribution
Value: 295.45 K
Expanded Uncertainty: 0.2 K
Coverage Factor: 1

+/- 0.1 C accuracy specification
< 0.1 C repeatability and stability

p_{total}:
Type B normal distribution
Value: 101.0 hPa
Expanded Uncertainty: 0.3 hPa
Coverage Factor: 1

+/- 0,2 hPa uncertainty of calibration around 100 hPa
+/- 0,2 hPa maximum variability, typically 0.1 hPa

x_{CO2}:
Result

FSR:
Type B normal distribution
Value: 0.048486 cm^{-1}
Expanded Uncertainty: 0.16 %
Coverage Factor: 2

FSRSP:
Type A summarized
Value: 43.487 SP #
Standard Uncertainty: 0.023 SP #
Degrees of Freedom: 5

Area:
Type B normal distribution
Value: 25.751811 SP #
Expanded Uncertainty: 0.016399 SP #
Coverage Factor: 1

The uncertainty includes the repeatability of areas combining the uncertainty from Voigt function and that of the variability between 9 replicates with 100 scans for each one.
relative uncertainty = 0.064 %
Area/cm^{-1} / r_{sweep}/(cm^{-1}/SP) = 0.02843/0.001104 = 25.751811 SP
u(Area)/cm^{-1} / r_{sweep}/(cm^{-1}/SP) = 0.0000181046/0.001104 = 0.016399 SP

S_{To}:
Type B normal distribution
Value: $1.273 \cdot 10^{-21}$ cm
Expanded Uncertainty: $0.045 \cdot 10^{-21}$ cm
Coverage Factor: 2

3.5 % is the half of the relative uncertainty values (2 to 5 %)

T_0:
Constant

Value: 296 K

h:
Type B normal distribution
Value: $6.6260693 \cdot 10^{-34}$ J s
Expanded Uncertainty: $0.0000011 \cdot 10^{-34}$ J s
Coverage Factor: 1

Value 6.626 0693 x 10-34 J s
Standard uncertainty 0.000 0011 x 10-34 J s
Relative standard uncertainty 1.7 x 10-7
From: CODATA Internationally recommended values of the Fundamental Physical constants, NIST(2000)

c:
Constant
Value: 299792458 m/s

Value 299 792 458 m s-1
From: CODATA Internationally recommended values of the Fundamental Physical constants, NIST(2000)

E:
Constant
Value: 60.8709 cm-1

ν_0:
Type B normal distribution
Value: 4987.3087 cm^{-1}
Expanded Uncertainty: 0.0040 cm^{-1}
Coverage Factor: 1

0.001 cm^{-1} for u(ν_0) form HITRAN and 0.003 cm^{-1} from the possible line shift of ν_0

Q_{To}:
Type B normal distribution
Value: 33.4082828864 Arbitrary
Expanded Uncertainty: 0.3 %
Coverage Factor: 1

Q_T:
Type B normal distribution
Value: 33.2066 Arbitrary
Expanded Uncertainty: 0.3 %
Coverage Factor: 1

Uncertainty Budget:

Quantity	Value	Standard Uncertainty	Degrees of Freedom	Sensitivity Coefficient	Uncertainty Contribution	Index
S_T	$1.2828 \cdot 10^{-21}$ cm	$23.3 \cdot 10^{-24}$ cm				
L	100.000 cm	0.289 cm	∞	$-900 \cdot 10^{-6}$	$-260 \cdot 10^{-6}$ mol/mol	2.4 %
k_B	$13.8065050 \cdot 10^{-24}$ J/K	$24.0 \cdot 10^{-30}$ J/K	50	$6.5 \cdot 10^{21}$	$160 \cdot 10^{-9}$ mol/mol	0.0 %
T	295.450 K	0.200 K	50	$580 \cdot 10^{-6}$	$120 \cdot 10^{-6}$ mol/mol	0.5 %
p_{total}	101.000 hPa	0.300 hPa	50	$-900 \cdot 10^{-6}$	$-270 \cdot 10^{-6}$	2.5 %

Quantity	Value	Standard Uncertainty	Degrees of Freedom	Sensitivity Coefficient	Uncertainty Contribution	Index
					mol/mol	
FSR	0.0484860 cm^{-1}	$38.8 \cdot 10^{-6}$ cm^{-1}	50	1.9	$72 \cdot 10^{-6}$ mol/mol	0.2 %
FSRSP	43.4870 SP #	0.0230 SP #	5	$-2.1 \cdot 10^{-3}$	$-48 \cdot 10^{-6}$ mol/mol	0.1 %
Area	25.7518 SP #	0.0164 SP #	50	$3.5 \cdot 10^{-3}$	$58 \cdot 10^{-6}$ mol/mol	0.1 %
S_{To}	$1.2730 \cdot 10^{-21}$ cm	$22.5 \cdot 10^{-24}$ cm	50	$-71 \cdot 10^{18}$	$-1.6 \cdot 10^{-3}$ mol/mol	89.1 %
T_0	296.0 K					
h	$662.606930 \cdot 10^{-36}$ J s	$110 \cdot 10^{-42}$ J s	50	$29 \cdot 10^{27}$	$3.2 \cdot 10^{-12}$ mol/mol	0.0 %
c	$299.792458 \cdot 10^{6}$ m/s					
E	60.8709 cm-1					
ν_0	4987.30870 cm^{-1}	$4.00 \cdot 10^{-3}$ cm^{-1}	50	0.0	0.0 mol/mol	0.0 %
Q_{To}	33.408 Arbitrary	0.100 Arbitrary	50	$-2.7 \cdot 10^{-3}$	$-270 \cdot 10^{-6}$ mol/mol	2.6 %
Q_T	33.2066 Arbitrary	0.0996 Arbitrary	50	$2.7 \cdot 10^{-3}$	$270 \cdot 10^{-6}$ mol/mol	2.6 %
x_{CO2}	0.0904 mol/mol	$1.69 \cdot 10^{-3}$ mol/mol	62			

Result:

Quantity: x_{CO2}
Value: 0.0904 mol/mol
Relative Expanded Uncertainty: ±3.7 %
Coverage Factor: 2.0
Coverage: t-table 95%

Example for a $9 \cdot 10^{-2}$ mol/mol CO_2/N_2 gas mixture (Table 6.1)

Changing S_T from HITRAN to the measured S_T of chapter 5

Model Equation:

$S_T=S_{To}*(Q_{To}/Q_T)*exp(-h*c*E/k_B*(1/T-1/T_0))*(1-exp(-h*c*\nu_0/(k_B*T)))/(1-exp(-h*c*\nu_0/(k_B*T_0)));$

x_{CO2} = FSR/FSR*SP*Area*10^6*k_B*T/(S_T*P_{total}*10^2* L);*

List of Quantities:

Quantity	Unit	Definition
S_T	cm	Line strength at temperature T
L	cm	Cell Pathlegth
k_B	J/K	Boltzmann constant
T	K	Temperature in Gascell

Quantity	Unit	Definition
P_{total}	hPa	Total-Pressure in Gascell
x_{CO2}	mol/mol	Amount of substance fraction of CO_2
FSR	cm^{-1}	Free spectral range (FSR) of a Si - etalon
FSRSP	SP #	FSR of a Si - etalon in SP # digitalized by the adquisition card
Area	SP #	Area under the Voigt profile
S_{To}	cm	Linestrength for norm temperature To = 296 K
T_0	K	Norm temperature
h	J s	Planck constant
c	m/s	Ligth speed in vacuum
E	cm-1	Lower state energy
ν_0	cm^{-1}	linecenter
Q_{To}	Arbitrary	internal partition sum for temperature To
Q_T	Arbitrary	internal partition sum for temperature T

S_T:
Interim Result

L:
Type B rectangular distribution
Value: 100 cm
Halfwidth of Limits: 0.5 cm

1 cm expanded uncertainty, not informative type B uncertainty source gives 0.5 cm

k_B:
Type B normal distribution
Value: $1.3806505 \cdot 10^{-23}$ J/K
Expanded Uncertainty: $0.0000024 \cdot 10^{-23}$ J/K
Coverage Factor: 1

Value 1.380 6505 x 10-23 J K-1
Standard uncertainty 0.000 0024 x 10-23 J K-1
Relative standard uncertainty 1.8 x 10-6
From: CODATA Internationally recommended values of the Fundamental Physical constants, NIST(2000)

T:
Type B normal distribution
Value: 295.45 K
Expanded Uncertainty: 0.2 K
Coverage Factor: 1

+/- 0.1 C accuracy specification
< 0.1 C repeatability and stability

P_{total}:
Type B normal distribution
Value: 101.0 hPa
Expanded Uncertainty: 0.3 hPa
Coverage Factor: 1

+/- 0.2 hPa uncertainty of calibration around 100 hPa
+/- 0.2 hPa maximum variability, typically 0.1 hPa

x_{CO2}:
Result

FSR:
Type B normal distribution
Value: 0.048486 cm^{-1}
Expanded Uncertainty: 0.16 %
Coverage Factor: 2

FSRSP:
Type A summarized
Value: 43.487 SP #
Standard Uncertainty: 0.023 SP #
Degrees of Freedom: 5

Area:
Type B normal distribution
Value: 25.751811 SP #
Expanded Uncertainty: 0.016399 SP #
Coverage Factor: 1

The uncertainty includes the repeatability of areas combining the uncertainty from Voigt function and that of the variability between 9 replicates with 100 scans for each one.
relative uncertainty = 0.064 %
Area/cm^{-1} / r_{sweep}/(cm^{-1}/SP) = 0.02843/0.001104 = 25.751811 SP
u(Area)/cm^{-1} / r_{sweep}/(cm^{-1}/SP) = 0.0000181046/0.001104 = 0.016399 SP

S_{To}:
Type B normal distribution
Value: $1.2549 \cdot 10^{-21}$ cm
Expanded Uncertainty: $0.0072 \cdot 10^{-21}$ cm
Coverage Factor: 1

from the measured linestrength value (see chapter 5)

T_0:
Constant
Value: 296 K

h:
Type B normal distribution
Value: $6.6260693 \cdot 10^{-34}$ J s
Expanded Uncertainty: $0.0000011 \cdot 10^{-34}$ J s
Coverage Factor: 1

Value 6.626 0693 x 10-34 J s
Standard uncertainty 0.000 0011 x 10-34 J s
Relative standard uncertainty 1.7 x 10-7
From: CODATA Internationally recommended values of the Fundamental Physical constants, NIST(2000)

c:
Constant
Value: 299792458 m/s

Value 299 792 458 m s-1
From: CODATA Internationally recommended values of the Fundamental Physical constants, NIST(2000)

E:
Constant
Value: 60.8709 cm-1

with E = hcv
u_r (E) = E * sqrt(u_r^2 (h)+u_r^2(v))
u (h) = 0.0000011e-34

ν_0:
Type B normal distribution
Value: 4987.3087 cm^{-1}
Expanded Uncertainty: 0.0040 cm^{-1}
Coverage Factor: 1

0.001 cm^{-1} for u(ν_0) form HITRAN and 0.003 cm^{-1} from the possible line shift of ν_0

Q_{To}:
Type B normal distribution
Value: 33.4082828864 Arbitrary
Expanded Uncertainty: 0.3 %
Coverage Factor: 1

Q_T:
Type B normal distribution
Value: 33.2066 Arbitrary
Expanded Uncertainty: 0.3 %
Coverage Factor: 1

Uncertainty Budget:

Quantity	Value	Standard Uncertainty	Degrees of Freedom	Sensitivity Coefficient	Uncertainty Contribution	Index
S_T	$1.26459 \cdot 10^{-21}$ cm	$9.06 \cdot 10^{-24}$ cm				
L	100.000 cm	0.289 cm	∞	$-920 \cdot 10^{-6}$	$-260 \cdot 10^{-6}$ mol/mol	11.7 %
k_B	$13.8065050 \cdot 10^{-24}$ J/K	$24.0 \cdot 10^{-30}$ J/K	50	$6.6 \cdot 10^{21}$	$160 \cdot 10^{-9}$ mol/mol	0.0 %
T	295.450 K	0.200 K	50	$580 \cdot 10^{-6}$	$120 \cdot 10^{-6}$ mol/mol	2.3 %
P_{total}	101.000 hPa	0.300 hPa	50	$-910 \cdot 10^{-6}$	$-270 \cdot 10^{-6}$ mol/mol	12.4 %
FSR	0.0484860 cm^{-1}	$38.8 \cdot 10^{-6}$ cm^{-1}	50	1.9	$73 \cdot 10^{-6}$ mol/mol	0.9 %
FSRSP	43.4870 SP #	0.0230 SP #	5	$-2.1 \cdot 10^{-3}$	$-48 \cdot 10^{-6}$ mol/mol	0.4 %
Area	25.7518 SP #	0.0164 SP #	50	$3.6 \cdot 10^{-3}$	$58 \cdot 10^{-6}$ mol/mol	0.6 %
S_{To}	$1.25490 \cdot 10^{-21}$ cm	$7.20 \cdot 10^{-24}$ cm	50	$-73 \cdot 10^{18}$	$-530 \cdot 10^{-6}$ mol/mol	46.4 %
T_0	296.0 K					
h	$662.606930 \cdot 10^{-36}$ J s	$110 \cdot 10^{-42}$ J s	50	$29 \cdot 10^{27}$	$3.2 \cdot 10^{-12}$ mol/mol	0.0 %
c	$299.792458 \cdot 10^{6}$					

Quantity	Value	Standard Uncertainty	Degrees of Freedom	Sensitivity Coefficient	Uncertainty Contribution	Index
	m/s					
E	60.8709 cm-1					
ν_0	4987.30870 cm^{-1}	$4.00 \cdot 10^{-3}$ cm^{-1}	50	0.0	0.0 mol/mol	0.0 %
Q_{To}	33.408 Arbitrary	0.100 Arbitrary	50	$-2.7 \cdot 10^{-3}$	$-280 \cdot 10^{-6}$ mol/mol	12.7 %
Q_T	33.2066 Arbitrary	0.0996 Arbitrary	50	$2.8 \cdot 10^{-3}$	$280 \cdot 10^{-6}$ mol/mol	12.7 %
x_{CO2}	0.09170 mol/mol	$773 \cdot 10^{-6}$ mol/mol	190			

Result:

Quantity: x_{CO2}
Value: 0.0917 mol/mol
Relative Expanded Uncertainty: ±1.7 %
Coverage Factor: 2.0
Coverage: t-table 95%

Example for a $408 \cdot 10^{-6}$ mol/mol CO_2/N_2 gas mixture (Table 6.2)

Model Equation:

$S_T=S_{To}*(Q_{To}/Q_T)*exp(-h*c*E/k_B*(1/T-1/T_0))*(1-exp(-h*c*\nu_0/(k_B*T)))/(1-exp(-h*c*\nu_0/(k_B*T_0)));$

x_{CO2} = FSR/FSR*SP*Area*10^6*k_B*T/(S_T*P_{total}*10^2* L);

List of Quantities:

Quantity	Unit	Definition
S_T	cm	Line strength at temperature T
L	cm	Cell Pathlegth
k_B	J/K	Boltzmann constant
T	K	Temperature in Gascell
P_{total}	hPa	Total-Pressure in Gascell
x_{CO2}	mol/mol	Amount of substance fraction of CO_2
FSR	cm^{-1}	Free spectral range (FSR) of a Si - etalon
FSRSP	SP #	FSR of a Si - etalon in SP # digitalized by the adquisition card
Area	SP #	Area under the Voigt profile
S_{To}	cm	Linestrength for norm temperature To = 296 K
T_0	K	Norm temperature
h	J s	Planck constant
c	m/s	Ligth speed in vacuum
E	cm-1	Lower state energy
ν_0	cm^{-1}	linecenter

Quantity	Unit	Definition
Q_{To}	Arbitrary	internal partition sum for temperature To
Q_T	Arbitrary	internal partition sum for temperature T

S_T:
Interim Result

L:
Type B rectangular distribution
Value: 100 cm
Halfwidth of Limits: 0.5 cm

1 cm expanded uncertainty, not informative type B uncertainty source gives 0.5 cm

k_B:
Type B normal distribution
Value: $1.3806505 \cdot 10^{-23}$ J/K
Expanded Uncertainty: $0.0000024 \cdot 10^{-23}$ J/K
Coverage Factor: 1

Value 1.380 6505 x 10-23 J K-1
Standard uncertainty 0.000 0024 x 10-23 J K-1
Relative standard uncertainty 1.8 x 10-6
From: CODATA Internationally recommended values of the Fundamental Physical constants, NIST(2000)

T:
Type B normal distribution
Value: 294.96 K
Expanded Uncertainty: 0.2 K
Coverage Factor: 1

+/- 0.1 C accuracy specification
< 0.1 C repeatability and stability

P_{total}:
Type B normal distribution
Value: 100.15 hPa
Expanded Uncertainty: 0.3 hPa
Coverage Factor: 1

+/- 0.1 hPa uncertainty of calibration around 100 hPa
+/- 0.2 hPa maximum variability, pooled standard uncertanity from repeatability 0.1 hPa

x_{CO2}:
Result

FSR:
Type B normal distribution
Value: 0.048486 cm^{-1}
Expanded Uncertainty: 0.16 %
Coverage Factor: 1

FSRSP:
Type A summarized
Value: 43.487 SP #
Standard Uncertainty: 0.023 SP #
Degrees of Freedom: 5

Area:
Type A summarized
Value: 0.114724 SP #
Standard Uncertainty: 1.41796 %
Degrees of Freedom: 999
The uncertainty includes the repeatability of areas combining the uncertainty from Voigt function and that of the variability between 10 replicates with 100 scans for each one or n = 1000 scans. Degrees of freedom = 999 relative uncertainty = 1.41796 %
Area/cm^{-1} / r_{sweep}/(cm^{-1}/SP) = 1.26656E-4/0.001104 = 0.114724 SP

S_{To}:
Type B normal distribution
Value: $1.2549 \cdot 10^{-21}$ cm
Expanded Uncertainty: $0.0072 \cdot 10^{-21}$ cm
Coverage Factor: 1

from the measured linestrength value (see chapter 5)

T_0:
Constant
Value: 296 K

h:
Type B normal distribution
Value: $6.6260693 \cdot 10^{-34}$ J s
Expanded Uncertainty: $0.0000011 \cdot 10^{-34}$ J s
Coverage Factor: 1

Value 6.626 0693 x 10-34 J s
Standard uncertainty 0.000 0011 x 10-34 J s
Relative standard uncertainty 1.7 x 10-7
From: CODATA Internationally recommended values of the Fundamental Physical constants, NIST(2000)

c:
Constant
Value: 299792458 m/s

Value 299 792 458 m s-1
From: CODATA Internationally recommended values of the Fundamental Physical constants, NIST(2000)

E:
Constant
Value: 60.8709 cm-1

ν_0:
Type B normal distribution
Value: 4987.3087 cm^{-1}
Expanded Uncertainty: 0.0040 cm^{-1}
Coverage Factor: 1

0.001 cm^{-1} for u(ν_0) form HITRAN and 0.003 cm^{-1} from the possible line shift of ν_0

Q_{To}:
Type B normal distribution
Value: 33.4082828864 Arbitrary
Expanded Uncertainty: 0.3 %
Coverage Factor: 1

Q_T:
Type B normal distribution
Value: 33.028 Arbitrary
Expanded Uncertainty: 0.3 %
Coverage Factor: 1

Uncertainty Budget:

Quantity	Value	Standard Uncertainty	Degrees of Freedom	Sensitivity Coefficient	Uncertainty Contribution	Index
S_T	$1.27329 \cdot 10^{-21}$ cm	$9.12 \cdot 10^{-24}$ cm				
L	100.000 cm	0.289 cm	∞	$-4.1 \cdot 10^{-6}$	$-1.2 \cdot 10^{-6}$ mol/mol	3.0 %
k_B	$13.8065050 \cdot 10^{-24}$ J/K	$24.0 \cdot 10^{-30}$ J/K	50	$30 \cdot 10^{18}$	$710 \cdot 10^{-12}$ mol/mol	0.0 %
T	294.960 K	0.200 K	50	$2.6 \cdot 10^{-6}$	$520 \cdot 10^{-9}$ mol/mol	0.6 %
P_{total}	100.150 hPa	0.300 hPa	50	$-4.1 \cdot 10^{-6}$	$-1.2 \cdot 10^{-6}$ mol/mol	3.3 %
FSR	0.0484860 cm^{-1}	$77.6 \cdot 10^{-6}$ cm^{-1}	50	$8.4 \cdot 10^{-3}$	$650 \cdot 10^{-9}$ mol/mol	0.9 %
FSRSP	43.4870 SP #	0.0230 SP #	5	$-9.4 \cdot 10^{-6}$	$-220 \cdot 10^{-9}$ mol/mol	0.1 %
Area	0.11472 SP #	$1.63 \cdot 10^{-3}$ SP #	1000	$3.6 \cdot 10^{-3}$	$5.8 \cdot 10^{-6}$ mol/mol	73.4 %
S_{To}	$1.25490 \cdot 10^{-21}$ cm	$7.20 \cdot 10^{-24}$ cm	50	$-330 \cdot 10^{15}$	$-2.3 \cdot 10^{-6}$ mol/mol	12.0 %
T_0	296.0 K					
h	$662.606930 \cdot 10^{-36}$ J s	$110 \cdot 10^{-42}$ J s	50	$250 \cdot 10^{24}$	$27 \cdot 10^{-15}$ mol/mol	0.0 %
c	$299.792458 \cdot 10^{6}$ m/s					
E	60.8709 cm-1					
ν_0	4987.30870 cm^{-1}	$4.00 \cdot 10^{-3}$ cm^{-1}	50	0.0	0.0 mol/mol	0.0 %
Q_{To}	33.408 Arbitrary	0.100 Arbitrary	50	$-12 \cdot 10^{-6}$	$-1.2 \cdot 10^{-6}$ mol/mol	3.3 %
Q_T	33.0280 Arbitrary	0.0991 Arbitrary	50	$12 \cdot 10^{-6}$	$1.2 \cdot 10^{-6}$ mol/mol	3.3 %
x_{CO2}	$408.5 \cdot 10^{-6}$ mol/mol	$6.76 \cdot 10^{-6}$ mol/mol	1100			

Result:

Quantity: x_{CO2}
Value: $408 \cdot 10^{-6}$ mol/mol
Relative Expanded Uncertainty: ±3.3 %
Coverage Factor: 2.0
Coverage: t-table 95%

Example for a $1 \cdot 10^{-2}$ mol/mol CO_2/N_2 gas mixture (Table 6.2)

Model Equation:

$S_T=S_{To}*(Q_{To}/Q_T)*exp(-h*c*E/k_B*(1/T-1/T_0))*(1-exp(-h*c*\nu_0/(k_B*T)))/(1-exp(-h*c*\nu_0/(k_B*T_0)));$

x_{CO2} = FSR/FSR*SP*Area*10^6*k_B*T/(S_T*P_{total}*10^2* L);

List of Quantities:

Quantity	Unit	Definition
S_T	cm	Line strength at temperature T
L	cm	Cell Pathlegth
k_B	J/K	Boltzmann constant
T	K	Temperature in Gascell
P_{total}	hPa	Total-Pressure in Gascell
x_{CO2}	mol/mol	Amount of substance fraction of CO_2
FSR	cm^{-1}	Free spectral range (FSR) of a Si - etalon
FSRSP	SP #	FSR of a Si - etalon in SP # digitalized by the adquisition card
Area	SP #	Area under the Voigt profile
S_{To}	cm	Linestrength for norm temperature To = 296 K
T_0	K	Norm temperature
h	J s	Planck constant
c	m/s	Ligth speed in vacuum
E	cm-1	Lower state energy
ν_0	cm^{-1}	linecenter
Q_{To}	Arbitrary	internal partition sum for temperature To
Q_T	Arbitrary	internal partition sum for temperature T

S_T:
Interim Result

L:
Type B rectangular distribution
Value: 100 cm
Halfwidth of Limits: 0.5 cm

1 cm expanded uncertainty, not informative type B uncertainty source gives 0.5 cm

k_B:
Type B normal distribution
Value: $1.3806505 \cdot 10^{-23}$ J/K
Expanded Uncertainty: $0.0000024 \cdot 10^{-23}$ J/K
Coverage Factor: 1

Value 1.380 6505 x 10-23 J K-1
Standard uncertainty 0.000 0024 x 10-23 J K-1
Relative standard uncertainty 1.8 x 10-6
From: CODATA Internationally recommended values of the Fundamental Physical constants, NIST(2000)

T:
Type B normal distribution

Value: 295.3 K
Expanded Uncertainty: 0.2 K
Coverage Factor: 1

+/- 0.1 C accuracy specification
< 0.1 C repeatability and stability

P_{total}:
Type B normal distribution
Value: 99.25 hPa
Expanded Uncertainty: 0.3 hPa
Coverage Factor: 1

+/- 0.2 hPa uncertainty of calibration around 100 hPa
+/- 0.2 hPa maximum variability, typically 0.1 hPa

x_{CO2}:
Result

FSR:
Type B normal distribution
Value: 0.048486 cm^{-1}
Expanded Uncertainty: 0.16 %
Coverage Factor: 1

FSRSP:
Type A summarized
Value: 43.487 SP #
Standard Uncertainty: 0.023 SP #
Degrees of Freedom: 5

Area:
Type A summarized
Value: 2.81703 SP #
Standard Uncertainty: 0.53245 %
Degrees of Freedom: 999

The uncertainty includes the repeatability of areas combining the uncertainty from Voigt function and that of the variability between 10 replicates with 100 scans for each one or n = 1000 scans. Degrees of freedom = 999 relative uncertainty = 0.53245 %
Area/cm^{-1} / r_{sweep}/(cm^{-1}/SP) = 0.00311/0.001104 = 2.81703 SP

S_{To}:
Type B normal distribution
Value: $1.2549 \cdot 10^{-21}$ cm
Expanded Uncertainty: $0.0072 \cdot 10^{-21}$ cm
Coverage Factor: 1

from the measured linestrength value (see chapter 5)

T_0:
Constant
Value: 296 K

h:
Type B normal distribution
Value: $6.6260693 \cdot 10^{-34}$ J s
Expanded Uncertainty: $0.0000011 \cdot 10^{-34}$ J s
Coverage Factor: 1

Value 6.626 0693 x 10-34 J s
Standard uncertainty 0.000 0011 x 10-34 J s
Relative standard uncertainty 1.7 x 10-7
From: CODATA Internationally recommended values of the Fundamental Physical constants, NIST(2000)

c:
Constant
Value: 299792458 m/s

Value 299 792 458 m s-1
From: CODATA Internationally recommended values of the Fundamental Physical constants, NIST(2000)

E:
Constant
Value: 60.8709 cm-1

ν_0:
Type B normal distribution
Value: 4987.3087 cm^{-1}
Expanded Uncertainty: 0.0040 cm^{-1}
Coverage Factor: 1

0.001 cm^{-1} for u(ν_0) form HITRAN and 0.003 cm^{-1} from the possible line shift of ν_0

Q_{To}:
Type B normal distribution
Value: 33.4082828864 Arbitrary
Expanded Uncertainty: 0.3 %
Coverage Factor: 1

Q_T:
Type B normal distribution
Value: 33.152 Arbitrary
Expanded Uncertainty: 0.3 %
Coverage Factor: 1

Uncertainty Budget:

Quantity	Value	Standard Uncertainty	Degrees of Freedom	Sensitivity Coefficient	Uncertainty Contribution	Index
S_T	$1.26724 \cdot 10^{-21}$ cm	$9.07 \cdot 10^{-24}$ cm				
L	100.000 cm	0.289 cm	∞	$-100 \cdot 10^{-6}$	$-29 \cdot 10^{-6}$ mol/mol	8.2 %
k_B	$13.8065050 \cdot 10^{-24}$ J/K	$24.0 \cdot 10^{-30}$ J/K	50	$740 \cdot 10^{18}$	$18 \cdot 10^{-9}$ mol/mol	0.0 %
T	295.300 K	0.200 K	50	$65 \cdot 10^{-6}$	$13 \cdot 10^{-6}$ mol/mol	1.6 %
P_{total}	99.250 hPa	0.300 hPa	50	$-100 \cdot 10^{-6}$	$-31 \cdot 10^{-6}$ mol/mol	9.0 %
FSR	0.0484860 cm^{-1}	$77.6 \cdot 10^{-6}$ cm^{-1}	50	0.21	$16 \cdot 10^{-6}$ mol/mol	2.5 %
FSRSP	43.4870 SP #	0.0230 SP #	5	$-230 \cdot 10^{-6}$	$-5.4 \cdot 10^{-6}$ mol/mol	0.3 %

Quantity	Value	Standard Uncertainty	Degrees of Freedom	Sensitivity Coefficient	Uncertainty Contribution	Index
Area	2.8170 SP #	0.0150 SP #	1000	$3.6 \cdot 10^{-3}$	$54 \cdot 10^{-6}$ mol/mol	28.0 %
S_{To}	$1.25490 \cdot 10^{-21}$ cm	$7.20 \cdot 10^{-24}$ cm	50	$-8.1 \cdot 10^{18}$	$-58 \cdot 10^{-6}$ mol/mol	32.5 %
T_0	296.0 K					
h	$662.606930 \cdot 10^{-36}$ J s	$110 \cdot 10^{-42}$ J s	50	$4.2 \cdot 10^{27}$	$460 \cdot 10^{-15}$ mol/mol	0.0 %
c	$299.792458 \cdot 10^{6}$ m/s					
E	60.8709 cm-1					
ν_0	4987.30870 cm^{-1}	$4.00 \cdot 10^{-3}$ cm^{-1}	50	0.0	0.0 mol/mol	0.0 %
Q_{To}	33.408 Arbitrary	0.100 Arbitrary	50	$-300 \cdot 10^{-6}$	$-31 \cdot 10^{-6}$ mol/mol	8.9 %
Q_T	33.1520 Arbitrary	0.0995 Arbitrary	50	$310 \cdot 10^{-6}$	$31 \cdot 10^{-6}$ mol/mol	8.9 %
x_{CO2}	0.01018 mol/mol	$102 \cdot 10^{-6}$ mol/mol	370			

Result:

Quantity: x_{CO2}
Value: 0.01018 mol/mol
Relative Expanded Uncertainty: ±2.0 %
Coverage Factor: 2.0
Coverage: t-table 95%

Example for a $5 \cdot 10^{-2}$ mol/mol CO_2/N_2 gas mixture (Table 6.2)

Model Equation:

$S_T=S_{To}*(Q_{To}/Q_T)*exp(-h*c*E/k_B*(1/T-1/T_0))*(1-exp(-h*c*\nu_0/(k_B*T)))/(1-exp(-h*c*\nu_0/(k_B*T_0)));$

x_{CO2} = FSR/FSR$SP*Area*10\text{^}6*k_B*T/(S_T*P_{total}*10\text{^}2*L);$

List of Quantities:

Quantity	Unit	Definition
S_T	cm	Line strength at temperature T
L	cm	Cell Pathlegth
k_B	J/K	Boltzmann constant
T	K	Temperature in Gascell
P_{total}	hPa	Total-Pressure in Gascell
x_{CO2}	mol/mol	Amount of substance fraction of CO_2
FSR	cm^{-1}	Free spectral range (FSR) of a Si - etalon
FSRSP	SP #	FSR of a Si - etalon in SP # digitalized by the adquisition card
Area	SP #	Area under the Voigt profile

Quantity	Unit	Definition
S_{To}	cm	Linestrength for norm temperature To = 296 K
T_0	K	Norm temperature
h	J s	Planck constant
c	m/s	Ligth speed in vacuum
E	cm-1	Lower state energy
ν_0	cm^{-1}	linecenter
Q_{To}	Arbitrary	internal partition sum for temperature To
Q_T	Arbitrary	internal partition sum for temperature T

S_T:
Interim Result

L:
Type B rectangular distribution
Value: 100 cm
Halfwidth of Limits: 0.5 cm

1 cm expanded uncertainty, not informative type B uncertainty source gives 0.5 cm

k_B:
Type B normal distribution
Value: $1.3806505 \cdot 10^{-23}$ J/K
Expanded Uncertainty: $0.0000024 \cdot 10^{-23}$ J/K
Coverage Factor: 1

Value 1.380 6505 x 10-23 J K-1
Standard uncertainty 0.000 0024 x 10-23 J K-1
Relative standard uncertainty 1.8 x 10-6
From: CODATA Internationally recommended values of the Fundamental Physical constants, NIST(2000)

T:
Type B normal distribution
Value: 294.3 K
Expanded Uncertainty: 0.2 K
Coverage Factor: 1

+/- 0.1 C accuracy specification
< 0.1 C repeatability and stability

P_{total}:
Type B normal distribution
Value: 100.45 hPa
Expanded Uncertainty: 0.3 hPa
Coverage Factor: 1

+/- 0.2 hPa uncertainty of calibration around 100 hPa
+/- 0.2 hPa maximum variability, typically 0.1 hPa

x_{CO2}:
Result

FSR:
Type B normal distribution
Value: 0.048486 cm^{-1}
Expanded Uncertainty: 0.16 %

Coverage Factor: 1

FSRSP:
Type A summarized
Value: 43.487 SP #
Standard Uncertainty: 0.023 SP #
Degrees of Freedom: 5

Area:
Type A summarized
Value: 14.59239 SP #
Standard Uncertainty: 0.17279 %
Degrees of Freedom: 999

The uncertainty includes the repeatability of areas combining the uncertainty from Voigt function and that of the variability between 10 replicates with 100 scans for each one or n = 1000 scans. Degrees of freedom = 999
relative uncertainty = 0.17279 %
Area/cm^{-1} / r_{sweep}/(cm^{-1}/SP) = 0.01611/0.001104 = 14.59239 SP

S_{To}:
Type B normal distribution
Value: $1.2549 \cdot 10^{-21}$ cm
Expanded Uncertainty: $0.0072 \cdot 10^{-21}$ cm
Coverage Factor: 1

from the measured linestrength value (see chapter 5)

T_0:
Constant
Value: 296 K

h:
Type B normal distribution
Value: $6.6260693 \cdot 10^{-34}$ J s
Expanded Uncertainty: $0.0000011 \cdot 10^{-34}$ J s
Coverage Factor: 1

Value 6.626 0693 x 10-34 J s
Standard uncertainty 0.000 0011 x 10-34 J s
Relative standard uncertainty 1.7 x 10-7
From: CODATA Internationally recommended values of the Fundamental Physical constants, NIST(2000)

c:
Constant
Value: 299792458 m/s

Value 299 792 458 m s-1
From: CODATA Internationally recommended values of the Fundamental Physical constants, NIST(2000)

E:
Constant
Value: 60.8709 cm-1

ν_0:
Type B normal distribution
Value: 4987.3087 cm^{-1}
Expanded Uncertainty: 0.0040 cm^{-1}

Coverage Factor: 1

0.001 cm^{-1} for u(ν_0) form HITRAN and 0.003 cm^{-1} from the possible line shift of ν_0

Q_{To}:
Type B normal distribution
Value: 33.4082828864 Arbitrary
Expanded Uncertainty: 0.3 %
Coverage Factor: 1

Q_T:
Type B normal distribution
Value: 32.7880 Arbitrary
Expanded Uncertainty: 0.3 %
Coverage Factor: 1

Uncertainty Budget:

Quantity	Value	Standard Uncertainty	Degrees of Freedom	Sensitivity Coefficient	Uncertainty Contribution	Index
S_T	$1.28514 \cdot 10^{-21}$ cm	$9.20 \cdot 10^{-24}$ cm				
L	100.000 cm	0.289 cm	∞	$-510 \cdot 10^{-6}$	$-150 \cdot 10^{-6}$ mol/mol	11.0 %
k_B	$13.8065050 \cdot 10^{-24}$ J/K	$24.0 \cdot 10^{-30}$ J/K	50	$3.7 \cdot 10^{21}$	$89 \cdot 10^{-9}$ mol/mol	0.0 %
T	294.300 K	0.200 K	50	$330 \cdot 10^{-6}$	$65 \cdot 10^{-6}$ mol/mol	2.2 %
P_{total}	100.450 hPa	0.300 hPa	50	$-510 \cdot 10^{-6}$	$-150 \cdot 10^{-6}$ mol/mol	11.8 %
FSR	0.0484860 cm^{-1}	$77.6 \cdot 10^{-6}$ cm^{-1}	50	1.1	$82 \cdot 10^{-6}$ mol/mol	3.4 %
FSRSP	43.4870 SP #	0.0230 SP #	5	$-1.2 \cdot 10^{-3}$	$-27 \cdot 10^{-6}$ mol/mol	0.4 %
Area	14.5924 SP #	0.0252 SP #	1000	$3.5 \cdot 10^{-3}$	$88 \cdot 10^{-6}$ mol/mol	3.9 %
S_{To}	$1.25490 \cdot 10^{-21}$ cm	$7.20 \cdot 10^{-24}$ cm	50	$-41 \cdot 10^{18}$	$-290 \cdot 10^{-6}$ mol/mol	43.5 %
T_0	296.0 K					
h	$662.606930 \cdot 10^{-36}$ J s	$110 \cdot 10^{-42}$ J s	50	$51 \cdot 10^{27}$	$5.6 \cdot 10^{-12}$ mol/mol	0.0 %
c	$299.792458 \cdot 10^{6}$ m/s					
E	60.8709 cm-1					
ν_0	4987.30870 cm^{-1}	$4.00 \cdot 10^{-3}$ cm^{-1}	50	0.0	0.0 mol/mol	0.0 %
Q_{To}	33.408 Arbitrary	0.100 Arbitrary	50	$-1.5 \cdot 10^{-3}$	$-150 \cdot 10^{-6}$ mol/mol	11.9 %
Q_T	32.7880 Arbitrary	0.0984 Arbitrary	50	$1.6 \cdot 10^{-3}$	$150 \cdot 10^{-6}$ mol/mol	11.9 %
x_{CO2}	0.05121 mol/mol	$445 \cdot 10^{-6}$ mol/mol	210			

Result:
Quantity: x_{CO2}
Value: 0.05121 mol/mol
Relative Expanded Uncertainty: ±1.7 %
Coverage Factor: 2.0
Coverage: t-table 95%

Example for a $10 \cdot 10^{-2}$ mol/mol CO_2/N_2 gas mixture (Table 6.2)

Model Equation:
$S_T=S_{To}*(Q_{To}/Q_T)*exp(-h*c*E/k_B*(1/T-1/T_0))*(1-exp(-h*c*\nu_0/(k_B*T)))/(1-exp(-h*c*\nu_0/(k_B*T_0)));$

x_{CO2} = FSR/FSR$SP*Area*10^6*k_B*T/(S_T*P_{total}*10^2*L);$

List of Quantities:

Quantity	Unit	Definition
S_T	cm	Line strength at temperature T
L	cm	Cell Pathlegth
k_B	J/K	Boltzmann constant
T	K	Temperature in Gascell
P_{total}	hPa	Total-Pressure in Gascell
x_{CO2}	mol/mol	Amount of substance fraction of CO_2
FSR	cm^{-1}	Free spectral range (FSR) of a Si - etalon
FSRSP	SP #	FSR of a Si - etalon in SP # digitalized by the adquisition card
Area	SP #	Area under the Voigt profile
S_{To}	cm	Linestrength for norm temperature To = 296 K
T_0	K	Norm temperature
h	J s	Planck constant
c	m/s	Ligth speed in vacuum
E	cm-1	Lower state energy
ν_0	cm^{-1}	linecenter
Q_{To}	Arbitrary	internal partition sum for temperature To
Q_T	Arbitrary	internal partition sum for temperature T

S_T:
Interim Result

L:
Type B rectangular distribution
Value: 100 cm
Halfwidth of Limits: 0.5 cm

1 cm expanded uncertainty, not informative type B uncertainty source gives 0.5 cm

k_B:
Type B normal distribution
Value: $1.3806505 \cdot 10^{-23}$ J/K
Expanded Uncertainty: $0.0000024 \cdot 10^{-23}$ J/K

Coverage Factor: 1

Value 1.380 6505 x 10-23 J K-1
Standard uncertainty 0.000 0024 x 10-23 J K-1
Relative standard uncertainty 1.8 x 10-6
From: CODATA Internationally recommended values of the Fundamental Physical constants, NIST(2000)

T:
Type B normal distribution
Value: 295.4 K
Expanded Uncertainty: 0.2 K
Coverage Factor: 1

+/- 0.1 C accuracy specification
< 0.1 C repeatability and stability

P_{total}:
Type B normal distribution
Value: 100.6 hPa
Expanded Uncertainty: 0.3 hPa
Coverage Factor: 1

+/- 0.2 hPa uncertainty of calibration around 100 hPa
+/- 0.2 hPa maximum variability, typically 0.1 hPa

x_{CO2}:
Result

FSR:
Type B normal distribution
Value: 0.048486 cm^{-1}
Expanded Uncertainty: 0.16 %
Coverage Factor: 1

FSRSP:
Type A summarized
Value: 43.487 SP #
Standard Uncertainty: 0.023 SP #
Degrees of Freedom: 5

Area:
Type A summarized
Value: 28.75 SP #
Standard Uncertainty: 0.07622 %
Degrees of Freedom: 899

The uncertainty includes the repeatability of areas combining the uncertainty from Voigt function and that of the variability between 9 replicates with 100 scans for each one or n = 1000 scans. Degrees of freedom = 899
relative uncertainty = 0.07622 %
Area/cm^{-1} / r_{sweep}/(cm^{-1}/SP) = 0.03174/0.001104 = 28.75 SP

S_{To}:
Type B normal distribution
Value: $1.2549 \cdot 10^{-21}$ cm
Expanded Uncertainty: $0.0072 \cdot 10^{-21}$ cm
Coverage Factor: 1

from the measured linestrength value (see chapter 5)

T_0:
Constant
Value: 296 K

h:
Type B normal distribution
Value: $6.6260693 \cdot 10^{-34}$ J s
Expanded Uncertainty: $0.0000011 \cdot 10^{-34}$ J s
Coverage Factor: 1

Value 6.626 0693 x 10-34 J s
Standard uncertainty 0.000 0011 x 10-34 J s
Relative standard uncertainty 1.7 x 10-7
From: CODATA Internationally recommended values of the Fundamental Physical constants, NIST(2000)

c:
Constant
Value: 299792458 m/s

Value 299 792 458 m s-1
From: CODATA Internationally recommended values of the Fundamental Physical constants, NIST(2000)

E:
Constant
Value: 60.8709 cm-1

ν_0:
Type B normal distribution
Value: 4987.3087 cm^{-1}
Expanded Uncertainty: 0.0040 cm^{-1}
Coverage Factor: 1

0.001 cm^{-1} for u(ν_0) form HITRAN and 0.003 cm^{-1} from the possible line shift of ν_0

Q_{T0}:
Type B normal distribution
Value: 33.4082828864 Arbitrary
Expanded Uncertainty: 0.3 %
Coverage Factor: 1

Q_T:
Type B normal distribution
Value: 33.188 Arbitrary
Expanded Uncertainty: 0.3 %
Coverage Factor: 1

Uncertainty Budget:

Quantity	Value	Standard Uncertainty	Degrees of Freedom	Sensitivity Coefficient	Uncertainty Contribution	Index
S_T	$1.26549 \cdot 10^{-21}$ cm	$9.06 \cdot 10^{-24}$ cm				
L	100.000 cm	0.289 cm	∞	$-1.0 \cdot 10^{-3}$	$-300 \cdot 10^{-6}$ mol/mol	11.4 %
k_B	$13.8065050 \cdot 10^{-}$	$24.0 \cdot 10^{-30}$ J/K	50	$7.4 \cdot 10^{21}$	$180 \cdot 10^{-9}$	0.0 %

Quantity	Value	Standard Uncertainty	Degrees of Freedom	Sensitivity Coefficient	Uncertainty Contribution	Index
	^{24} J/K				mol/mol	
T	295.400 K	0.200 K	50	$650 \cdot 10^{-6}$	$130 \cdot 10^{-6}$ mol/mol	2.2 %
P_{total}	100.600 hPa	0.300 hPa	50	$-1.0 \cdot 10^{-3}$	$-310 \cdot 10^{-6}$ mol/mol	12.2 %
FSR	0.0484860 cm^{-1}	$77.6 \cdot 10^{-6}$ cm^{-1}	50	2.1	$160 \cdot 10^{-6}$ mol/mol	3.5 %
FSRSP	43.4870 SP #	0.0230 SP #	5	$-2.4 \cdot 10^{-3}$	$-54 \cdot 10^{-6}$ mol/mol	0.4 %
Area	28.7500 SP #	0.0219 SP #	900	$3.6 \cdot 10^{-3}$	$78 \cdot 10^{-6}$ mol/mol	0.8 %
S_{To}	$1.25490 \cdot 10^{-21}$ cm	$7.20 \cdot 10^{-24}$ cm	50	$-82 \cdot 10^{18}$	$-590 \cdot 10^{-6}$ mol/mol	45.0 %
T_0	296.0 K					
h	$662.606930 \cdot 10^{-36}$ J s	$110 \cdot 10^{-42}$ J s	50	$36 \cdot 10^{27}$	$4.0 \cdot 10^{-12}$ mol/mol	0.0 %
c	$299.792458 \cdot 10^{6}$ m/s					
E	60.8709 cm-1					
ν_0	4987.30870 cm^{-1}	$4.00 \cdot 10^{-3}$ cm^{-1}	50	0.0	0.0 mol/mol	0.0 %
Q_{To}	33.408 Arbitrary	0.100 Arbitrary	50	$-3.1 \cdot 10^{-3}$	$-310 \cdot 10^{-6}$ mol/mol	12.3 %
Q_T	33.1880 Arbitrary	0.0996 Arbitrary	50	$3.1 \cdot 10^{-3}$	$310 \cdot 10^{-6}$ mol/mol	12.3 %
x_{CO2}	0.10269 mol/mol	$879 \cdot 10^{-6}$ mol/mol	200			

Result:

Quantity: x_{CO2}
Value: 0.1027 mol/mol
Relative Expanded Uncertainty: ±1.7 %
Coverage Factor: 2.0
Coverage: t-table 95%

Example for a $14 \cdot 10^{-2}$ mol/mol CO_2/N_2 gas mixture (Table 6.2)

Model Equation:

$S_T=S_{To}*(Q_{To}/Q_T)*exp(-h*c*E/k_B*(1/T-1/T_0))*(1-exp(-h*c*\nu_0/(k_B*T)))/(1-exp(-h*c*\nu_0/(k_B*T_0)));$

x_{CO2} = FSR/FSR*SP*Area*10^6*k_B*T/(S_T*P_{total}*10^2* L);

List of Quantities:

Quantity	Unit	Definition
S_T	cm	Line strength at temperature T

Quantity	Unit	Definition
L	cm	Cell Pathlegth
k_B	J/K	Boltzmann constant
T	K	Temperature in Gascell
P_{total}	hPa	Total-Pressure in Gascell
x_{CO2}	mol/mol	Amount of substance fraction of CO_2
FSR	cm^{-1}	Free spectral range (FSR) of a Si - etalon
FSRSP	SP #	FSR of a Si - etalon in SP # digitalized by the adquisition card
Area	SP #	Area under the Voigt profile
S_{To}	cm	Linestrength for norm temperature To = 296 K
T_0	K	Norm temperature
h	J s	Planck constant
c	m/s	Ligth speed in vacuum
E	cm-1	Lower state energy
ν_0	cm^{-1}	linecenter
Q_{To}	Arbitrary	internal partition sum for temperature To
Q_T	Arbitrary	internal partition sum for temperature T

S_T:
Interim Result

L:
Type B rectangular distribution
Value: 100 cm
Halfwidth of Limits: 0.5 cm

1 cm expanded uncertainty, not informative type B uncertainty source gives 0.5 cm

k_B:
Type B normal distribution
Value: $1.3806505 \cdot 10^{-23}$ J/K
Expanded Uncertainty: $0.0000024 \cdot 10^{-23}$ J/K
Coverage Factor: 1

Value 1.380 6505 x 10-23 J K-1
Standard uncertainty 0.000 0024 x 10-23 J K-1
Relative standard uncertainty 1.8 x 10-6
From: CODATA Internationally recommended values of the Fundamental Physical constants, NIST(2000)

T:
Type B normal distribution
Value: 293.9 K
Expanded Uncertainty: 0.2 K
Coverage Factor: 1

+/- 0.1 C accuracy specification
< 0.1 C repeatability and stability

P_{total}:
Type B normal distribution
Value: 50.25 hPa
Expanded Uncertainty: 0.3 hPa

Coverage Factor: 1

+/- 0.2 hPa uncertainty of calibration around 100 hPa
+/- 0.2 hPa maximum variability, typically 0.1 hPa

x_{CO2}:
Result

FSR:
Type B normal distribution
Value: 0.048486 cm^{-1}
Expanded Uncertainty: 0.16 %
Coverage Factor: 1

FSRSP:
Type A summarized
Value: 43.487 SP #
Standard Uncertainty: 0.023 SP #
Degrees of Freedom: 5

Area:
Type A summarized
Value: 19.81884 SP #
Standard Uncertainty: 0.22614 %
Degrees of Freedom: 999

The uncertainty includes the repeatability of areas combining the uncertainty from Voigt function and that of the variability between 10 replicates with 100 scans for each one or n = 1000 scans. Degrees of freedom = 999 relative uncertainty = 0.22614 %
Area/cm^{-1} / r_{sweep}/(cm^{-1}/SP) = 0.02188/0.001104 = 19.81884 SP

S_{To}:
Type B normal distribution
Value: $1.2549 \cdot 10^{-21}$ cm
Expanded Uncertainty: $0.0072 \cdot 10^{-21}$ cm
Coverage Factor: 1

from the measured linestrength value (see chapter 5)

T_0:
Constant
Value: 296 K

h:
Type B normal distribution
Value: $6.6260693 \cdot 10^{-34}$ J s
Expanded Uncertainty: $0.0000011 \cdot 10^{-34}$ J s
Coverage Factor: 1

Value 6.626 0693 x 10-34 J s
Standard uncertainty 0.000 0011 x 10-34 J s
Relative standard uncertainty 1.7 x 10-7
From: CODATA Internationally recommended values of the Fundamental Physical constants, NIST(2000)

c:
Constant
Value: 299792458 m/s

Value 299 792 458 m s-1

From: CODATA Internationally recommended values of the Fundamental Physical constants, NIST(2000)

E:
Constant
Value: 60.8709 cm-1

ν_0:
Type B normal distribution
Value: 4987.3087 cm^{-1}
Expanded Uncertainty: 0.0040 cm^{-1}
Coverage Factor: 1

0.001 cm^{-1} for u(ν_0) form HITRAN and 0.003 cm^{-1} from the possible line shift of ν_0

Q_{To}:
Type B normal distribution
Value: 33.4082828864 Arbitrary
Expanded Uncertainty: 0.3 %
Coverage Factor: 1

Q_T:
Type B normal distribution
Value: 33.643 Arbitrary
Expanded Uncertainty: 0.3 %
Coverage Factor: 1

Uncertainty Budget:

Quantity	Value	Standard Uncertainty	Degrees of Freedom	Sensitivity Coefficient	Uncertainty Contribution	Index
S_T	$1.25398 \cdot 10^{-21}$ cm	$8.98 \cdot 10^{-24}$ cm				
L	100.000 cm	0.289 cm	∞	$-1.4 \cdot 10^{-3}$	$-410 \cdot 10^{-6}$ mol/mol	8.0 %
k_B	$13.8065050 \cdot 10^{-24}$ J/K	$24.0 \cdot 10^{-30}$ J/K	50	$10 \cdot 10^{21}$	$250 \cdot 10^{-9}$ mol/mol	0.0 %
T	293.900 K	0.200 K	50	$910 \cdot 10^{-6}$	$180 \cdot 10^{-6}$ mol/mol	1.6 %
P_{total}	50.250 hPa	0.300 hPa	50	$-2.8 \cdot 10^{-3}$	$-850 \cdot 10^{-6}$ mol/mol	34.1 %
FSR	0.0484860 cm^{-1}	$77.6 \cdot 10^{-6}$ cm^{-1}	50	2.9	$230 \cdot 10^{-6}$ mol/mol	2.4 %
FSRSP	43.4870 SP	0.0230 SP #	5	$-3.3 \cdot 10^{-3}$	$-75 \cdot 10^{-6}$ mol/mol	0.3 %
Area	19.8188 SP	0.0448 SP #	1000	$7.2 \cdot 10^{-3}$	$320 \cdot 10^{-6}$ mol/mol	4.9 %
S_{To}	$1.25490 \cdot 10^{-21}$ cm	$7.20 \cdot 10^{-24}$ cm	50	$-110 \cdot 10^{18}$	$-820 \cdot 10^{-6}$ mol/mol	31.5 %
T_0	296.0 K					
h	$662.606930 \cdot 10^{-36}$ J s	$110 \cdot 10^{-42}$ J s	50	$180 \cdot 10^{27}$	$19 \cdot 10^{-12}$ mol/mol	0.0 %
c	$299.792458 \cdot 10^{6}$ m/s					
E	60.8709 cm-1					

Quantity	Value	Standard Uncertainty	Degrees of Freedom	Sensitivity Coefficient	Uncertainty Contribution	Index
ν_0	4987.30870 cm^{-1}	$4.00 \cdot 10^{-3}$ cm^{-1}	50	0.0	0.0 mol/mol	0.0 %
Q_{To}	33.408 Arbitrary	0.100 Arbitrary	50	$-4.3 \cdot 10^{-3}$	$-430 \cdot 10^{-6}$ mol/mol	8.6 %
Q_T	33.643 Arbitrary	0.101 Arbitrary	50	$4.2 \cdot 10^{-3}$	$430 \cdot 10^{-6}$ mol/mol	8.6 %
x_{CO2}	0.1423 mol/mol	$1.45 \cdot 10^{-3}$ mol/mol	220			

Result:

Quantity: x_{CO2}
Value: 0.1423 mol/mol
Relative Expanded Uncertainty: ±2.0 %
Coverage Factor: 2.0
Coverage: t-table 95%